

**Design, Preparation and Application of
Multifunctional Materials:
From 2D Nonwovens to 3D Nanofiber-Grass Coatings**

DISSERTATION

zur Erlangung des akademischen Grades einer Doktorin der
Naturwissenschaften (Dr. rer. nat.)

in der Bayreuther Graduiertenschule für Mathematik und Naturwissenschaften

(BayNAT)

der Universität Bayreuth

vorgelegt von

Lu Chen

aus Shaanxi, VR China

Bayreuth 2020

This doctoral thesis was prepared at the department of Macromolecular Chemistry II at the University of Bayreuth from September 2013 until Juli 2017 and was supervised by Prof. Dr. Andreas Greiner.

This is a full reprint of the thesis submitted to obtain the academic degree of Doctor of Natural Sciences (Dr. rer. nat.) and approved by the Bayreuth Graduate School of Mathematical and Natural Sciences (BayNAT) of the University of Bayreuth.

Date of submission: 28.04.2020

Date of defence: 25.10.2021

Acting director: Prof. Dr. Hans Keppler

Doctoral committee:

Prof. Dr. Andreas Greiner	(reviewer)
Prof. Dr. Peter Strohriegl	(reviewer)
Prof. Dr. Andreas Möglich	(chairman)
Prof. Dr. Werner Köhler	

No sooner said than done.

- Confucius

Table of Contents

Table of Contents	I
List of symbols and abbreviations	III
1 Introduction and theoretical background	1
1.1 Superhydrophobic surface from nature to artificial	2
1.2 Electrospinning technique for preparation of superhydrophobic materials	9
1.3 Three-dimensional structures prepared by electrospinning	12
1.4 Flocking technique as a three-dimensional coating method	15
2 Aim and Concept of this thesis	19
3 Two-dimensional superhydrophobic Nonwovens via Green Electrospinning	25
3.1 Preparation of Poly (perfluorodecyl acrylate) via emulsion polymerization	25
3.2 Preparation and Characterization of superhydrophobic nonwovens via green electrospinning	35
3.3 Preparation and Characterization of aligned nanofibers and their hydrophobicity	59
3.4 Conclusion	69
4 Three-Dimensional Matrixes with Versatile Functionalities via Flocking technique	73
4.1 Preparation and Characterization of three-dimensional matrixes via flocking with Polyamide 6.6	73
4.2 Three-dimensional flock fibers matrix as the loading material for artemisone	88
4.3 Preparation and characterization of copper flocks	93
4.4 Conclusion	107
5 Flocking with short fibers prepared via Electrospinning	110
5.1 Preparation and characterization of short nanofibers via electrospinning	110

Table of Contents

5.2 Preparation and characterization of short yarn fibers and the possibility as flock materials	117
5.3 Conclusion	123
6 Experimental part	126
6.1 Materials	126
6.2 Characterization	128
6.3 Synthesis of Poly (perfluorodecyl acrylate)	131
6.4 Preparation of multifunctional three-dimensional platform via flocking technique	133
6.5 Flocking of electrospun nanofibers	136
7 Summary	139
8 Zusammenfassung	143
9 Outlook	147
10 References	149
11 Acknowledgements	161

List of symbols and abbreviations

A	Ampere
AgNP	Silver nanoparticle
Al	Aluminum
Al ₂ O ₃	Aluminum oxide
cm	Centimeter
CFU/mL	Colony forming unit per milliliter
CTAB	Cetyltrimethylammonium bromide
CVD	Chemical Vapor Deposition
DSC	Differential scanning calorimetry
DLS	Dynamic light scattering
DMF	Dimethylformamide
DTMS	n-Decyltrimethoxysilane
<i>e.g.</i>	for example, (latin “ <i>exempli gratia</i> ”)
<i>et al.</i>	et alii; et aliae
ETD	Everhart-Thornley detector
g	Gram
GPC	Gel permeation chromatography
h	Hour
HCl	Hydrochloride acid
HFIP	Hexafluoro-2-propanol
H ₂ O	Water
k	Kilo
kΩ	Kilo ohm
kV	Kilovolt
L	Liter

List of symbols and abbreviations

LFD	Large field detector
mg	Milligram
Min	Minute
mL	Milliliter
M_n	Number average molecular weight
mol	Mole
$M\Omega$	Mega ohm
mPas	Millipascal second
M_w	Weight average molecular weight
nm	Nanometer
Pa	Pascal
PA	Polyamide
PAN	Polyacrylonitrile
PBS	Phosphate buffered saline
PEI	Poly (ethylene imine)
PFDA	^1H , ^1H , ^2H , ^2H -Perfluorodecyl Acrylate
Poly-PFDA	Poly (perfluorodecyl acrylate)
PPX	Poly (para-xylene)
PTFE	Polytetrafluoroethylene
PU	Polyurethane
PVA	Poly (vinyl alcohol)
rpm	Revolutions per minute
s	Second
s^{-1}	Per second
S	Siemens
$\text{S}\cdot\text{m}^{-1}$	Siemens per meter

List of symbols and abbreviations

SE2	Secondary electrons
SEM	Scanning electron microscope
T	Temperature
T _c	Crystallization temperature
TEOS	Tetraethyl orthosilane
TEM	Transmission electron microscopy
T _g	Glass transition temperature
TGA	Thermogravimetric analysis
THF	Tetrahydrofuran
TiO ₂	Titanium dioxide
T _m	Melting temperature
TSC	Total solid concentration
V-50	2,2'-Azo-bis(2-methylpropionamidin)-dihydrochloride
SAXS	Small-angle X-ray scattering
wt%	Weight percentage
Đ	Polydispersity index
μL	Microliter
μm	Micrometer
Ω	Ohm
°	Degree
°C	Centigrad

1 Introduction and theoretical background

Nowadays, functional materials with complex structures draw more and more concerns for their wide application fields. Among them, superhydrophobic materials showed diverse properties, such as anti-fouling, anti-icing, and self-cleaning. ^[1-4] According to the studies on natural superhydrophobic creatures, sufficient surface roughness and low surface energy are two essential matters to design and prepare artificial superhydrophobic materials. ^[5-6] To combine these principles in one-step, the electrospinning technique is applied. Electrospinning is a well-developed method to create nanofibers out of polymer solutions. ^[7] The resulted nonwovens are very porous, and build up the macro-scaled roughness; meanwhile, the random oriented nanofibers offer an additional roughness in nano/micro-scale. ^[8-10] By choosing proper materials with low surface energy, superhydrophobic nonwovens could be prepared in a quite simple process. ^[11-12] However, most of the electrospun superhydrophobic materials are prepared with organic solvents, which could cause lots of health and environmental issues. ^[13-16] To realize a sustainable procedure, the green electrospinning technique, where water is applied as the solvent, comes into concern. ^[17-23] Furthermore, the electrospun nonwovens obtain a two-dimensional structure. To expand the application areas, a three dimensional matrix is essential due to its high surface-to-volume ratio. ^[24-26] It is of interest to prepare a three-dimensional matrix through electrospinning, or use the electrospun nanofibers to build up such matrixes.

1.1 Superhydrophobic surface from nature to artificial

The famous example in Mother Nature of superhydrophobic surface is the lotus leaf (**Figure 1-1**).^[27-30] Water droplets roll away from leaf surface, and various contaminations are also collected and removed along with them. This famous phenomenon is well-known as self-cleaning ability or lotus effect, which is driven by the superhydrophobicity.^[31-35] Barthlott and Neinhuis stated for the first time in 1997, a wettable leaf exhibits usually smooth microstructure; on contrast, the water repellent surface in most plants possesses surface sculpture, which in most cases are wax-covered papillae epidermal.^[36] The hierarchical structure of cuticles over leaves minimizes the contamination of leaves' surface with water droplets.^[4, 37-40] With the combination of these two characters, the lotus leaves have contact angles as high as 160° , and a small sliding angle around 2° . Hence, it exhibits an excellent water-repellence effect.

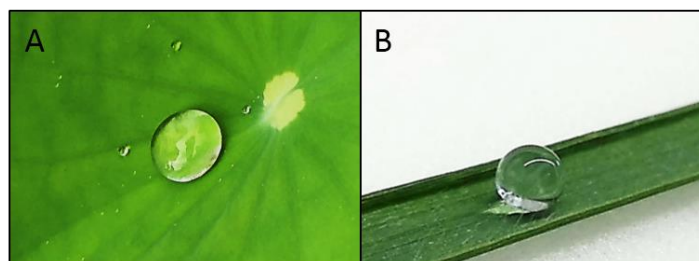


Figure 1-1. Water droplets sit on the surfaces of lotus (A) and bamboo (B) leaves.

In animal world, there are also examples exhibiting spectacular anti-adhesion property to water. The superhydrophobicity of legs of a water strider allows it to float and move freely on water surface. There are numerous oriented *setae* and they build up a three-dimensional hierarchical structure.^[41] The feathers of some birds, such as pigeons, prevent them from wetting, as a result of the hierarchical structure and

the wax material. ^[40, 42] The microstructure of some butterflies' wing surface are like roof tiles, the scales overlap with each other and arrange regularly. ^[43] Besides of the water-repellence function, this kind of structure is also used by some animals in the desert to collect water. ^[44] Mosquito's eye has also the similar structure, and this enables its antifog functionality. ^[45]

With knowledge from nature examples and the consideration of design principles of water-repellent surface, lots of artificial superhydrophobic materials are achieved by top-down or bottom-up approaches. ^[13, 46-52] Usually the two kinds of approaches are combined together to fabric superhydrophobic surfaces. Silicon cone arrays with controllable morphologies were prepared by using colloidal lithography. With the adjusting of the diameters and the size of silicon arrays, the hydrophobicity of the substrate is tunable. ^[53] To mimic the structure of mosquito's eye, soft lithography was used. With this method, micro-hemisphere and nanosphere structures were created and thereby the water-resistance is strongly enhanced. This surface prevent microscale moisture from condensing on the artificial eye surface, and showed excellent anti-fogging property. ^[45] Polystyrene (PS) nanopillars were fabricated with different tip geometries. The adhesive property of water to the surface is tunable by altering the tip geometries. The concave PS tips have the highest adhesion, and the flat tips with aligned nanotube surface exhibits lower adhesion to water. All the surfaces showed superhydrophobicity with contact angles higher than 150°. ^[54] With anodic aluminum oxide (AAO) template extrusion method, superhydrophobic surface composed of high-density polyethylene (HDPE) nanofibers was fabricated. ^[55] Chemical vapor deposition (CVD) is used to

directly prepare a rough surface or to coat a hydrophobic thin layer over a rough substrate. [3, 56] Well-aligned InGaN nanotips were successfully fabricated by CVD and after different modification it showed tunable surface wettability. [57] The initial nanotips were hydrophilic and after oxidation, it could be completely wetted. With a post modification of octyl-phosphonic acid (OPA), it showed a contact angle of 154°. This superhydrophobic surface became hydrophilic again and was completely wetted again.

When the liquid droplet contacts with the substrate surface, a contact angle between substrate and droplet can be measured. According to Young Equation,

$$\cos \theta = \frac{\gamma_{SV} - \gamma_{SL}}{\gamma_{LV}} \dots \dots \dots (1)$$

the Young contact angle θ of a smooth surface could be defined, where L, S, V relate to liquid, solid and vapor phase, and γ represents the interfacial tension (**Figure 1-2**). [58] If the contact angle is less than 90°, the surface is classified as hydrophilic. Hydrophobic surface obtains a contact angle more than 90°. [59-60] The so-called superhydrophobic surface has a contact angle more than 150°, and this special surface could be achieved by adding roughness into the smooth surface. In this case, the surface roughness factor r should be taken into account for the calculation of contact angle of rough surface, where roughness factor r is the ratio of actual surface area to the apparent area. For these rough surfaces there are two wetting states: Wenzel and Cassie-Baxter (**Figure 1-3**). [9, 61-64]

1 Introduction and theoretical background

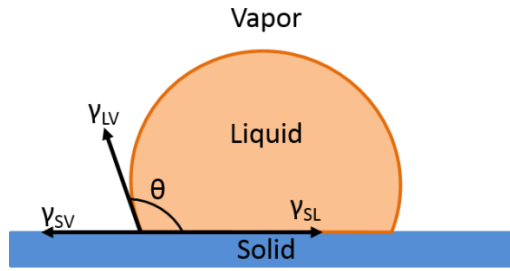


Figure 1-2. Schematically illustration of the contact angle θ of the liquid droplet on a solid surface according to Young Equation.

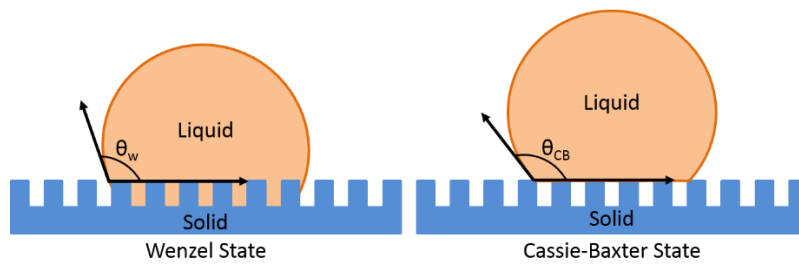


Figure 1-3. Two wetting models of the liquid droplet on a solid surface.

In the Wenzel wetting model, the liquid droplet penetrates into the surface and the interface is a homogenous surface. Its contact angle is closely related to the contact solid surface area. The contact angle in Wenzel model θ_w could be calculated by equation 2.

$$\cos \theta_w = r \cos \theta \dots \dots \dots (2)$$

The roughness amplifies the original hydrophobicity or hydrophilicity of a smooth surface. For a hydrophobic surface, the increasing of surface roughness leads to a more hydrophobic one. That means, the water contact angle will be even larger than the smooth surface. For a hydrophilic surface, it becomes more hydrophilic with higher roughness.

In contrast, model the water droplet in the Cassie-Baxter state is sitting on the surface, but does not penetrate into the surface. Therefore, the

interface composes not only of the solid phase but also vapor phase, it is a heterogeneous surface. The contact angle is related to the two components. The Cassie's law explains how to calculate a contact angle θ_{CB} on a composite surface as below,

$$\cos \theta_{CB} = f_1 \cos \theta_1 + f_2 \cos \theta_2 \dots \dots \dots (3)$$

where f_1 and f_2 represent for the surface areal fraction of phase 1 and phase 2. θ_1 and θ_2 are the contact angle for the homogenous phase 1 and 2, respectively. Usually, one of the phases is air and it has a water contact angle of 180° . For a two components surface, the areal fraction of air could be described as $(1-f)$, when the other has the fraction of f . So the equation 3 could be simplified to equation 4,

$$\cos \theta_{CB} = f(\cos \theta_1 + 1) - 1 \dots \dots \dots (4)$$

The areal fraction f is always smaller than 1; and with an increasing roughness, f will be further reduced. Therefore, $\cos \theta_{CB}$ is always smaller than $\cos \theta$. For the Cassie-Baxter model, higher roughness leads to higher contact angle, regardless of the hydrophobicity or hydrophilicity of the solid phase.

According to the two wetting states, the roughness of substrate is very important. On the other hand, the hydrophilicity/hydrophobicity of substrate material should also be emphasized for a superhydrophobicity. These are the two design principles for an artificial surface. In order to realize this, the roughness of surfaces should be increased. Meanwhile, the surface material should have less surface free energy, or lower surface energy, when no adsorption happens at the interfaces. [5, 65, 132-133] With

the combination of high roughness and low surface energy materials, surface could exhibit superhydrophobic property.

Superhydrophobic surfaces are well-known for their high water contact angle and low roll off angles, which are the key issues of self-cleaning properties. Coaxial electrospinning of TiO_2 dispersion as shell and cellulose acetate as core material is carried out by Bedford and Steckl. ^[66] Due to the well-known photocatalyst TiO_2 , the fiber mats became self-cleaning under certain indoor lighting conditions after deacetylation of initial electrospinning nonwovens. As compared to other kinds of compositions, such as pure cellulose nanofibers, TiO_2 loaded cellulose nanofibers, cellulose as core and TiO_2 /cellulose as shell; it showed the best photocatalytic property. This work introduced a new access to preparing self-cleaning materials by facile coaxial electrospinning, which is also environmental-friendly.

According to the definition of superhydrophobic surface, the contact angle is very high and the water droplet could not penetrate into the surface, therefore, it is so-called non-wettable materials. ^[42] Take this advantage, new application fields could also be found, such as anticorrosion, anti-ice/frost. Jerome and coworkers created superhydrophobic aluminum surfaces with outstanding anticorrosion performance by electrospinning of fluorinated diblock copolymer solution. ^[67] The two blocks composed of polyacrylonitrile (PAN) and poly (heptadecafluorodecylacrylate-co acrylic acid). The surface energy of fluorinated block is very low and therefore this part of blocks brought hydrophobicity into the chains. Meanwhile, the carboxylic acid acts as anchor to fix the polymer film onto the aluminum surface after annealing.

On the other hand, the PAN showed good thermal. The use of PAN block could keep the stability of surface structure during annealing at 130°C. All the surfaces showed superhydrophobic behavior before and after annealing. The film of polymer could also slightly influence the superhydrophobicity, as thicker films the performance is better. The superhydrophobic surface showed adhesion and corrosion inhibition properties. Also thicker films exhibited better results.

Another important concept using superhydrophobic surfaces are SLIPS, which represents for slippery, liquid-infused porous surfaces SLIPS is a well-studied method to create anti-ice or anti-frost surfaces. Aizenberg and coworkers produced SLIPS-coated icephobic aluminum surfaces. ^[68] A water-immiscible liquid is infused into chemically functionalized nanostructure surface and this lubricant layer is very stable, ultra-smooth and low-hysteresis. It has a high affinity to infiltrated liquid and could keep it in place. Condensed water droplets will slide off from this surface before frozen, therefore the ice accumulation reduced dramatically. It could be used in refrigeration and aviation industry or other fields, where an icephobic surface is desired.

The hydrophobic nature of materials, the superhydrophobic surfaces is oleophilic, so that it could also be used for water-oil separation, such as to remove oil pollution in the sea. ^[69-71] Through coaxial electrospinning of PCL core and Teflon shell, superhydrophobic nonwovens could be created and this fiber mat is both superhydrophobic and oleophobic. ^[38] On the other hand, electrospinning could also produce nanofibers with porous morphology; this could also help to separate water from oil. ^[30] Besides the functions mentioned above, superhydrophobic materials

could also be applied for biomedical field, such as substrates for protein adsorption, cellular/bacteria interactions, drug delivery and diagnostic applications, etc. [35, 72-86]

1.2 Electrospinning technique for preparation of superhydrophobic materials

Electrospinning shown in **Figure 1-4** is a versatile method to prepare thin fibers from liquids or melts both in small or large scales. [3, 56, 87-90] The diameter of these thin fibers could be several nanometers to micrometers. Electrospinning is suitable to prepare nanofibers with complex structures. For electrospinning a polymer solution is loaded in a syringe and with a liquid pump, this solution will form a Taylor cone at needle tip. [90-94] High voltage is applied between electrodes and with this electrical field, the Taylor cone is charged. As the stretch force is larger than the surface tension of liquid, a jet of polymer solution was emitted and formed thin fibers. When the molecular cohesion is large enough, the thin beam will not break and endless thinner fibers could be produced. Furthermore, the fiber diameters could be influenced by other parameters, such as polymer properties, viscosity and conductivity of polymer solution, distance between needles and collector, and even ambient humidity and temperature. [93, 95]

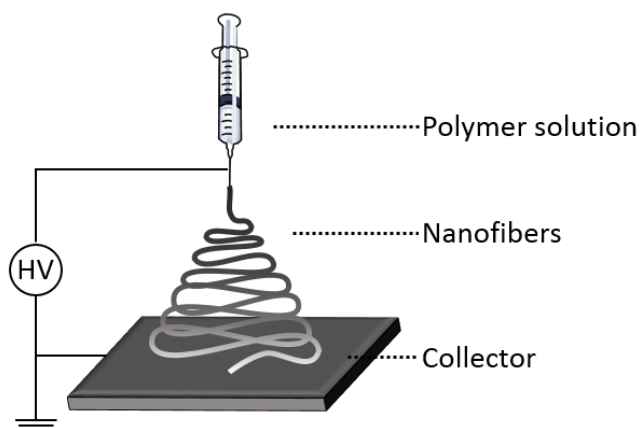


Figure 1-4. Schematically illustration of a typical electrospinning setup.

Mostly, polymer dissolves in organic solvents, which are usually toxic and highly flammable. Therefore, the usage of organic solvents in electrospinning is not sustainable. With this consideration, green electrospinning becomes a hot topic. In this case, water is used as solvent in green electrospinning. Besides, there are other methods to enable a green electrospinning. ^[23]

One of the methods to enable a green electrospinning process is emulsion electrospinning. As compared to solution electrospinning, the preparation of a stable emulsion is difficult. Three components should be satisfied: a water phase, a water not miscible solvent and an emulgator. Except of emulsion electrospinning, there is also a so-called “suspension electrospinning”, it is also a green electrospinning method. In work of Stoiljkovic and coworkers, they used a latex suspension of polystyrene and polyacrylates to make nanofibers. ^[96-97] Emulsion polymerization could produce a primary suspension directly and with help of a certain amount of template polymers, such as PVA, nanofibers with good stability against water could be made. Another method to get a stable suspension is to make a secondary suspension, by dissolving a polymer firstly in

organic phase and after adding of water and removal of organic solvent, a stable secondary suspension could be formed. ^[98] In work of Sun and coworkers, they prepared a secondary suspension of biodegradable block copolyester. ^[99] In their study, there is no used of surfactants and the resulted nonwovens is also water stable.

As shown above, the electrospinning could provide multistage roughness, not only the macroscopic roughness of nonwovens but also the microscopic roughness between each nanofiber. Besides with using of hydrophobic materials, we could combine higher surface roughness and lower surface energy in one simple step. This enriches the surface hydrophobicity dramatically and opens a new access to prepare superhydrophobic surfaces.

In work of Agarwal and coworkers made superhydrophobic nonwovens of homo- and copolymer of fluorinated styrene (PFS) and styrene (PS). ^[100] By dissolving polymers in organic solvents such as tetrahydrofuran (THF) and Dimethylformamide (DMF), they could produce nanofibers with different morphologies by tuning the composition of homo- and copolymers in electrospinning solution, such as particles, particles connected by nanofibers and fibers. Homopolymer of fluorinated styrene showed overall outstanding superhydrophobicity with particle structure and particles connected by nanofibers structure. The water contact angle is 160° or even higher, and the roll-off angle is 0°. For the copolymer of styrene and fluorinated styrene, they found that the fluorinated part should be not less than 30 mol-% as compared to the PS backbone. And these copolymers produced morphology of particles connected by

nanofibers and their roll off angles were also only 0° and the water contact angle is extreme hard to measure accurately.

Furthermore, superhydrophobic surface could also be made by blend PS homopolymer with PS-co-PDMS copolymer. ^[10] The electrospinning used also organic solvents THF and DMF. With a microphase separation, PDMS microdomains dispersed in PS matrix and segregated to surface and reduced the surface energy. The water contact angle on the fiber mat's surface is higher than 163°.

All the examples mentioned above are all out of organic solvents. Because of their toxicity and flammability the definition of "green electrospinning" come to concern, where the solvent is water and therefore the electrospinning system is environmentally friendly. Until now, there are not a lot works in this field so the purpose of this work is to fill this empty space. In the work by Doimoto et al, superhydrophobic surface out of water solution could be produced. ^[88] In his work, fluorinated acrylate polymer is produced by emulsion polymerization and after electrospinning and post-treatment, superhydrophobic surface could be prepared.

1.3 Three-dimensional structures prepared by electrospinning

Comparing two-dimensional structures, the three-dimensional ones have higher specific surface and porous structures. Three-dimensional structures draw more and more attention and are applied in many fields, such as packaging, constructions, scaffolds for tissue engineering, drug loading and delivery systems etc. ^[101-104] Scaffolds for tissue engineering should have special characteristics, such as biocompatible and bioresorbable, three-dimensional and high porous structures,

appropriate surface chemistry for cell attachment and growth, certain mechanical properties and so on. ^[105] Usually, the scaffolds could be made of polymers, synthetic or natural, organic or inorganic. As a result of different materials, there are different methods to create three-dimensional scaffolds for tissue engineering.

As mentioned before, electrospinning technique could produce nanofibers or nonwovens with special morphologies. Prof. Greiner and coworkers used electrospun fibers and freeze drying technique and successfully created ultralight and multifunctional sponges in a very simple way. ^[106] At first, the initial electrospun nanofibers were cut into short fibers with desirable fiber length and dispersed into solution. Then following with freeze-drying of the dispersion, sponges composed of short electrospun nanofibers were prepared. The sponges are ultralight and have three-dimensional network, can uptake liquid and also showed hydrophobic properties, because the main composed material is air. ^[107] This technique opens a new access to make three-dimensional network of electrospun nanofibers and there is also no limit of polymer sources. ^[107-108] The porosity could be tuned with changing the freeze rate during freeze-drying procedure. The sponges made of polyimide short fibers showed thermal insulating property, and after loading this sponge with silver nanowires, it also showed electrical conductivity and the sponge is still compression resistance. ^[108-109] The ultralight sponges are also used as drug carriers for a controllable release system. ^[110]

Besides, polymers could also form a three-dimensional scaffold from organic solvents with help of solvent-casting particulate-leaching technique. After vaporization of solvents and salt leaching in water, three-

dimensional polymer scaffolds with expected pore size could be created. [26, 111-112] However, the organic solvents are usually not biocompatible and may cause other healthy issues. In order to get rid of usage of them, gas foaming technique came into concern. [113-114] With this method, gas such as carbon dioxide CO₂ is used to form the porous structure inside of polymer matrix. Nowadays, the three-dimensional printing technique is really well developed and with this technique three-dimensional scaffolds could be prepared. [25, 115-117] Except the methods mentioned above, solvent-free techniques are also used to make three-dimensional structures. [107, 118] Expanded PS was used as matrix and then ultralight poly (para-xylene) foams and open cell sponges were produced by chemical vapor deposition.

Aerogels have three-dimensional structure and highly porous materials, which composed mainly of air and therefore aerogels are very light. [119-121] This kind of materials have ultra high specific surface and the pore size could also be tuned, to fulfill different applications such as scaffolds for tissue engineering, catalyst supports, thermal isolation, etc. Ding and coworkers combined electrospinning with freeze technique, three-dimensional ultra light aerogels could be produced. [122-123] The aerogels showed outstanding properties, such as deformation resistance, thermal insulation, electric conductivity etc. The density could be tuned and desirable three-dimensional shapes could also be created. Nanofibers functioned not only for the crosslinking, but also for the high porosity.

1.4 Flocking technique as a three-dimensional coating method

Flocking is a well-developed process in textile industry. ^[124] The first prove of flocking technique in history could be traced back to 1000 BC in china and they fixed natural fibers with resin. In middle ages in France, people used this method to decorate their stuffs. ^[125] The first electrostatic flock process showed up in 1936 and the further developed since 1950. With development of preparation of fibres and appearance of varied adhesives, flocking became an industrial process and could be widely used to change appearances, shapes and even physical properties. ^[126]

There were two kinds of typical flock processes: mechanical or electrostatic. Mechanical flock process was the first flocking technique, and during this process short fibres fell down and stuck onto the substrates. In order to get a better distribution of flock fibers and to fix the flock fibers better, the substrates were shaken in a vibration motion. This kind of process was not suitable for flat textile surfaces but rather for molded articles. With an electrostatic flock process, the short flock fibres were put in an electrical field and therefore charged. As known, if a particle is positive charged, it will attract to the negative electrode, a negative charged particles goes to positive electrode. When the substrates are put on counter electrodes and pre-coated with adhesive, the short fibres will fix on them, therefore we could get a three-dimensional coating. Usually in industrial field, these two techniques were combined together to make a better coating.

According to the preparation processes of flock short fibers, the materials could be classified into two kinds: milled/non-calibrated flock or cut/calibrated flock. The milled/non-calibrated flock could be made of

1 Introduction and theoretical background

natural cotton or synthetic polymer fibres and most used to imitate natural leather products. Because of the milling process, this kind of flock fibres has no universal length. The cut/calibrated flock fibers were mostly made of synthetic polymer fibres and the length of each fiber is almost the same thanks to the cutting process.

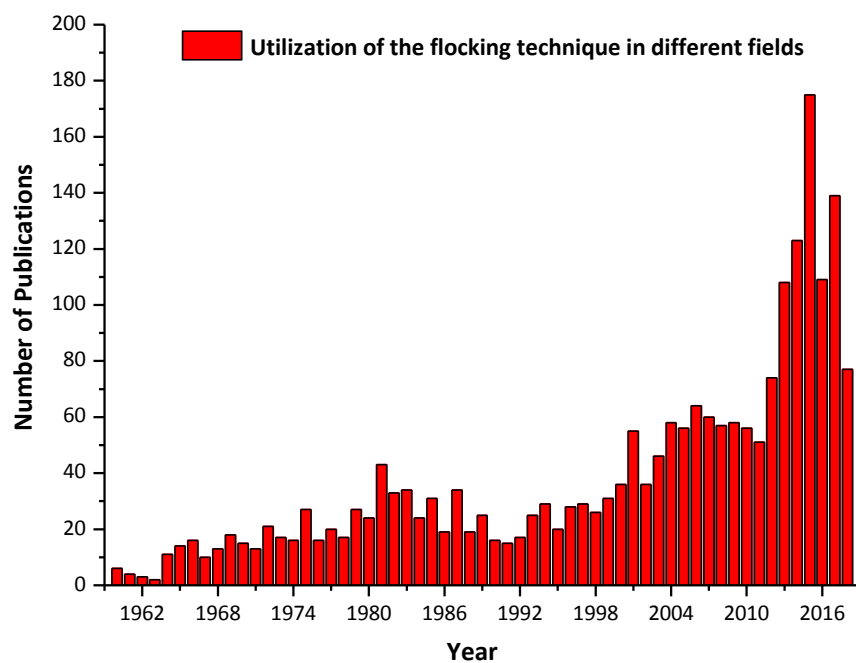


Figure 1-5. Number of publications per year concerning the utilization of the flocking technique in different fields (based on a SciFinder search on 10.08.2018 with the keyword: flocking; the number of patents is also included.)

1 Introduction and theoretical background

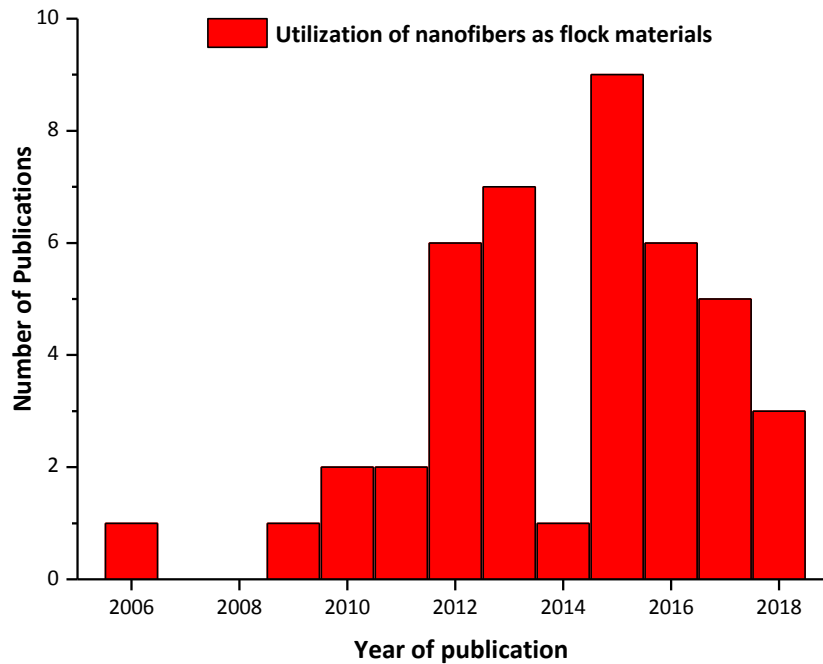


Figure 1-6. Number of publications per year concerning the utilization of nanofibers in the flocking technique (based on a SciFinder search on 10.08.2018 with the keyword: “nanofibers and flocking”; the number of patents is also included.)

If we look the flocking layer in detail, it could be considered as a three dimensional matrix with lot of air space between fibers. Therefore, it was widely studied in tissue engineering and could be applied as scaffolds.

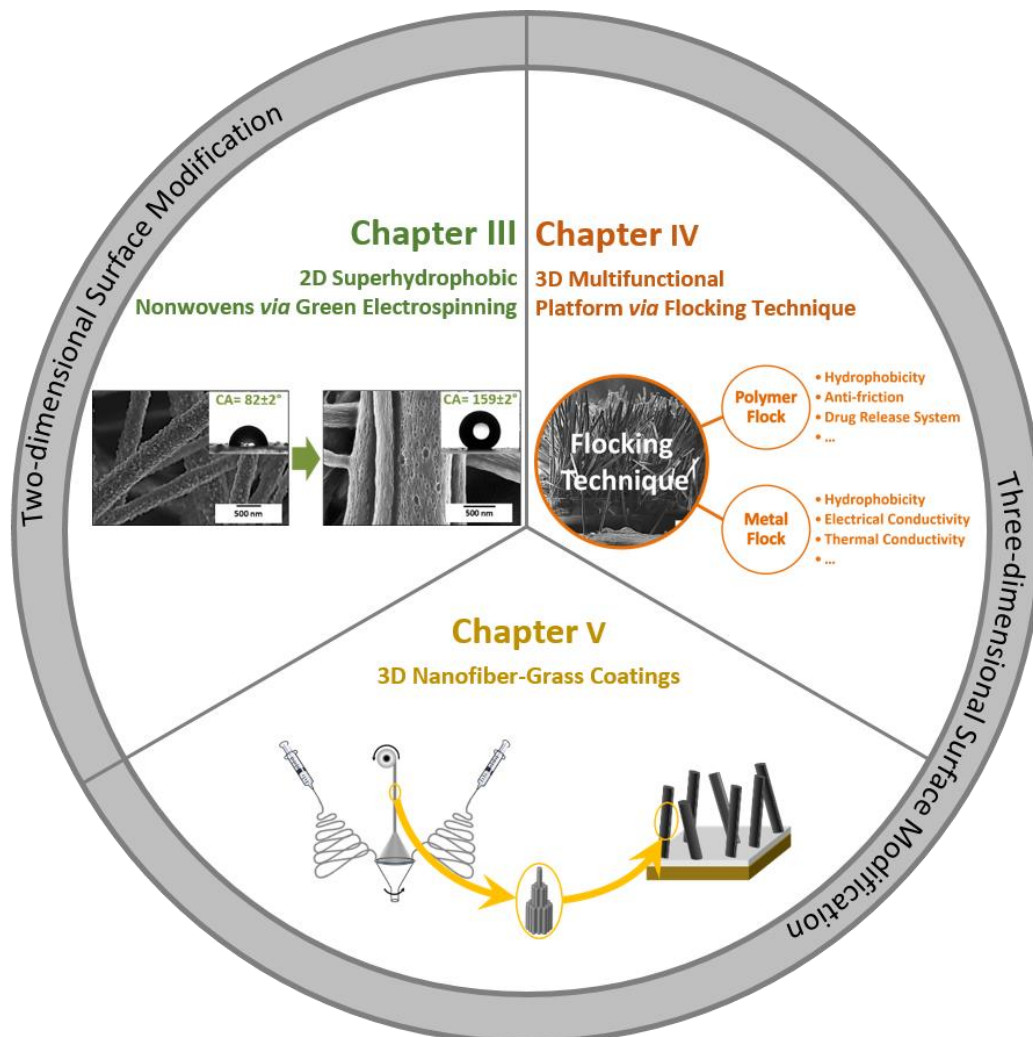
Figure 1-5 and 1-6 showed the published works since 1962 by using flocking technique to build up the scaffolds. ^[127] As comparing to scaffolds made by other methods, this technique offers higher compressive strength and also high porosity. ^[126, 128-129] The membrane of cross-linked and mineralized collagen was used as substrate and gelatin as adhesive. The pore size in flock scaffolds could be simply adjusted by changing the flocking time and those pores are higher interconnected. Walther and coworkers showed using flock technology and made highly oriented scaffolds from Polyamide 66 fibres for cartilage tissue engineering. ^[128]

They also used mineralized collagen as substrate and gelatin as adhesive. This scaffolds had high surface-to-volume ratio and made seeding and migration of cells much easier than other common scaffolds.

Besides as scaffolds for tissue engineering, this technique could also be used for other application. As is known, the design principle of a superhydrophobic surface includes two main parts: surface roughness and materials with low surface tension. With this flock technique a really rough surface could be made out of nylon-6, 6 flock fibers.^[130] The fibers were coated with poly acrylic acid and followed with perfluorooctylamine and the water contact angle changed from less than 10° to 178° . Instead of using vertical standing structure of flock fibers to create the three dimensional matrix, the aligned flock fibers could be pressed them into a film.^[131] With this process they could make fiber-reinforced polymer films with a laminate structure and improve the wear properties of this hybrid plastics.

2 Aim and Concept of the Thesis

The overall aim of the following chapters is to establish various surface modification methods, both for two-dimensional and three-dimensional structures. The two-dimensional nonwovens prepared through green electrospinning exhibits outstanding properties based on its superhydrophobicity (Chapter III). In addition, three-dimensional polymer matrixes, which are fabricated through flocking technique, show versatile functionalities (Chapter IV). Furthermore, the use of electrospun nanofibers as flocking materials for fundamental research into the preparation of more complex three-dimensional structures has been established in chapter V.



The concept of chapter III was the preparation of water-repellent nonwovens out of water dispersion by green electrospinning. The existing studies about the fabrication of superhydrophobic nonwovens *via* electrospinning are mainly out of organic solvents, which are not sustainable. In this work, a dispersion of poly(perfluorodecyl acrylate) particles was prepared through emulsion polymerization. Followed with green electrospinning of this polymer, nanofibers with rough surface morphologies were manufactured. The original nonwovens were overall hydrophilic due to their compositions. However, the nonwovens turned to superhydrophobic after the sol-gel treatment. The resulting nanofibers exhibited unique morphologies; instead of particles, numerous pores appeared on the nanofiber surfaces. This enhances the areal fraction of air inside the two-dimensional nonwovens. The nanofiber composition, parameters during electrospinning and sol-gel treatment did influence the superhydrophobicity of the nonwovens.

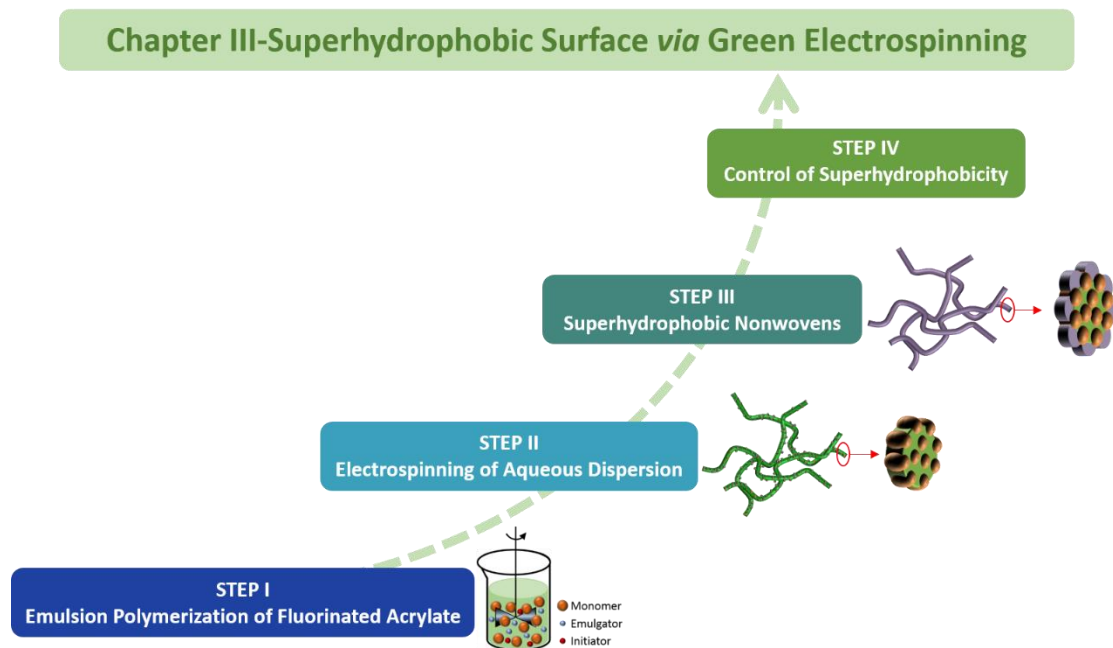


Fig. 2-1. Conceptual illustration of chapter 3: superhydrophobic surface creating by a green electrospinning process and with control of parameters the hydrophobicity could be adjusted.

Lotus leaves are known for its self-cleaning property, which is also called lotus effect. The secret of this phenomenon is at the basis of the surface morphology of lotus leaves. Lots of papillae in micrometer size rise from the surfaces, and create the roughness; meanwhile, the leaves are covered with wax-like materials, which can reduce the surface energy. In contrast to lotus leaves, the superhydrophobic nonwovens consist of numerous nanofibers, where micropores around 50 nm in diameter are found on the surface. The hierarchical structure of electrospun nanofibers and the micropores contribute to the surface roughness, both in macroscopic and microscopic scales respectively. Furthermore, the siloxane layer from sol-gel treatment reduces the surface energy. Due to the differences, we defined this kind of structure as “anti-lotus” structure.

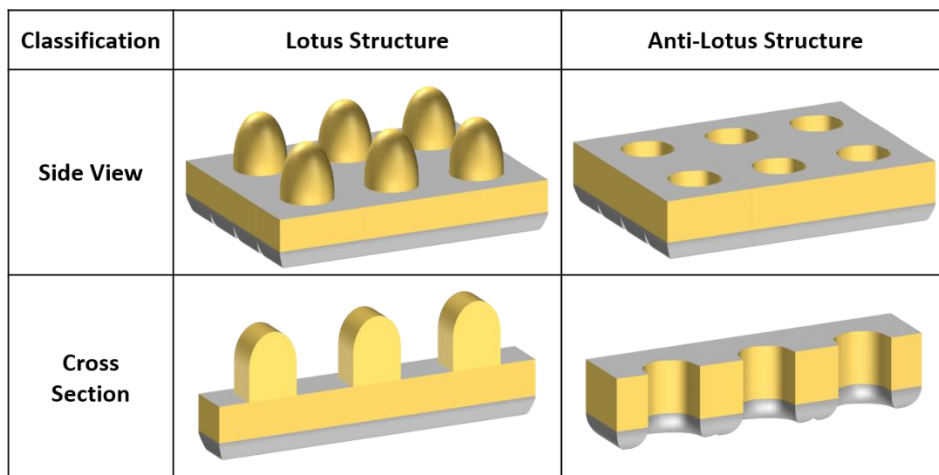


Fig. 2-2. Schematic illustration of surface morphologies of lotus structure and anti-lotus structure. *Lotus structure*: rough surface due to lots of papillae. *Anti-lotus structure*: numerous micropores, distributing along the surface, provide additionally roughness in microscopic scale. Both effects can lead to superhydrophobicity.

By virtue of the limit of a two-dimensional structure, a three-dimensional matrix can bring more advantages and can be applied in many other fields. In chapter IV, flocking technique from textile industry is the fundamental method here to create a three-dimensional polymer matrix. The resulting rough three-dimensional coating are composed of numerous fibers; in addition, there are lots of spaces between fibers, which are defined as pores for this special structure. As a consequence, the three-dimensional coating has higher porosity and higher area-to-volume ratio. According to the chapter III, the two design principles for a superhydrophobic material are high surface roughness and low surface energy. Since the three-dimensional coating is already rough, an additional hydrophobic coating is introduced into the system, to reduce the surface energy. Moreover, the roughness of the three-dimensional coating enables its anti-friction effect, and it can also be applied as a drug release system due to its high specific area. To enlarge the application possibilities, an additional copper layer is brought to the three-dimensional coatings. The resulting metal flock matrix shows good electrical and thermal conductivity. Meanwhile, the obtained metal flock matrix can be either hydrophobic or hydrophilic depending on the copper densities. Furthermore, the metal flock matrix can absorb certain wavelength, and convert the photon energy into thermal energy; therefore, it is also possible to use this matrix in the energy-harvesting facilities.

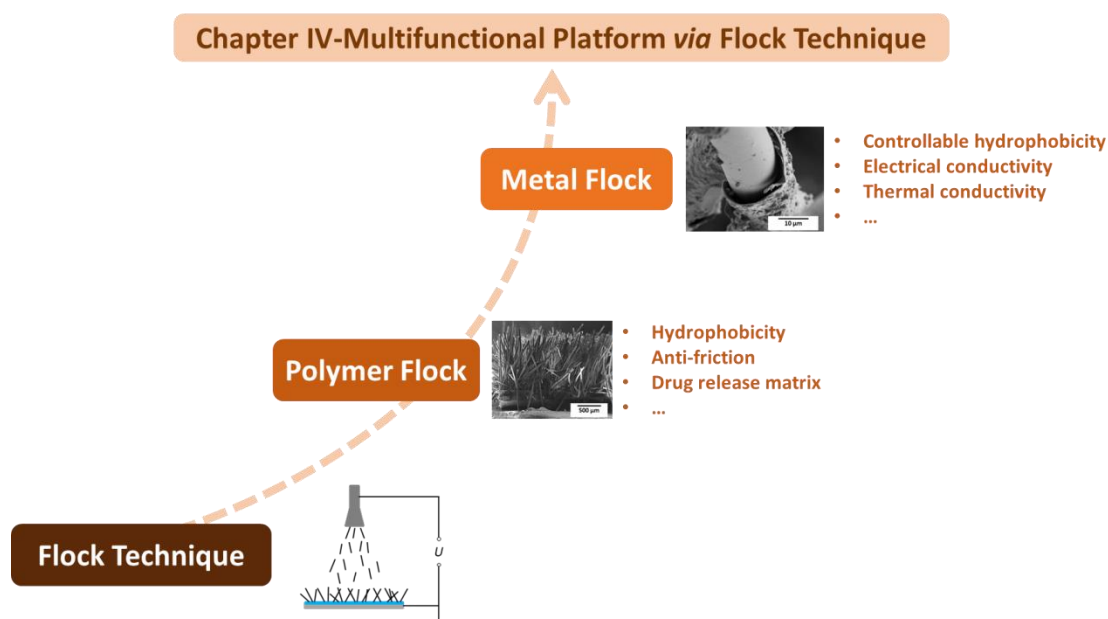


Fig. 2-3. Conceptual illustration of chapter IV: creating three dimensional polymer matrix by flocking technique and with different post treatment to build up a multifunctional platform.

Electrospinning can produce nanofibers with complex morphologies. It is of interest to combine electrospinning and flocking techniques to create a new three-dimensional coating with complex morphologies. Moreover, various polymer nanofibers can be produced by electrospinning; their different chemical properties can also introduce more applications into the three-dimensional coating systems, such as hydrophobicity, anti-bacterial property, thermal resistance, and so on. To begin with, the electrospun nanofibers are cut into short fibers with a stand mixer. However, the existing cutting methods cannot produce short fibers with a similar aspect ratio of commercial flock fibers. The only solution to reduce the aspect ratio is to increase the nanofiber thickness, which is realized by fabrication of yarn fibers. The yarn fibers, also produced by electrospinning, consist of thousands of nanofibers. Their diameters are usually in the range of several micrometers to millimeters. The endless

yarn fibers are cut into 1 mm length with different cutting models. It is studied, to use short electrospun nanofibers or yarn fibers as flock materials, in the last part of this work.

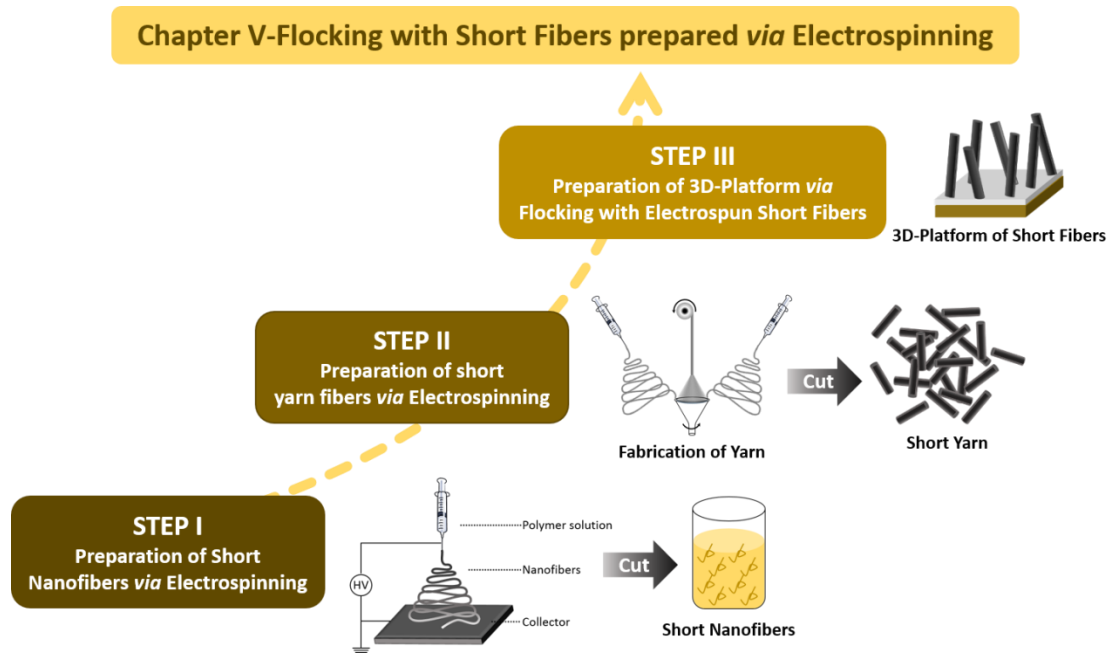


Fig. 2-4. Conceptual illustration of chapter V: combining electrospinning and flocking techniques together and create the three dimensional matrix out of electrospun short fibers.

3 Two-dimensional Superhydrophobic Nonwovens *via* Green Electrospinning

In this chapter, the preparation and characterization of superhydrophobic nonwovens are discussed. The poly (perfluorodecyl acrylate) (Poly-PFDA) is synthesized *via* emulsion polymerization. After blending with poly (vinyl alcohol) (PVA) in water, two-dimensional nonwovens could be produced by green electrospinning. The superhydrophobic nonwovens are achieved after the sol-gel treatment. The final superhydrophobicity could be controlled by changing the parameters all through the preparations.

3.1 Preparation of Poly(perfluorodecyl acrylate) *via* emulsion polymerization

3.1.1 Characterization of Poly (perfluorodecyl acrylate)

In order to realize a green preparation process, an emulsion polymerization was carried out. ^1H , ^1H , ^2H , ^2H -Perfluorodecyl acrylate (PFDA) is dispersed in a water/acetone mixture, Cetyltrimethylammonium bromide (CTAB) is the surfactant helping with the formation of Monomer-micelles. 2,2'-Azobis(2-amidinopropane) dihydrochloride (V-50) is used to initiate the reaction. The reaction is carried out at 65 °C and the chemical reaction formula is shown in **Figure 3-1_A**. Finally, a milk-like dispersion was obtained. This dispersion was stable at room temperature, and no precipitation was observable after two months. After precipitation in methanol, white solids shown in **Figure 3-1_B** were received (Sample 20130919.). The molar mass and its distribution of three different batches, they have the similar results.

3 Two-dimensional Superhydrophobic Nonwovens *via* Green Electrospinning

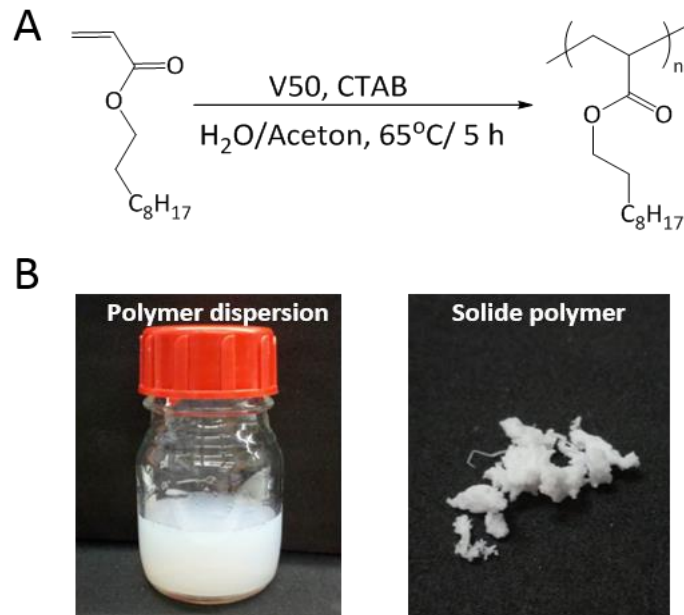


Figure 3-1. A. The chemical reaction of emulsion polymerization. B. The polymer dispersion (left) and white solid polymer after precipitation in methanol (right).

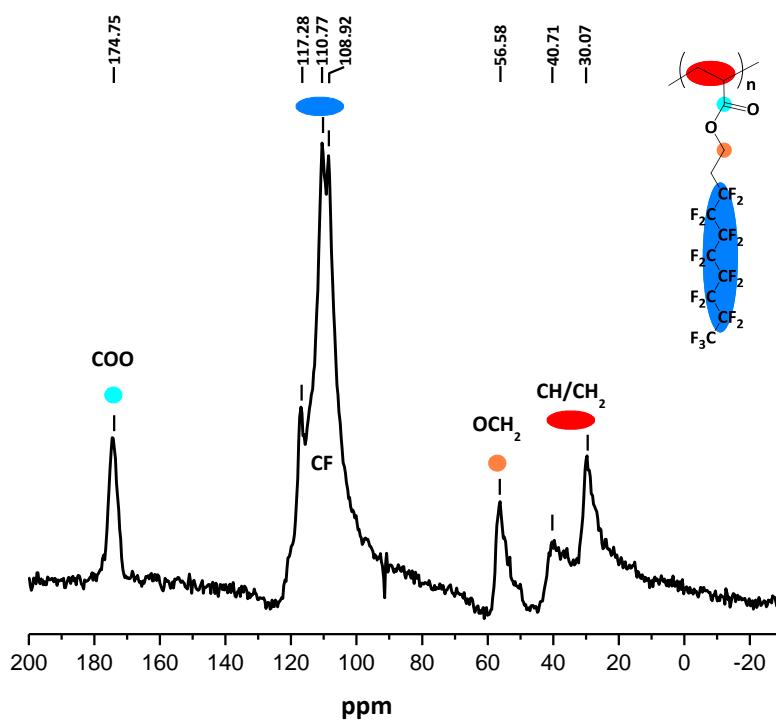


Figure 3-2. Solid-state ¹³C-NMR spectrum of Poly(perfluorodecyl acrylate). The chemical shift at 174 ppm represents for the carboxylate group in the side chain. The fluorinated side chain exhibits the chemical shift between 108 and 117 ppm.

Table 3-1. The molecular weight of Poly-PFDA in three preparation batches.

Sample	M_n^* / Da	\bar{D}	ρ / mg / mL
20130919	310,400	1.28	1.0
20131023	314,800	1.34	1.5
20131126	319,900	1.44	1.0

* The molecular weight of Poly-PFDA was measured with Hexafluoro-2-propanol (HFIP) GPC.

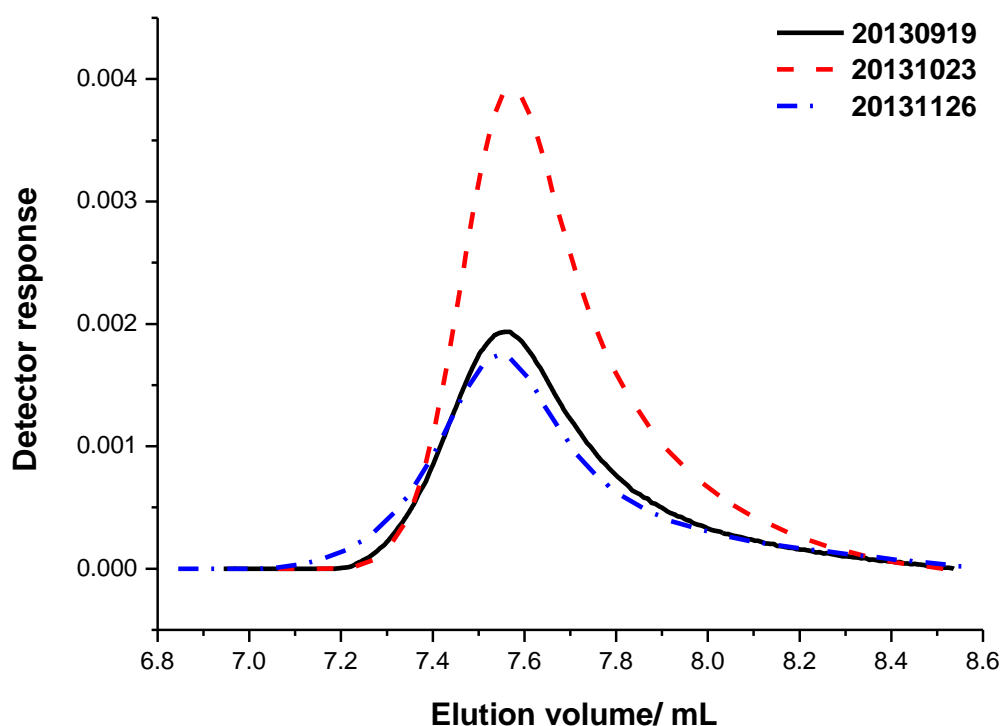


Figure 3-2. Elution curve of poly-PFDA *via* HFIP-GPC. The different height of peaks is the result of the different concentration of testing samples.

Fluorinated acrylate polymers (Poly-PFDA) from different polymerization batches also showed similar thermal behavior, which was studied *via* thermogravimetric analysis (TGA) and differential scanning calorimetry (DSC). The 5% decomposition lay around 340°C (**Figure 3-3**). The decomposition of this

3 Two-dimensional Superhydrophobic Nonwovens *via* Green Electrospinning

acrylate polymer started around 385°C. In DSC curves, the fluorinated acrylate polymer (poly-PFDA) showed a melting temperature of 76 °C and a recrystallization temperature of the side chain at 65 °C. (Figure 3-4)

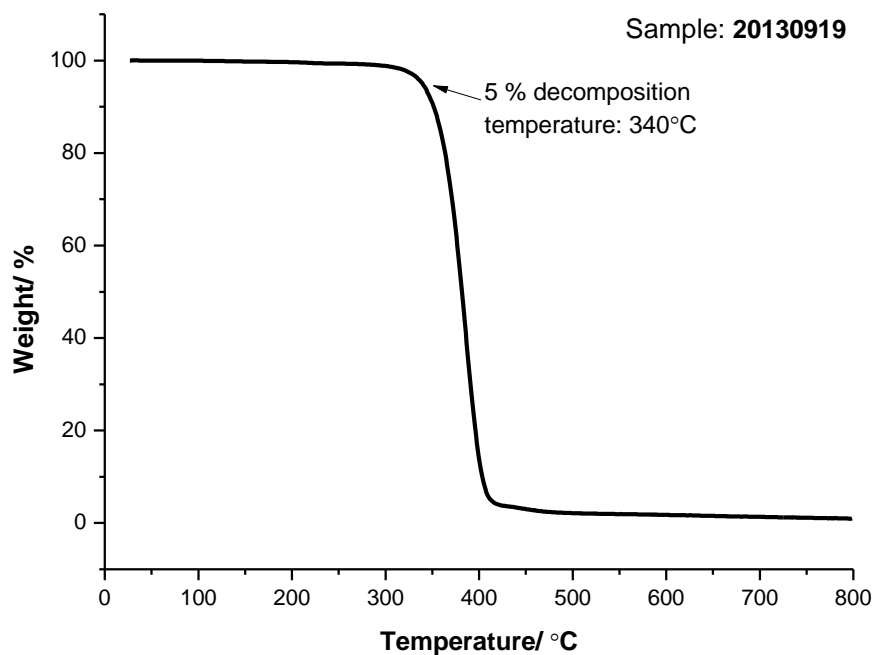


Figure 3-3. TGA curves of poly-PFDA(20130919). The 5% decomposition temperature is around 340 °C, and it decomposes from 385 °C. Polymers of other batches showed similar results.

3 Two-dimensional Superhydrophobic Nonwovens *via* Green Electrospinning

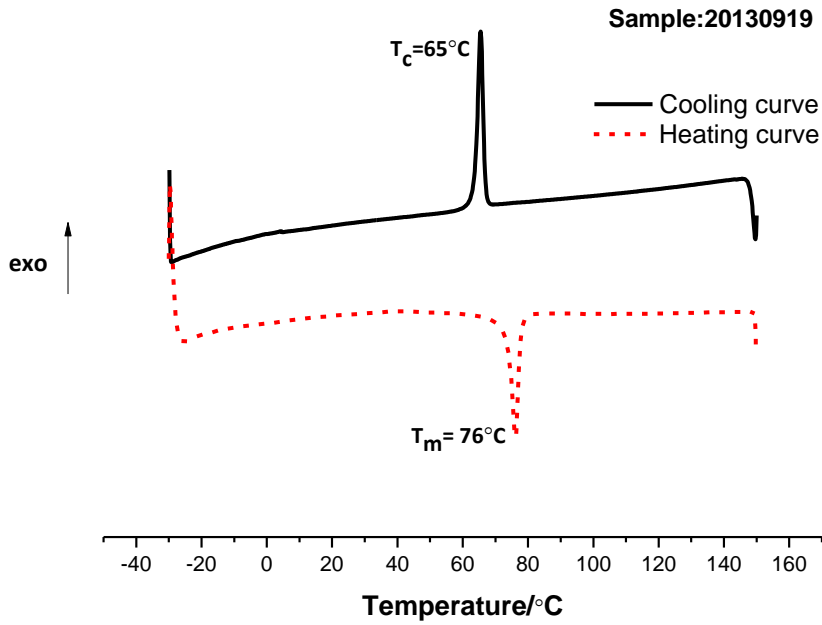


Figure3-4. DCS curves of poly-PFDA (20130919).It has a melting temperature of 76 °Cand a recrystallization temperature of 65 °C.Polymers of other batches showed similar results.

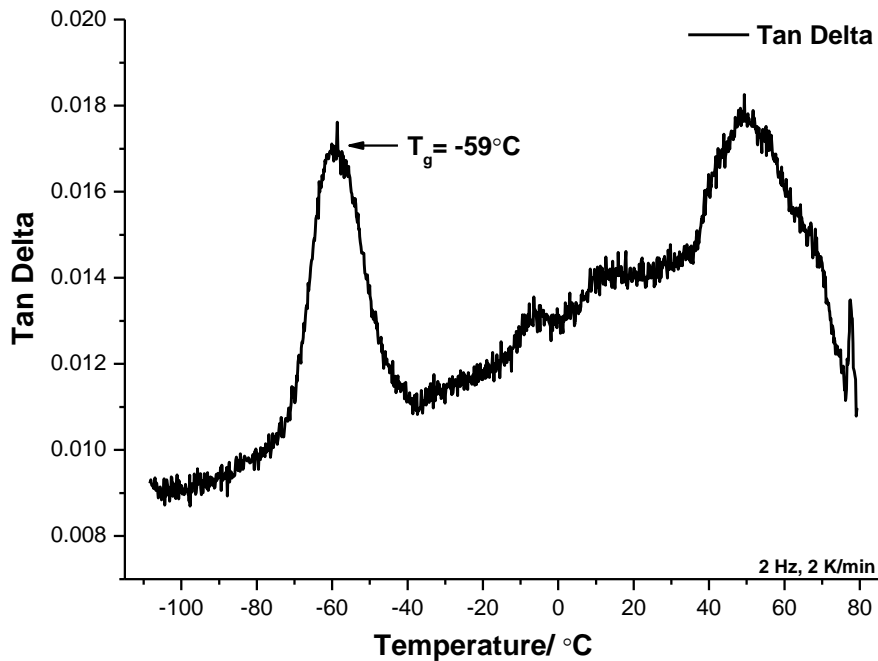


Figure 3-5. DMA curve of Poly-PFDA (Sample-20130919). It shows a glass transition temperature around -59°C.

The side chain crystallization of this fluorinated acrylate polymer in a smectic B phase is well known in the literature. ^[130-132] In order to prove its side chain crystallization behavior, small-angle X-ray scattering (SAXS) was carried out. **(Figure 3-5)** The temperature was increased from 25 °C to 80 °C and the melting process started from 55 °C. The peak intensity reduced at first slowly, and the change became obviously from 65 °C. Peaks A to D in **Figure 3-5** showed its lamella structure or crystalline form. The lamella structure was stable until the temperature higher than 75 °C. As temperature increasing distances between lamella sheets became bigger, shown through a left shift of peak E at $2\theta=18^\circ$. At 80 °C, the peak was almost disappeared by virtue of completely melting of the fluorinated acrylate polymer.

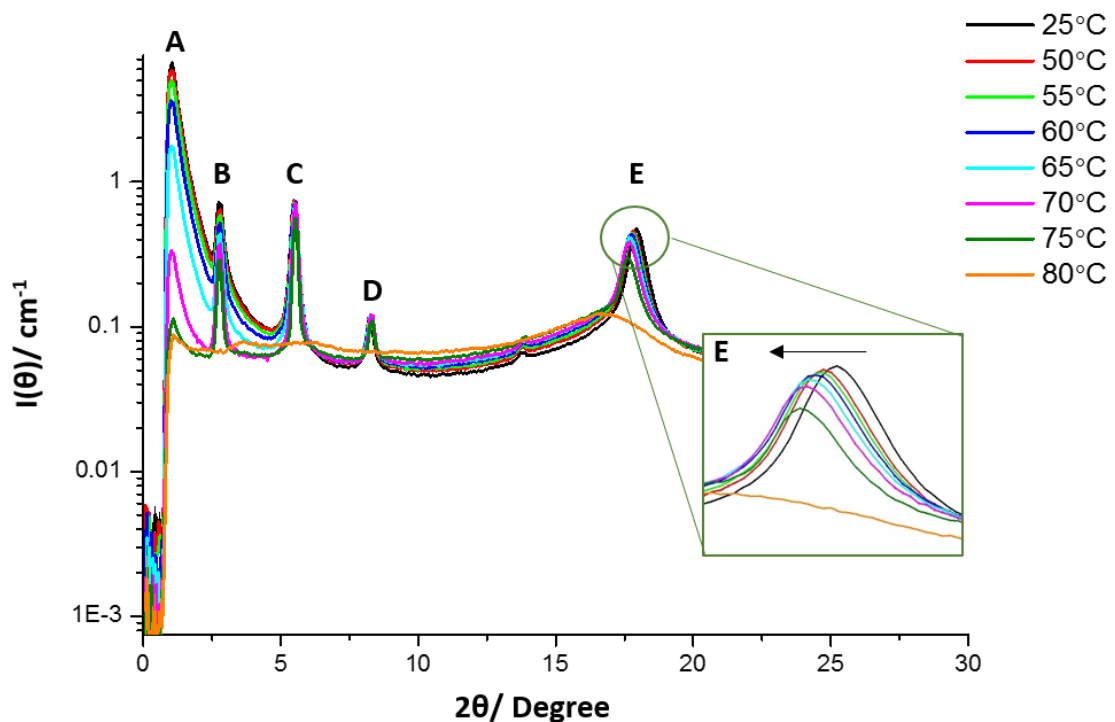


Figure 3-5. Proof of side chain crystallization *via* SAXS.

3.1.2 Influence of existence of acetone during emulsion polymerization on polymer particle dispersion

In an emulsion polymerization, the monomers are not soluble in water. Instead, with the help of surfactants, they are dissolved in micelles. Meanwhile, acetone is added as the co-solvent during the emulsion polymerization. In order to find out the influence of acetone on the polymerization, a comparable experiment is carried out, where no acetone was added into the starting materials. The remaining reaction conditions were kept the same as for the previous reaction.

3.1.1.1 Influence of existence of acetone on emulsion polymerization

Firstly, yields and total solid concentrations of the two systems are different. **Figure 3-6** showed TGA curves of dispersions with different processes. The total solid concentrations (TSC) of the first three dispersions are in **Table 3-2** were all around 32% and the yields are more than 85%. In contrast, the polymerization without acetone (Sample- 201312317) has a much lower yield of 36%, while the TSC is 22%.

Table 3-2. Samples with different preparation processes.

Sample	Polymerization with Acetone
20130919	Yes
20131023	Yes
20131126	Yes
20131217	No

3 Two-dimensional Superhydrophobic Nonwovens *via* Green Electrospinning

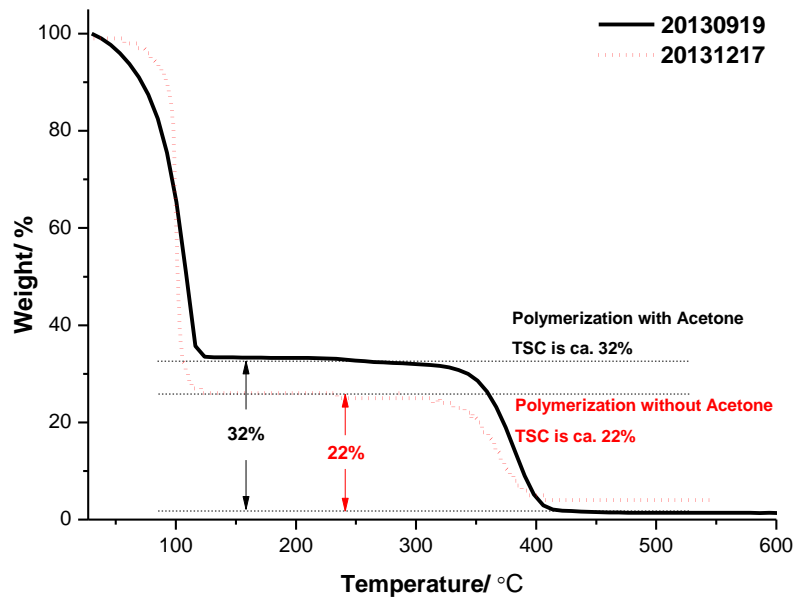


Figure 3-6. Total solid concentration (TSC) of polymer dispersions, measured *via* TGA.

Secondly, the stability of the dispersions is different. The dispersions produced with acetone during polymerization were quite stable at least for two months, while white solids precipitated after three days for the one without acetone in the reaction mixture. (**Figure 3-7**)

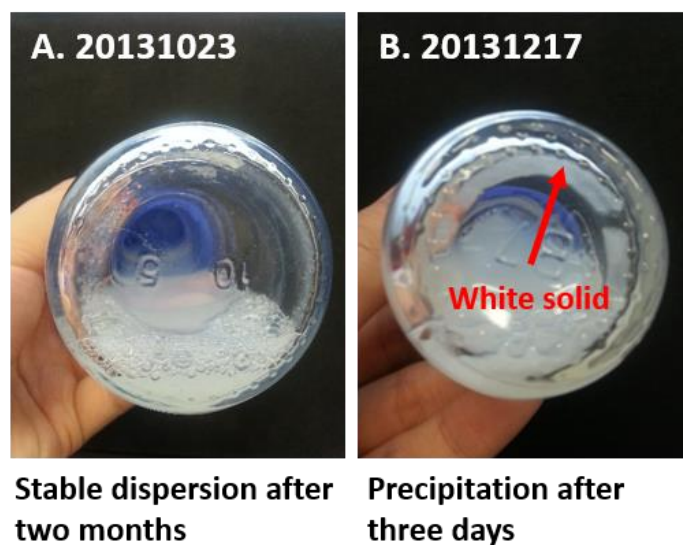


Figure 3-7. Different stability of polymer dispersions: Polymerization with acetone (A) and without acetone (B).

3.1.1.2 Influence of existence of acetone on particles size

The influence of acetone on particle size distribution was also studied both in dispersion with dynamic light scattering (DLS) and in solid state with scanning electron microscope (SEM). Polymer particles synthesized with acetone during emulsion polymerization (**Figure 3-8_A**) have a diameter of around 90 nm. However, the absence of acetone led to larger particles with a diameter of 100 nm. (**Table 3-3**) The fluorinated polymer particles were stable and kept their forms both in solution or in the solid-state.

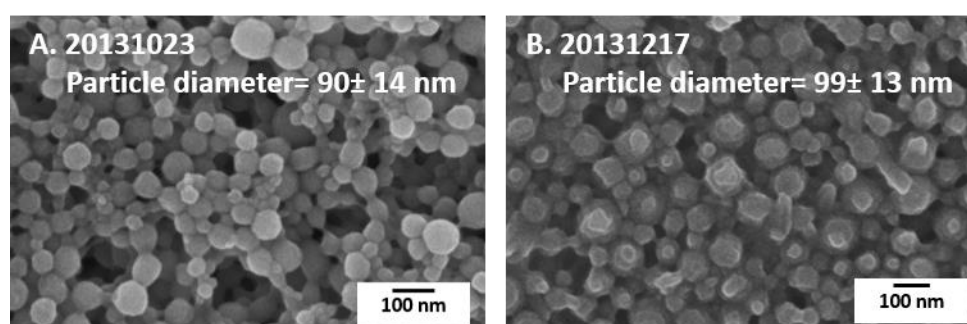


Figure 3-8. SEM images of particles in dry states. Sample 20131023 is polymerized with acetone (A); Sample 20131217 is polymerized without acetone (B).

Table 3-3. Polymer particle diameters with different preparation processes.

Sample Name	Diameter <i>via</i> DLS	Diameter <i>via</i> SEM
20131023	89.4±0.4 nm	90±14 nm
20131217	104±0.2 nm	99±13 nm

3.1.1.3 Influence of existence of acetone on electrospinning solution

As the stability of initial systems was quite different, **Figure3-9** showed the electrospun fibers fabricated with different initial polymer dispersions. The electrospun solution is composed of PVA and fluorinated acrylate polymer dispersions. The weight ratio of PVA and poly-PFDA was 83:17. On the basis of stable and homogenous acrylate polymer particle dispersion, the spin solution is

3 Two-dimensional Superhydrophobic Nonwovens *via* Green Electrospinning

also homogenous with acetone during polymerization (**Figure 3-9_A**). Nanofibers have a diameter of around 448 ± 83 nm and many particles are found on the nanofibers. In contrast, the absence of acetone during polymerization led to unstable polymer dispersion; therefore, the mixture was not homogenous (**Figure 3-9_B**). In this case, only thin nanofibers with a diameter of 263 ± 62 nm could be produced. The morphology of nanofibers is relatively flat; and due to the inhomogeneity of the spin solution, lots of beads were found within thin nanofibers.

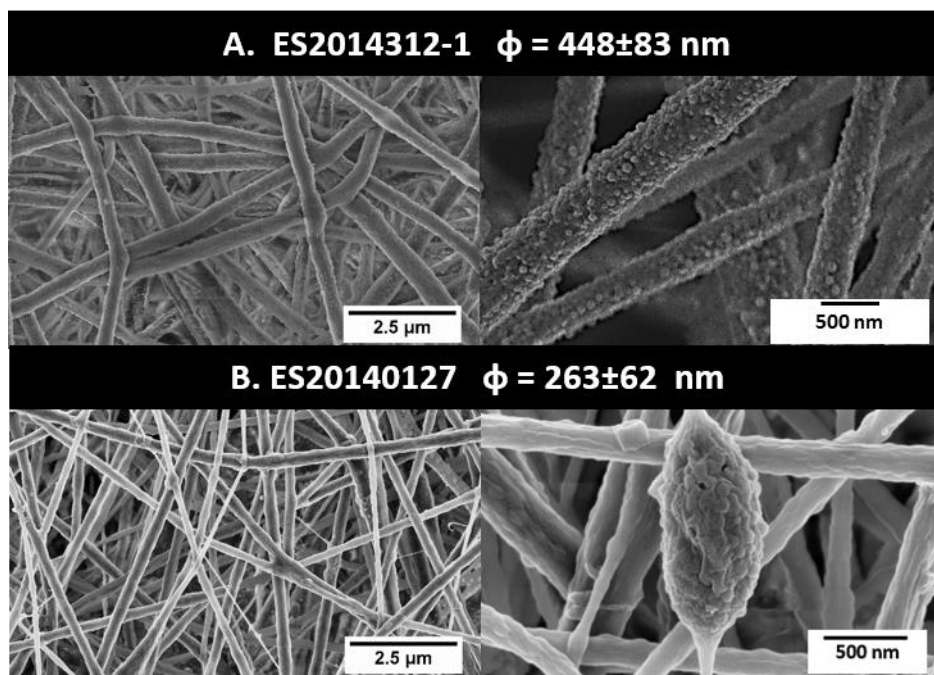


Figure 3-9. SEM images of as-spun nanofibers produced with different initial polymer dispersions. Meanwhile, they showed different fiber morphology.

3.2 Preparation and Characterization of superhydrophobic nonwovens *via* green electrospinning

3.2.1 Preparation of as-spun nanofibers and superhydrophobic nonwovens

To ensure the green electrospinning process, acetone was removed before making the spin solution and the reduced weight was balanced with the addition of distilled water. DLS measurements were carried out to determine the particle size before and after removal of acetone. As shown in **Figure 3-10**, the diameters of particles don't change within a measurement mistake and maintained around 90 nm.

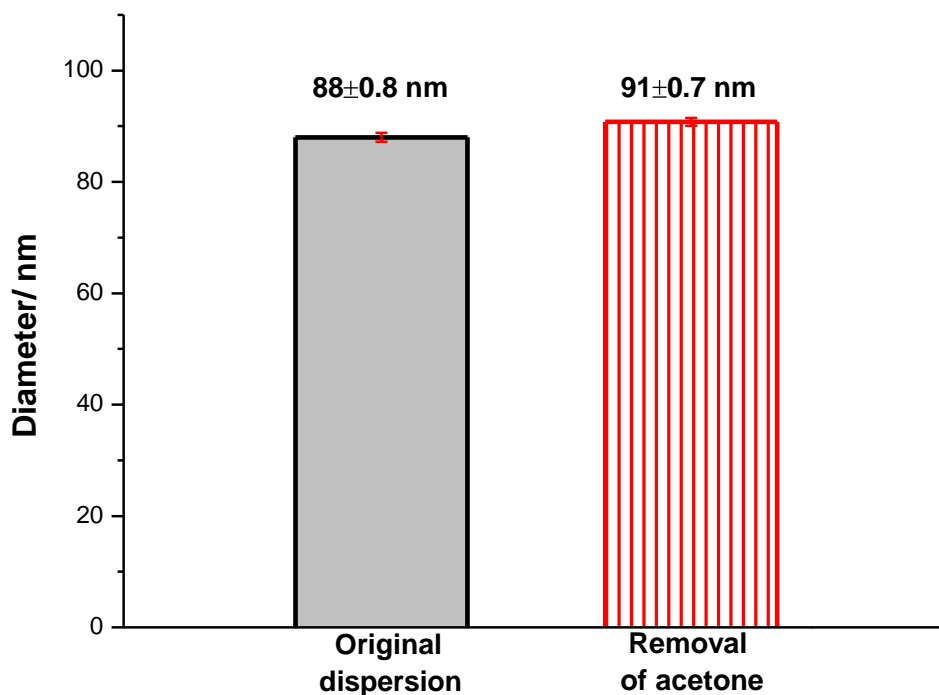


Figure 3-10. Diameter distribution of poly-PFDA particles before and after the removal of acetone *via* DLS.

3 Two-dimensional Superhydrophobic Nonwovens *via* Green Electrospinning

With only the acrylate polymer particle dispersion, nanofiber formation is impossible during electrospinning, as the viscosity is not enough. Therefore, PVA was added into the dispersion to improve the viscosity of the electrospinning solution. **Figure 3-11** showed the absorption peaks of polymer dispersion and electrospinning solution in the IR-spectroscopy. The absorption peak at around 3250 cm^{-1} represents for PVA. The C=O bond in fluorinated acrylate polymer showed a typical absorption peak at 1737 cm^{-1} . The peak at around 1200 cm^{-1} represents the CF_3 -group in the fluoride side chains; meanwhile, $\text{CF}_2\text{-CF}_3$ bonds exhibit the absorption at 1144 cm^{-1} .

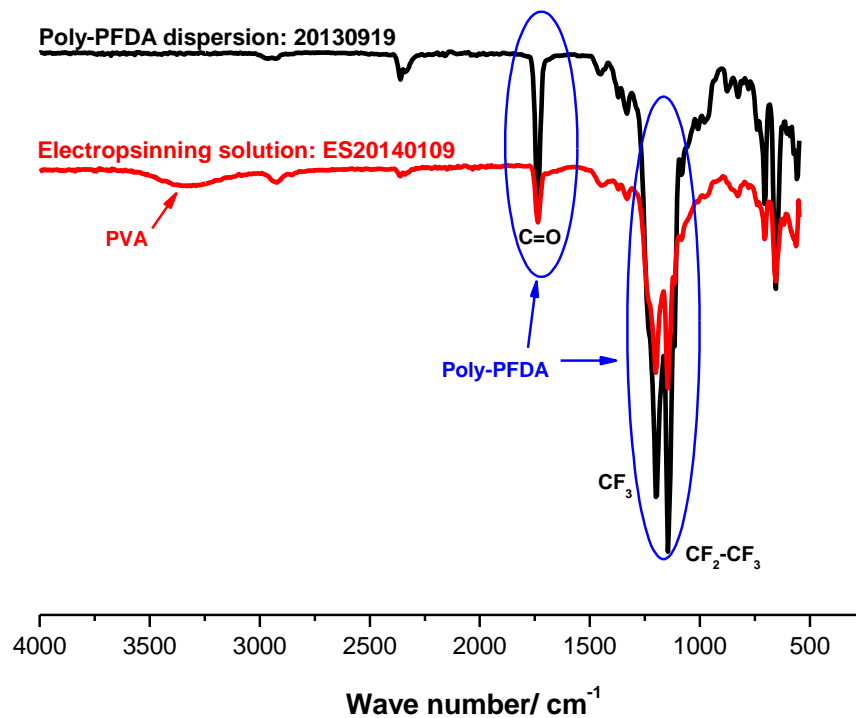


Figure 3-11. IR-spectroscopy of poly (perfluorodecyl acrylate) dispersion and electrospinning solution.

3 Two-dimensional Superhydrophobic Nonwovens *via* Green Electrospinning

Table 3-3. Compositions of different electrospinning solutions.

Sample	Poly-PFDA dispersion*	[PVA]/ wt%	Poly-PFDA: PVA (wt ratio)
ES20131025	20130919	4.1	83:17
ES20131127-1		3	50:50
ES20131127-2		3	73:27
ES20131130		3.7	83:17
ES20140109		3	87:13
ES20140127	20131217	3.6	87:13
ES20140312-1	20131023	3.5	87:13
ES20140312-2		4	87:13

* All the initial poly-PFDA dispersions are made with acetone during polymerization.

The electrospun nanofibers form two-dimensional nonwovens; after coating with siloxane (Sol-Gel treatment), a superhydrophobic surface is prepared. The process is showed in **Figure 3-12**.

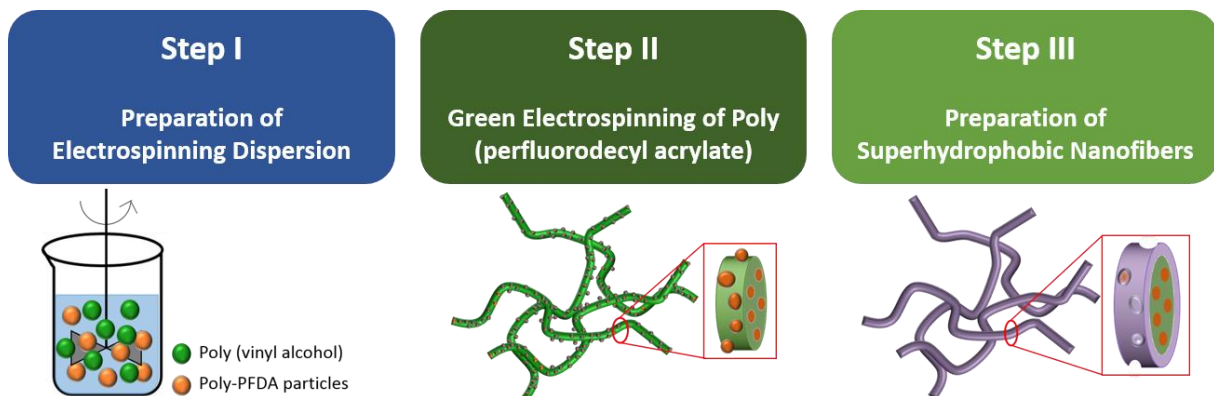


Figure 3-12. Schematically illustration of fabrication of superhydrophobic nonwovens

3 Two-dimensional Superhydrophobic Nonwovens *via* Green Electrospinning

As shown in the chapter 1, the key of creating a superhydrophobic surface is the proper combination of high roughness and low surface energy. Due to the formation of randomly oriented hierarchical structures with the electrospun nanofibers, a high surface roughness was obtained within the process. Due to the high concentration of PVA, the initial nonwovens were still hydrophilic. In order to make these nonwovens superhydrophobic, the surface was treated with the sol-gel process. This method is a wet-chemical technique, which is used for the preparation of glassy and ceramic materials. ^[134] In this work, sol-gel treatment is used to introduce siloxane layers onto nonwovens, and to reduce the surface energy. The resulted nonwovens exhibited superhydrophobicity.

(Figure 3-13)

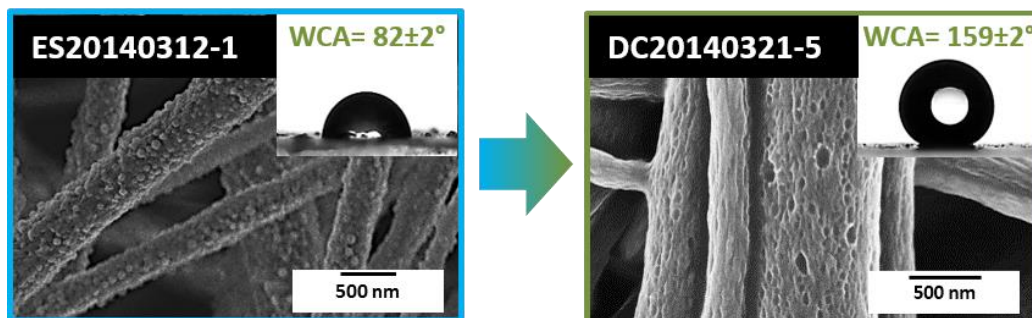
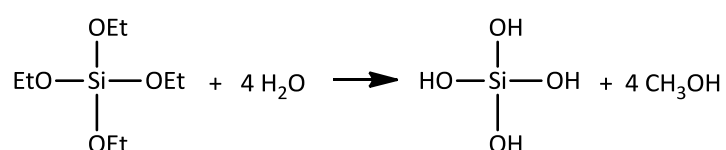


Figure 3-13. SEM images of original nanofibers (left) and treated nanofibers (right).

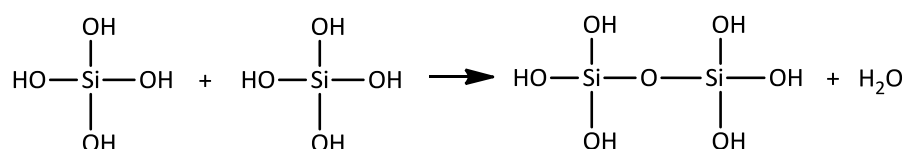
During the sol-gel treatment, hydrolysis and condensation reaction takes place simultaneously. Colloidal particles are synthesized and form the colloidal solution (Sol). This “Sol” is also the precursor to form the integrated network (Gel), which consists of either discrete particles or a polymer network depending on different chemical conditions. ^[135] Usually, metal alkoxides are used as the precursors due to their reactivity with water. The most widely used material is alkoxysilanes, such as tetraethoxysilane (TEOS) and tetramethoxysilane (TMOS). The hydrolysis and condensation take place simultaneously in the liquid. TEOS

hydrolyzes for example in water at first and then hydrated silica tetrahedral are formed, which interact in a condensation reaction, and eventually establish a network of silicon. At numerous reaction sites within the solution, sufficient Si-O-Si bonds are formed, which leads to the formation of colloidal particles. As colloidal particles and silica species gather, a three-dimensional network “Gel” is formed. With control of hydrolysis and condensation, the gel could be either discrete colloidal particles or a polymer network. The reactions are shown below.

Hydrolysis:



Condensation:



As shown in **Figure 3-14**, the as-spun nonwovens have a hydrophilic surface because of PVA in the nanofibers. When a water droplet was put on this surface, it penetrated into the nonwovens and wet the surface. However, siloxane-coated nonwovens showed a high contact angle up to 160°, and the roll-off angle was less than 10°. A water droplet could make multiple jumps on this surface and then rolled away.

3 Two-dimensional Superhydrophobic Nonwovens *via* Green Electrospinning

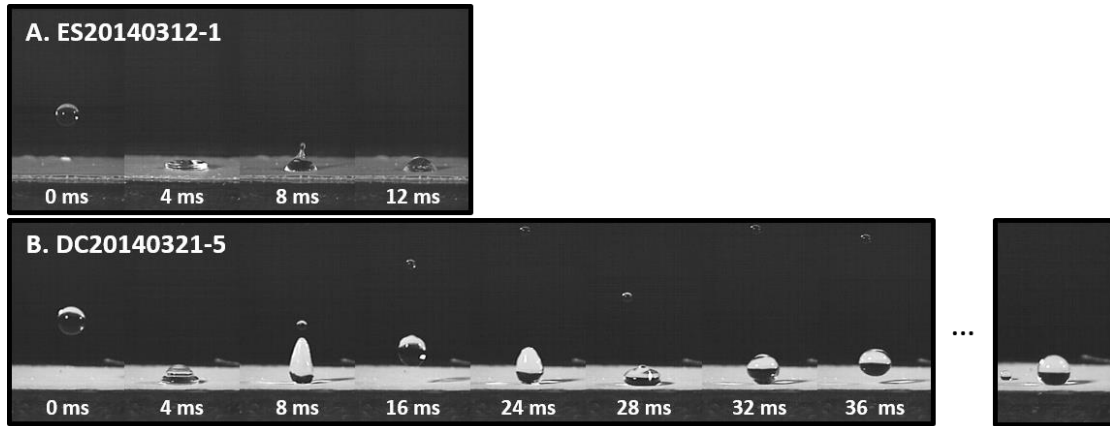


Figure 3-14. Different behaviors of a water droplet on as-spun (A) and siloxane-coated (B) nonwovens.

Figure 3-15 showed the self-cleaning property of this superhydrophobic nonwovens, where ketchup acted as the pollution. With pouring distilled water to nonwovens, the superhydrophobic surface remains clean and no macroscopic damage was observed.

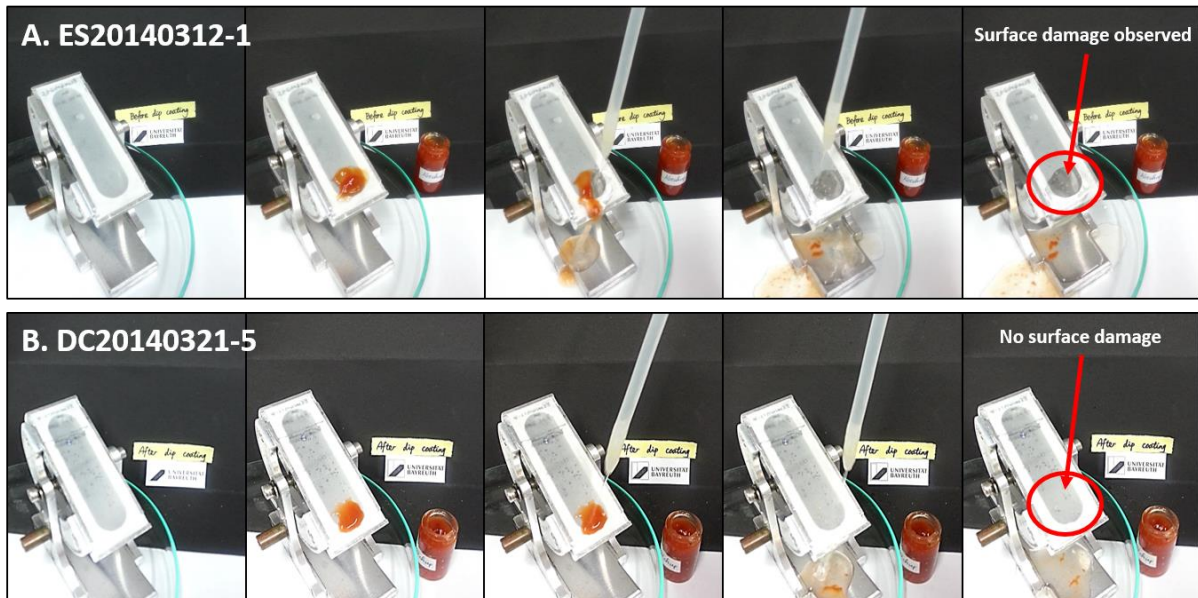


Figure 3-15. Surface damage after water washing on as-spun fibers (A) and self-cleaning properties of siloxane-coated nonwovens(B).

3.2.2 Characterization of as-spun and superhydrophobic nonwovens

3.2.2.1 Influence of existence of acetone during polymerization on superhydrophobicity

As discussed above, the existence of acetone is important to make a stable homogenous polymer dispersion. It also influenced electrospun fibers and their properties.

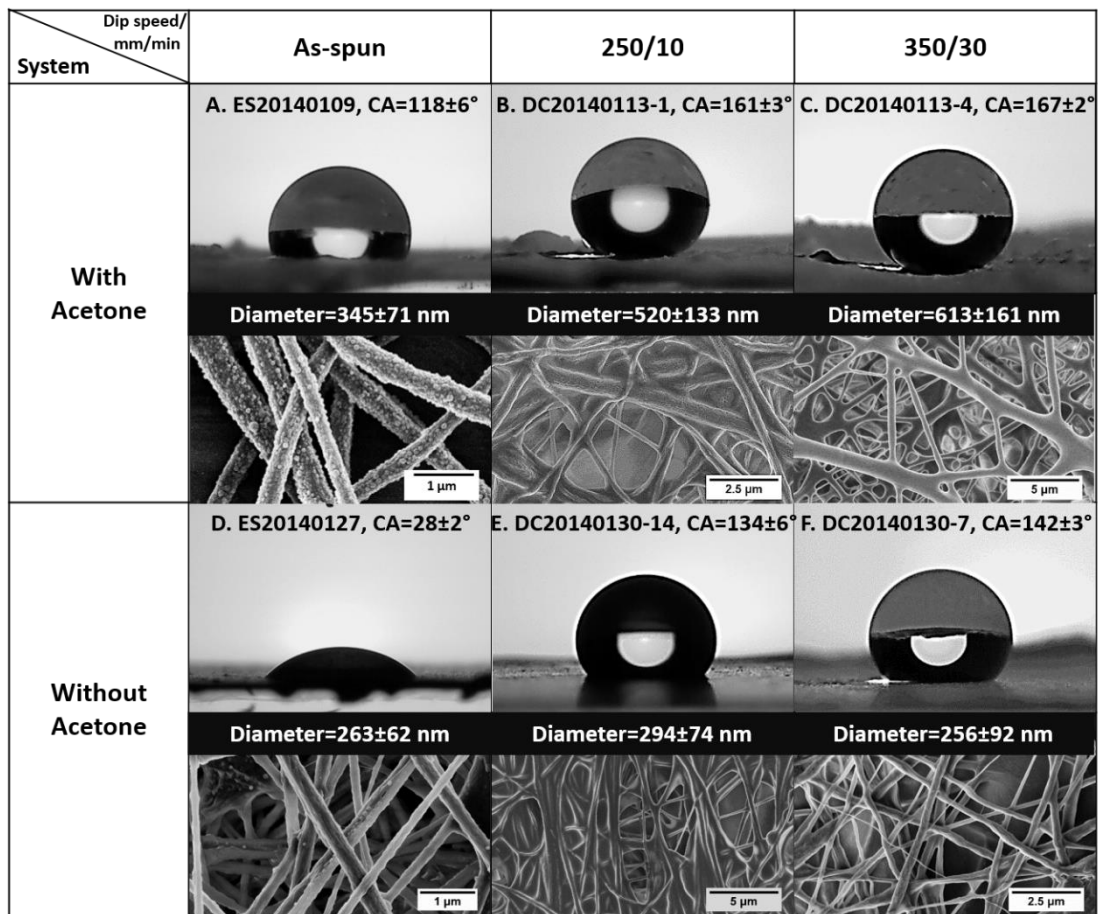


Figure 3-16. Contact angles and nanofiber morphologies of different samples

Nonwovens, fabricated from acrylate particle dispersion with acetone during polymerization (**Figure 3-16_A**), had a much higher water contact angle (118±6°) as compared to sample D (28±2°). After sol-gel treatment, the contact angle increased to more than 160° (**Figure 3-16_B** and **C**). For the system without

acetone during polymerization, the contact angles of nonwovens after coating with siloxane were only around 140° (**Figure 3-16_E** and **F**).

As already discussed the roughness has a high influence on the hydrophobicity. Hence, the differences in the fibre morphologies, achieved with the different electrospinning solutions, could explain this behavior. Firstly, nanofibers of **Figure 3-16_A** were much thicker; secondly, there were lots of particles along their fiber surfaces. For sample D, the nanofibers were smooth and almost no particles could be observed on the fiber surface. Thirdly, siloxane-coated nanofibers had numerous pores (**Figure 3-16_B**). In contrast, films were formed between the thinner nanofibers in sample E. Therefore, the areal fraction of air is strongly reduced, and leads to the lower contact angles.

3.2.3 Influence of Polymer/PVA ratio on superhydrophobicity of nonwovens

The composition of electrospinning solutions is the main factor to decide the nanofiber diameter and its morphologies. Electrospinning solution consists of a dispersion of polymer particles and PVA. If the amount of either of these polymer parts is varied, the morphology and properties of the electrospun nanofibers change as well.

Particles in different electrospinning solutions are determined with DLS (**Figure 3-17**). Take ES20131025 and ES20131030 as examples, they had the same polymer weight ratios and different concentrations. When the concentration of PVA is 4.1 wt%, the particles had a diameter of 327 ± 1.3 nm. Diluted the solution to a lower PVA concentration of 3.7 wt%, smaller particles with a diameter of 273 ± 1.3 nm were found. Samples ES20131127-1 and ES20131127-2 had the same PVA concentration of 3 wt%, and their polymer ratios are different. ES20131127-2 had much higher PVA ratio in the mixture (50%). The particles in

this solution were, therefore, larger than ES20131127-1. In summary, increasing PVA amount in the mixture led larger particles in the electrospinning solution.

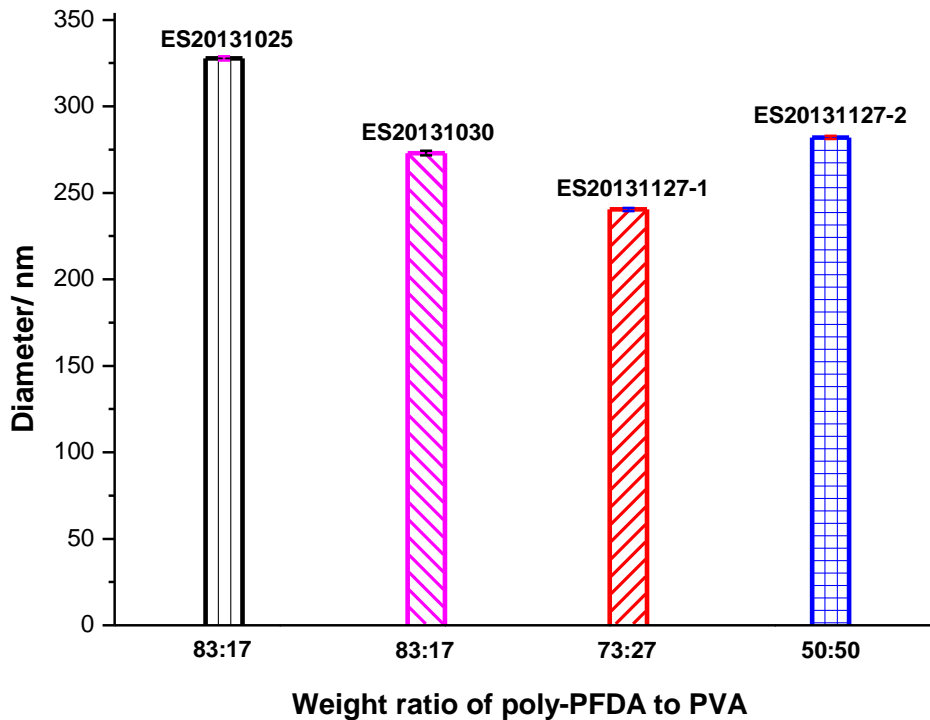


Figure 3-17. Particles in electrospinning solutions with different compositions: higher PVA amount in the mixture led larger particles in the electrospinning solutions.

The solution was placed in a syringe with a flattened needle tip. The syringe was connected to a liquid pump to enable a constant flow rate. The solution will form a Taylor cone at the needle tip; under high voltage between electrodes, the Taylor cone is charged. As the stretch force is larger than the surface tension of the solution, a jet of the polymer solution was emitted and formed thin fibers.^[90]

Table 3-3 shows the different parameters used during electrospinning experiments.

Table 3-3. Electrospinning parameters for different samples.

Sample	Poly-PFDA:PVA	[PVA]/ wt%	Voltage/ kV	Flow rate/ mL/h	Relative humidity/ %
ES20131127-1	50:50	3	30	0.66	15
ES20131127-2	73:27	3	30	0.66	22
ES20140109	83:17	3	30	0.66	19-22
ES20140312-1		3.5	31	0.93	17-22
ES20140312-2		4	24	1.54	19

Due to the composition of the electrospinning solution, the PVA is dominant in the polymer blend. Therefore, the nanofibers consist mainly of PVA. The poly-PFDA particles are distributed along the PVA matrix. Different compositions led to different fiber thickness and morphologies, and they also influenced the hydrophobicity of the resulted nonwovens. Samples A, B and C in **Figure 3-18** had the same PVA concentration (3 wt %). However, the Polymer ratios were different. With higher PVA proportion in the polymer mixture, the fibers were thinner; meanwhile, there were more beads inside the fibers. Keeping the weight ratio of Poly-PFDA to PVA constant (83:17) and increased the concentrations of PVA, the as-spun nanofibers became thicker with increased PFDA amount. Meanwhile, more particles were located on the fiber surface.

3 Two-dimensional Superhydrophobic Nonwovens *via* Green Electrospinning

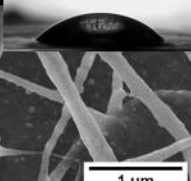
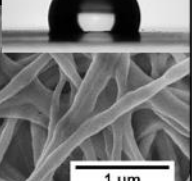
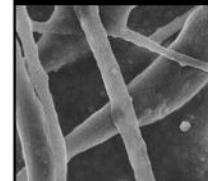
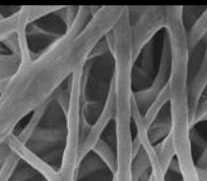
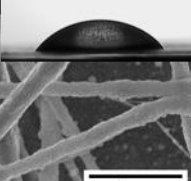
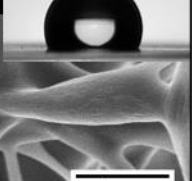
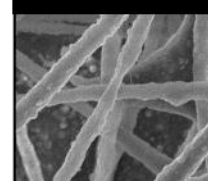
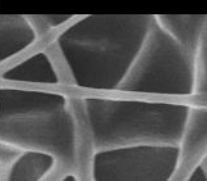
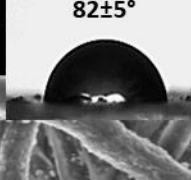
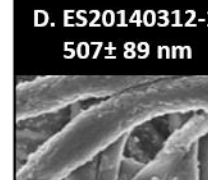
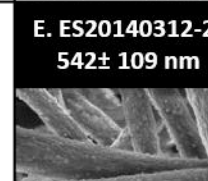
Poly-PFDA:PVA	[PVA] wt. %	As-spun nonwovens		Treated nonwovens	
50:50	3	A. ES20131127-1 137±38 nm	48±1° 	F. DC20140109-8 167±35 nm	138±3° 
					
73:27	3	B. ES20131127-2 207±24 nm	43±1° 	G. DC20140109-7 202±65 nm	136±2° 
					
83:17	3	C. ES20140109 345±71 nm	118±6° 	H. DC20140113-1 502±133 nm	161±3° 
					
	3.5	D. ES20140312-1 507± 89 nm	82±5° 	I. DC20140321-6 562±110 nm	159±2° 
					
4	E. ES20140312-2 542± 109 nm	49±1° 	J. DC20140321-5 583±134 nm	162±1° 	
					

Figure 3-18. Compositions of electrospinning solutions influence the nanofiber morphologies and the hydrophobicity of nonwovens significantly.

To determine the hydrophobicity, the contact angle of water was measured for each sample. Poly-PFDA has a lower surface energy compared to PVA; therefore,

the contact angle increased with the higher amount of poly-PFDA in the electrospinning solution. With the change of the nanofiber composition, the hydrophobicity of the nonwovens changed as well. Sample C in **Figure 3-18** had a lower amount of PVA than D and E; therefore, its contact angle was the highest at $118\pm 6^\circ$. When the PVA amount was increased up to 4 wt% in the solution, the water contact angle decreased down to 49° . (**Figure 3-18_E**)

The as-spun nanofibers were either smooth or have numerous particles on their surfaces. After sol-gel treatment, their morphologies changed enormously. The as-spun nanofibers in **Figure 3-18_A** and **B** are much thinner. The space between each single fibers disappeared after coating with siloxane; meanwhile, lots of films between nanofibers were formed. Due to a higher amount of PVA in D and E compared to C, the as-spun nanofibers are much thicker. No films were observed after coating. Although sample C have much thinner nanofibers, the fiber morphology of treated nonwovens is similar to the other two samples: particles are covered with siloxane layers, and numerous pores are formed on the fiber surfaces.

Silica and Fluor are typical materials with low surface energy. After sol-gel treatment, these two different components were combined in the hybrid material, which showed unique nanofiber morphology. The treated nonwovens could be considered as a heterogeneous surface, which was composed of air and fibers. According to Cassie-Baxter's wetting model, the contact angle on the heterogeneous surface could be calculated by equation 3 ^[61]

$$\cos \theta = f_1 \cdot \cos \theta_1 + f_2 \cdot \cos \theta_2 \dots \dots \dots (3)$$

where f_1 and f_2 are the areal fraction of two materials, $f_1+f_2=1$; θ_1 and θ_2 represent for the contact angle of each pure material to water. θ_1 is $95\pm 3^\circ$ for a pure siloxane film, and θ_2 is 180° for air. θ is the water contact angle on the

heterogeneous surface. So that the area of air pocket on fibers could be calculated. The results showed in **Table 3-4**. The samples with a higher areal fraction of air in nonwovens exhibited higher contact angles.

Table 3-4. Areal fractions of air pockets along and between nanofibers.

PVA/ wt%	Dip speed/ mm/min *	Fiber diameter/ nm	Contact angle/ Degree	Pore size/ nm	Air fraction / %**
4.0	250-10	583±134	162±1	53±15	94.6
	350-10	592±114	156±2	54±12	90.5
3.5	250-10	562±110	159±1	53±12	92.8
	350-10	501±89	161±4	55±15	94.1

* Dip speed 250-10 mm/min describes the immersion speed of 250 mm/min and a lift-up speed is 10 mm/min. The same explanation for 350-10.

** Air fraction is calculated by equation 3.

3.2.4 Influence of thermal behavior of fluorinated acrylate polymer on the hydrophobicity of nonwovens

In comparison with as-spun nanofibers, the siloxane-coated nanofibers were covered with pores (Diameter was approximately 55 nm). As discussed above, electrospinning builds up the hierarchical structures of nonwovens, which comprise their macroscopic roughness. Additionally, the formation of small pores along the fibers offered a microscopic scale of roughness. In fact, the siloxane layer is one of the essential elements for the formation of pores, and this is one of its roles. Another important function of siloxane layers is to prevent poly-FPDA particles from melting at a higher temperature. After the sol-gel treatment, siloxane-coated nonwovens were cured at 85°C, which was higher

than the melting temperature of poly-PFDA (approximate 75°C). It is clear to observe, that the coated nanofibers still maintained their high roughness, indicating that the poly-PFDA particles preserved their spherical structures over their melting temperature. Diverse coating procedures should have a strong effect on the nanofiber morphologies and the hydrophobicity of the resulted nonwovens. The siloxane coating process could be carried out on three different routes: standard coating (Route I), coating with a diluted solution (Route II), pre-cure and post-coat (Route III).

In Route I, as-spun nanofibers undergo a standard coating procedure. It means, they are coated with a standard sol-gel solution (concentration corresponding to the amount of tetraethyl orthosilane, 8.48 wt%). **Figure 3-19** shows the change of nanofiber morphology. The siloxane layer is thick due to the highest concentration of the sol-gel solution. Therefore, the resulted nanofibers should have the highest fiber diameters among the three different routes. Meanwhile, poly-PFDA particles survived from the thermal treatment after sol-gel process due to the thick siloxane layers. Nanofibers have plenty of pores (diameter around 53 ± 15 nm), which enhance the area fraction of air in the nonwovens. This leads to the high water contact angle and the superhydrophobicity of treated nonwovens.

3 Two-dimensional Superhydrophobic Nonwovens *via* Green Electrospinning

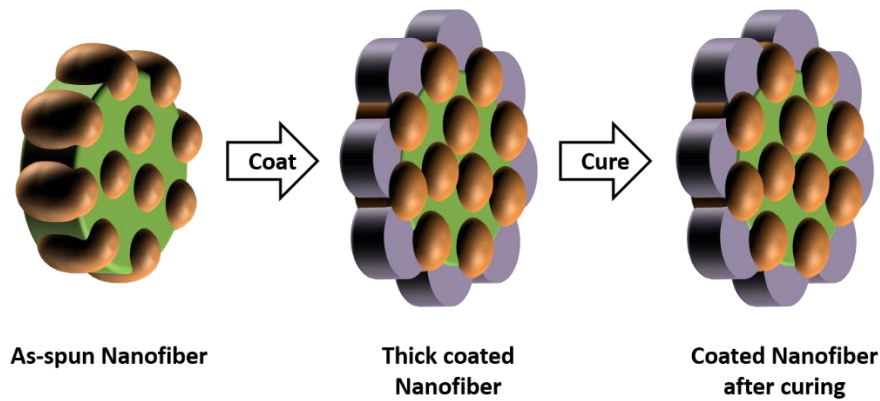


Figure 3-19. Illustration of nanofiber morphologies of Route I. The yellow spherical objects represent poly-PFDA particles. The green part is the PVA matrix and the siloxane layer is showed in lavender. Thicker siloxane layer prevents poly-PFDA particles from melting. The coated nanofibers exhibit high roughness as a result of numerous pores on them.

When the sol-gel solution is diluted (Route II), the siloxane layers are thus much thinner than the Route I. (**Figure 3-20**). The siloxanes layer is too thin to protect the polymer particles completely from melting. Therefore, the resulted nanofibers obtain much smoother surfaces compared with Route I, and the fiber diameter should be decreased. Moreover, there should be less or even no pores on the coated nanofibers.

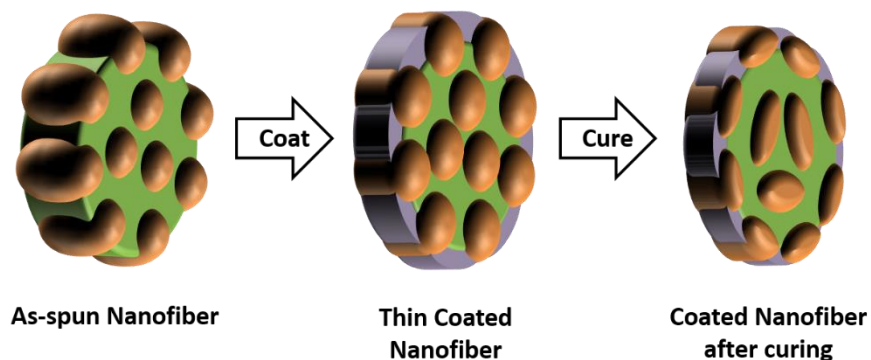


Figure 3-20. Illustration of nanofiber morphologies of Route II. The thinner siloxane layers are not able to prevent totally the melting behavior of poly-PFDA particles. The resulted nanofibers are much thinner and have relatively smooth surface morphology with fewer pores.

In addition, the sequence of coating process has also influence on the coated nanofiber morphologies. In Route III, as-spun fibers are firstly cured at 85°C, and these pre-cured nanofibers should have smooth surface morphology due to melting behavior of poly-PFDA. When they are coated with siloxane, the nanofibers remain smooth and almost no pores are formed by this route. (**Figure 3-21**)

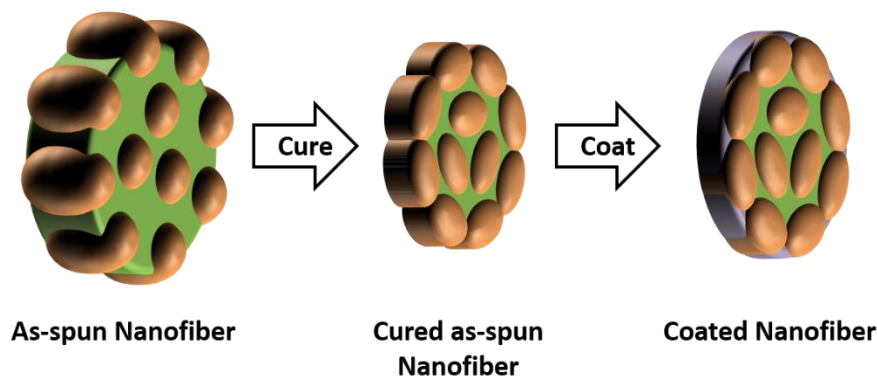


Figure 3-21. Illustration of nanofiber morphologies of Route III. The cured as-spun nanofibers possess smooth morphology as a result of particle melting. The additional coating layers could not change the morphology much.

To prove our hypothesis of these three coating routes, as-spun fibers are coated with different routes. Their surface morphologies are showed in **Figure 3-22**.

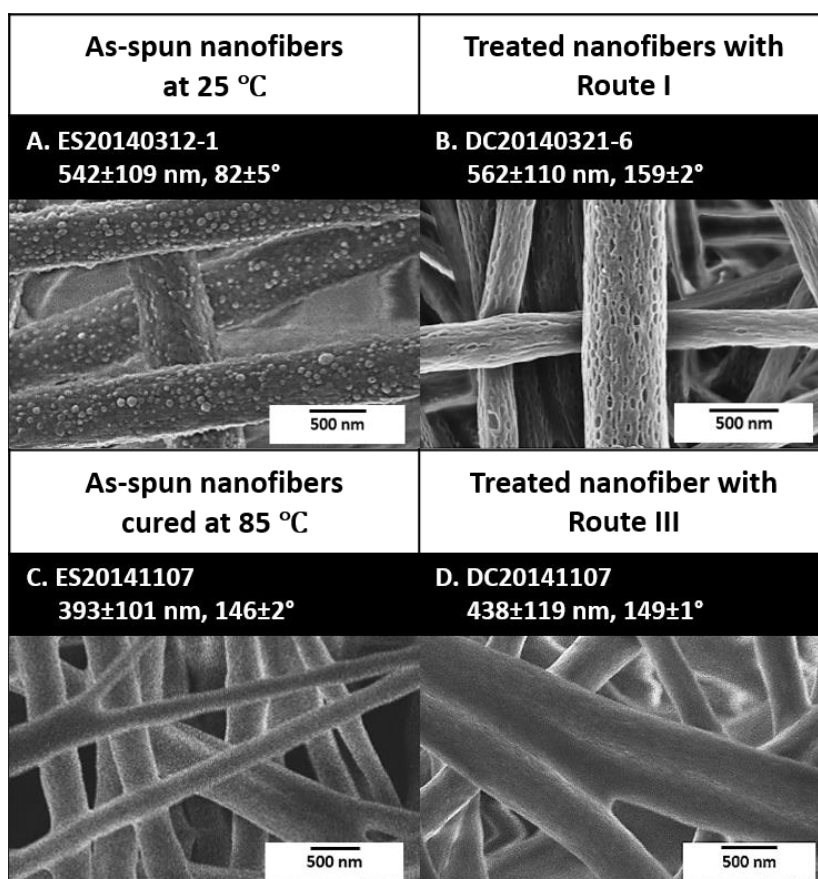


Figure 3-22. SEM images of nanofiber morphologies with different treatments routes.

The as-spun nanofibers in **Figure 3-22_A** have numerous poly-PFDA particles on the fiber surface. After a standard coating process (Route I), lots of pores appeared on their surface with diameters of 53 ± 15 nm. (**Figure 3-22_B**) This treated nonwovens was superhydrophobic and exhibited a contact angle of $159\pm 2^\circ$. If the sample A was firstly cured at 85°C , the poly-PFDA particles melted and the resulted nanofibers possessed smooth morphology. (**Figure 3-22_C**) Therefore, the fiber diameter reduced obviously to 393 ± 101 nm. The melted fluorinated polymer formed an outer layer over the nanofibers and showed an enhancement of hydrophobicity of the nonwovens. The contact angle of sample C was $146\pm 2^\circ$, much higher than the as-spun nonwovens (Sample A, $82\pm 5^\circ$). Further coated sample C with siloxane, the nanofiber diameter increased by 40 nm, and the contact angle was $149\pm 1^\circ$, similar to sample C. (**Figure 3-22_D**)

To summarize the results above, the formation of numerous pores on the nanofiber surface shows significant influence on the superhydrophobicity. A suitable thickness of siloxane layers prevents poly-PFDA particles efficiently from melting, and it also enhances the creation of pores. The experimental results agree to the hypotheses (Route I and III). The morphology changes through Route II will be discussed in the following chapter.

3.2.5 Influence of parameters of sol-gel process on the hydrophobicity of nonwovens

As discussed above, the siloxane layer should have a certain thickness to ensure its effects. The adjustment of layer thickness can be achieved by changing the parameters of sol-gel treatment, such as dip time, cure time, solution concentration, and dip cycle. The influence of each parameter on the hydrophobicity of nonwovens is discussed in the following parts.

3.2.5.1 Influence of dip/cure time on the hydrophobicity of nonwovens

In this part, the dip time of the coating process was changed to find out its influence on the hydrophobicity of nonwovens. The concentration was kept the same, 8.48 wt% corresponding to the amount of tetraethyl orthosilane (TEOS).

3 Two-dimensional Superhydrophobic Nonwovens *via* Green Electrospinning

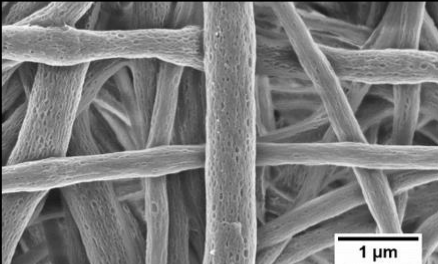
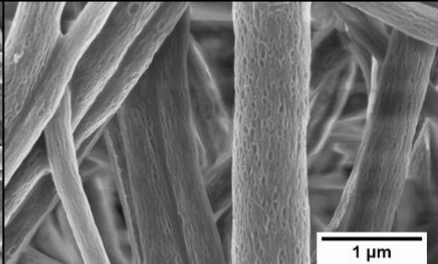
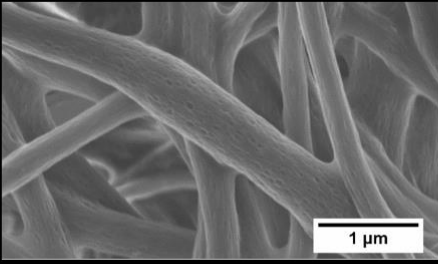
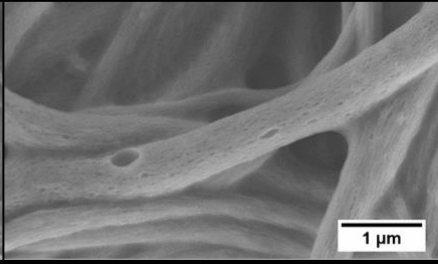
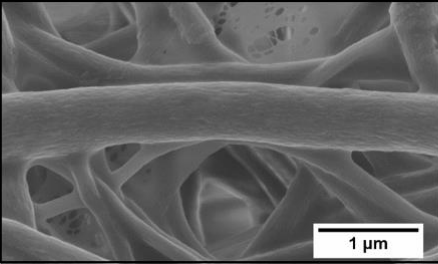
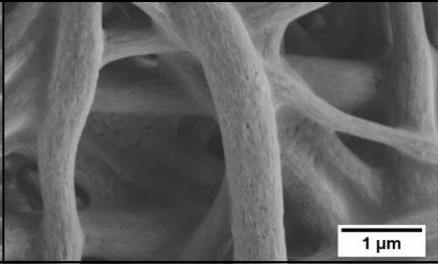
[PVA] Dip time	3.5 wt%	4 wt%
5 s	A. DC20140321-6 562±110 nm, 159±2°	D. DC20140321-5 583±134 nm, 162±1°
		
10 s	B. DC20140716-7 526±132 nm, 141±4°	E. DC20140716-6 438±87 nm, 144±2°
		
15 s	C. DC20140716-14 556±138 nm, 144±2°	F. DC20140716-13 495±145 nm, 146±1°
		

Figure 3-23. Longer dip time led to thicker siloxane layers; therefore, the nanofibers became smoother. The microscopic roughness reduced and the nonwovens became less hydrophobic.

With different dip time, not only the fiber diameter but also the contact angle change a lot. (**Figure 3-24**) With the same PVA concentration, fiber diameters increase along with longer dip time; however, nonwovens become less hydrophobic. The longer the fiber mats are immersed in the sol-gel solution, the treated nanofibers become smoother with shallower pores; meanwhile, films between nanofibers are observed with longer dip time. Therefore, the area

3 Two-dimensional Superhydrophobic Nonwovens *via* Green Electrospinning

fraction of air in the nonwovens and its roughness are decreased; the resulted fiber mats obtained lower contact angles.

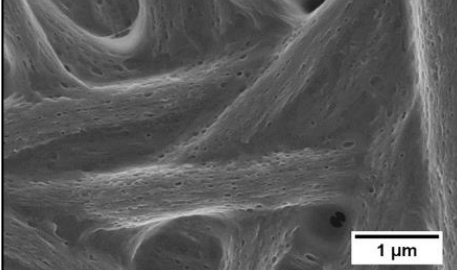
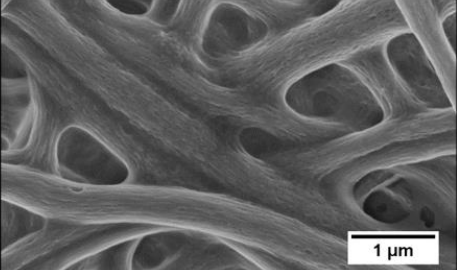
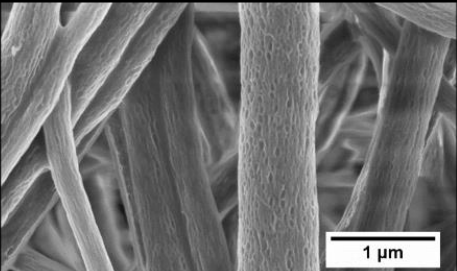
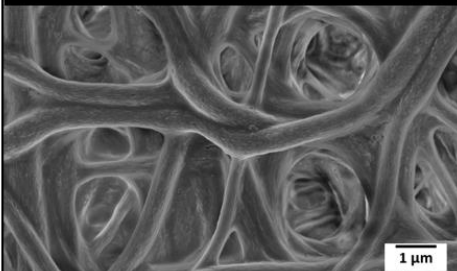
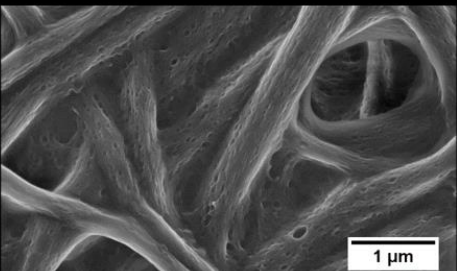
[PVA] Cure time	3.5 wt%	4 wt%
5 min	A. DC20140804-6 501±136 nm, 147±2° 	D. DC20140804-7 397±78 nm, 147±3° 
	10 min	D. DC20140321-5 583±134 nm, 162±1° 
15 min	C. DC20140804-13 430±92 nm, 150±2° 	F. DC20140716-13 366±75 nm, 147±2° 

Figure 3-24. The duration of cure time influenced the formation of pores along the fiber surfaces. The nanofibers became smoother and the pores were shallower with longer cure time, because the protective effect of siloxane layers became weaker.

Different from dip time, the contact angle increased at first with longer cure time, and then decreased again. As discussed already, the siloxane layer is a protection of fluorinated polymer particles from melting. As the cure time becomes longer,

the protection of siloxane is weaker and the nanofibers lose their roughness; therefore, the contact angle decreases. The SEM images clearly revealed the different morphologies of nanofibers with different cure time. The samples with 10 min (**Figure 3-24 B and D**) had more obvious pores along the fibers, it represents the best result. Comparing to other samples, nanofibers in these two samples are much thicker. The siloxane layers prevented the poly-PFDA particles from melting sufficiently, which led to the numerous pores along the nanofibers. This also enhanced the microscopic roughness of the total fiber mats.

3.2.5.2 Influence of concentration and dip cycle on the hydrophobicity of nonwovens

Using different concentrations of the sol-gel solution and dip cycles can also change the siloxane layer thickness, which prevents the particles from melting. Here, diluted solutions are used. The dip and cure time are 5 s and 10 min for all the treated samples.

With diluted solutions the siloxane layers became much thinner; therefore, the poly-PFDA particles were not protected sufficiently and melted during the curing process. Meanwhile, the fiber diameter decreased enormously. (**Figure 3-25 and 3-26**) Although nanofibers became smoother and fewer pores were created on their surface, the contact angles did not change too much. The reason is that the combination of siloxane layers and melted fluorinated acrylate polymer layers. According to the hypothesis, nanofibers, which are coated with a diluted solution (Route II), should have a smooth morphology. The experimental results agreed with the hypothesis.

3 Two-dimensional Superhydrophobic Nonwovens *via* Green Electrospinning

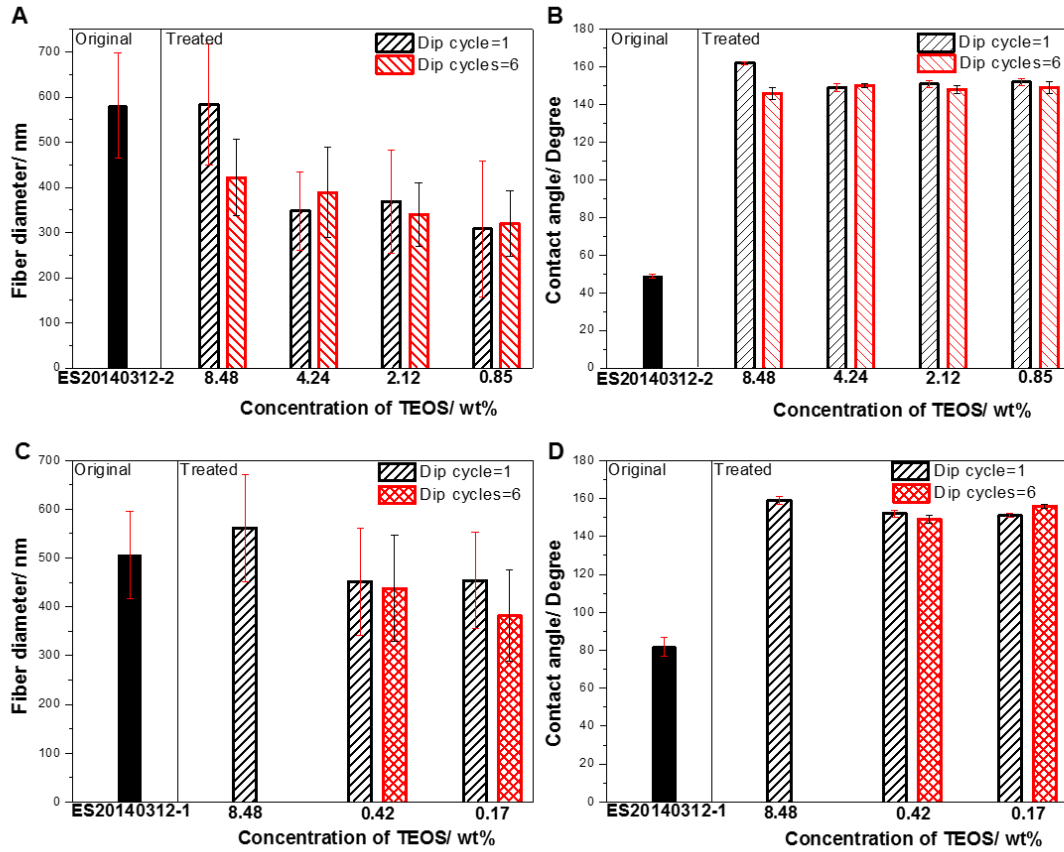


Figure 3-25. With the diluted sol-gel solution, the siloxane layers became thinner and they could not fully prevent the melting behavior of poly-PFDA. Therefore, the fiber diameter decreased with dilution. The melted poly-PFDA particles formed however an extra hydrophobic layer under siloxane layers, this contributed to the high contact angles to water. This effect is more obvious with more dip cycles.

3 Two-dimensional Superhydrophobic Nonwovens *via* Green Electrospinning

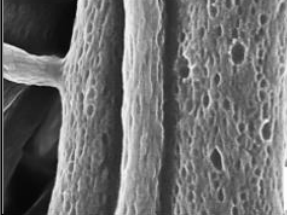
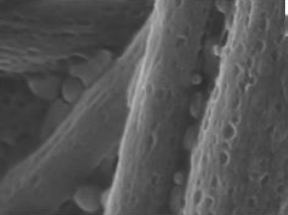
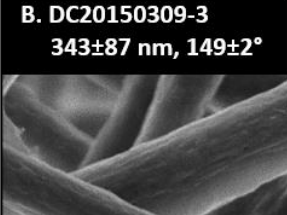
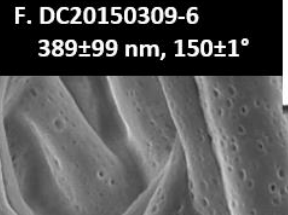
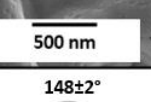
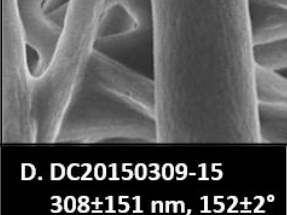
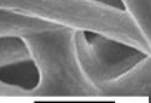
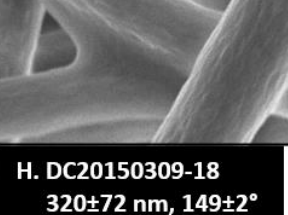
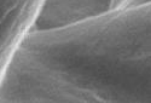
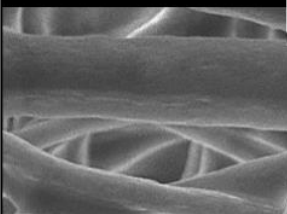
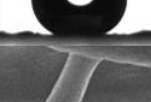
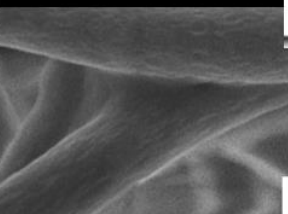
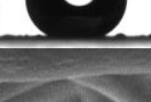
Dip cycles [TEOS]	1 time	6 Times
8.5 wt%	A. DC20140321-5 583 ± 134 nm, $162 \pm 1^\circ$   500 nm	E. DC20150112-1-3 422 ± 85 nm, $146 \pm 3^\circ$   500 nm
	B. DC20150309-3 343 ± 87 nm, $149 \pm 2^\circ$   500 nm	F. DC20150309-6 389 ± 99 nm, $150 \pm 1^\circ$   500 nm
4.3 wt%	C. DC20150309-9 369 ± 114 nm, $151 \pm 2^\circ$   500 nm	G. DC20150309-12 340 ± 70 nm, $148 \pm 2^\circ$   500 nm
	D. DC20150309-15 308 ± 151 nm, $152 \pm 2^\circ$   500 nm	H. DC20150309-18 320 ± 72 nm, $149 \pm 2^\circ$   500 nm
0.85 wt%	D. DC20150309-15 308 ± 151 nm, $152 \pm 2^\circ$   500 nm	H. DC20150309-18 320 ± 72 nm, $149 \pm 2^\circ$   500 nm

Figure 3-26. Fibers with thinner siloxane layers obtained smoother surfaces; however, the surface energy was lower enough to exhibit the superhydrophobic property (D). Meanwhile, more dip cycles lowered the surface roughness and made the nonwovens less hydrophobic.

3 Two-dimensional Superhydrophobic Nonwovens *via* Green Electrospinning

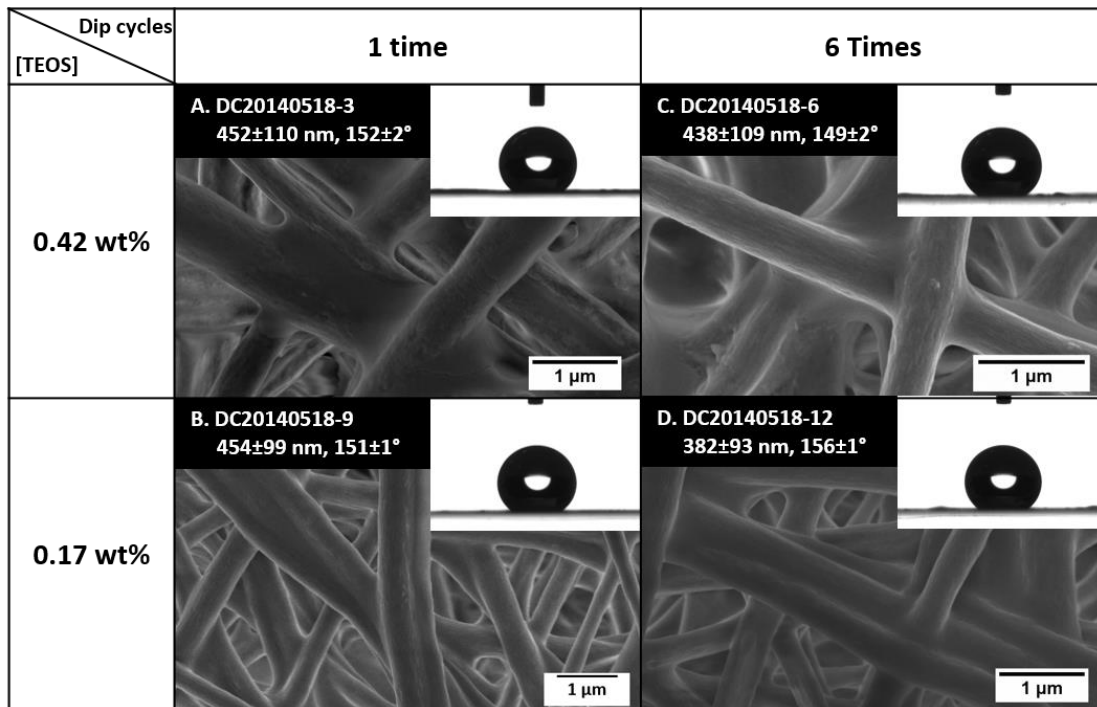


Figure 3-27. The nanofibers showed smooth surface morphologies with diluted sol-gel solutions. The poly-PFDA particles melted and created the extra layer under the siloxane layers. The combination of these two layers could also lead to the creation of superhydrophobic nonwovens.

With more dip cycles, the fiber diameter increases slightly; however, fewer pores are observed on the fiber surface. (**Figure 3-27**) According to Cassie formula (Equation 3), the areal fraction of air in nonwovens with different dip cycles could be calculated. (**Table 3-5**) With more dip cycles, the pores on nanofibers became smaller; therefore, the areal fraction of air decreased dramatically. This leads to a decrease of water contact angle droplet on nonwovens.

Table 3-5. The areal fraction of air of coated fibers with different dip cycles

Sample*	Dip cycles	Contact Angle/Degree	Pore diameter/nm	The areal fraction of air**/ %
DC20140321-5	1	162±1	53±15	94.6
DC20150112-1-2	3	146±2	34±3	75.4
DC20150112-1-3	6	146±3	33±8	73.4

* The original fiber mat is fabricated with ES20140312-2. All the samples were coated with an immerse speed of 250 mm/min and a lift speed of 10 mm/min. The concentration of the sol-gel solution is 8.5 wt% corresponding to TEOS.

** Calculated through Cassie formula: $\cos \theta = f_1 \cdot \cos \theta_1 + f_2 \cdot \cos \theta_2$, where θ_1 is 95°, water droplet on pure soa l-gel solution.

3.3 Preparation and characterization of aligned nanofibers and their hydrophobicity

Different from random nanofibers, rolling collector is used to prepare oriented nanofibers. The PVA concentration in the solution was constant of 3.5 wt%, and the weight ratio of Poly-PFDA to PVA was 83:17.

3.3.1 Influence of different parameters on fiber orientation

Usually, a stationary collector is used to collect fiber; therefore, nanofibers are randomly loaded on substrates. By using a rotating collector, aligned nanofibers could be simply prepared. The setup is shown in **Figure 3-28**.

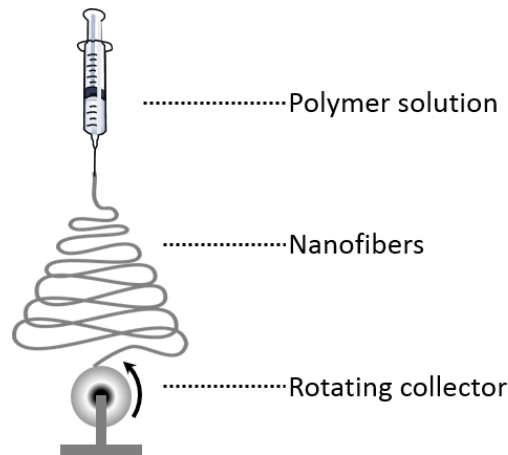


Figure 3-28. Setup of preparation of aligned nanofibers, where the nanofibers are collected with a rotating collector.

The degree of orientation S is an important factor to determine the alignment. According to the definition, the degree of orientation S could be calculated by

$$S = \frac{\langle 3(\cos \theta)^2 - 1 \rangle}{2} \dots \dots \dots (5)$$

where θ represents the angle nanofibers assume relative to the average orientation direction.^[90] When S equals zero, there is no orientation of nanofibers, e.g. nanofibers are randomly arranged. Nanofibers have a degree of alignment $S=1$ when all the fibers orient to one direction. As the rolling speed of collector increased, nanofibers are stretched more and more; therefore, the nanofibers were getting thinner. The nanofibers aligned with each other along the tangential direction; with an increasing speed, the alignment becomes also better.

3 Two-dimensional Superhydrophobic Nonwovens *via* Green Electrospinning

Table 3-6. Parameters of electrospinning for preparation of aligned nanofibers.

No.	Sample	Relative humidity/ %	Roll speed**/ $m \cdot s^{-1}$	DTC*/ cm	Voltage/ kV	S***
A	ES20140429	33	2	10	28	0
B	ES20140506		13		30	0.88
C	ES20140507		19			0.89
D	ES20140508		23			0.95
E	ES20140513	22	23			0.99
F	ES20140522	26	19	5	19	0.96

* DTC means distance to the collector.

**Tangential velocity of the collector.

***S represents for the degree of orientation and is calculated by Equation 5.

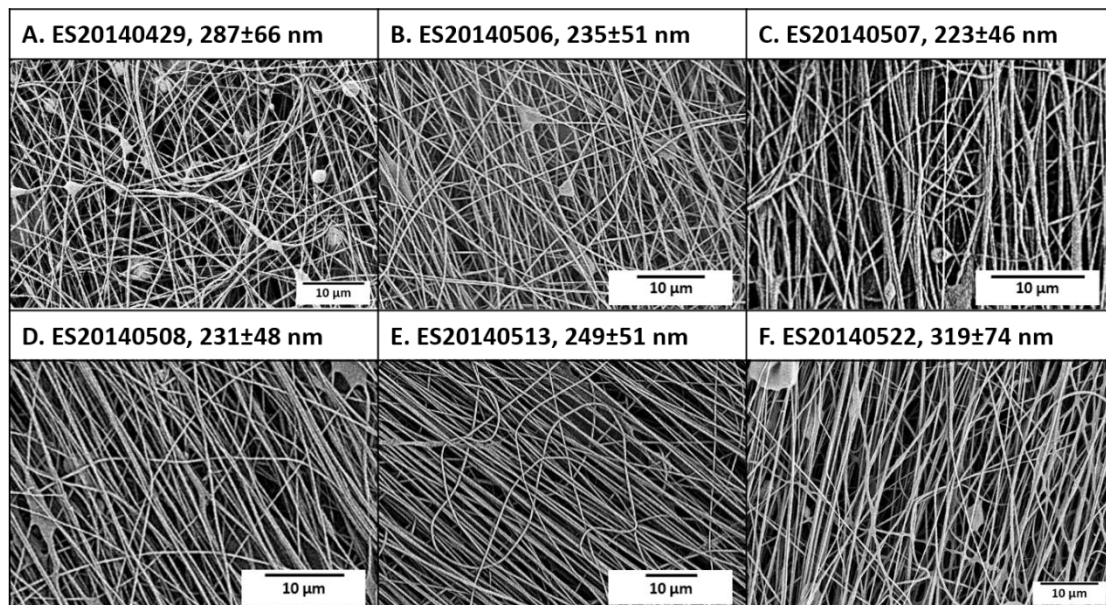


Figure 3-29. The alignment of nanofibers increased with higher rolling speed; meanwhile, the fiber diameter decreased.

Nanofibers showed no alignment with lower rolling speed (**Figure 3-29_A**). The alignment became better from B to D with an increased rolling speed. Thus, the degree of orientation *S* was improved from 0.88 to 0.95. Shorter distance to collector could reduce the free-flying time of nanofibers; therefore, the orientation became also better (**Figure 3-29_F**). Less humidity in the environment could also improve the fiber orientation (**Figure 3-29_E**).

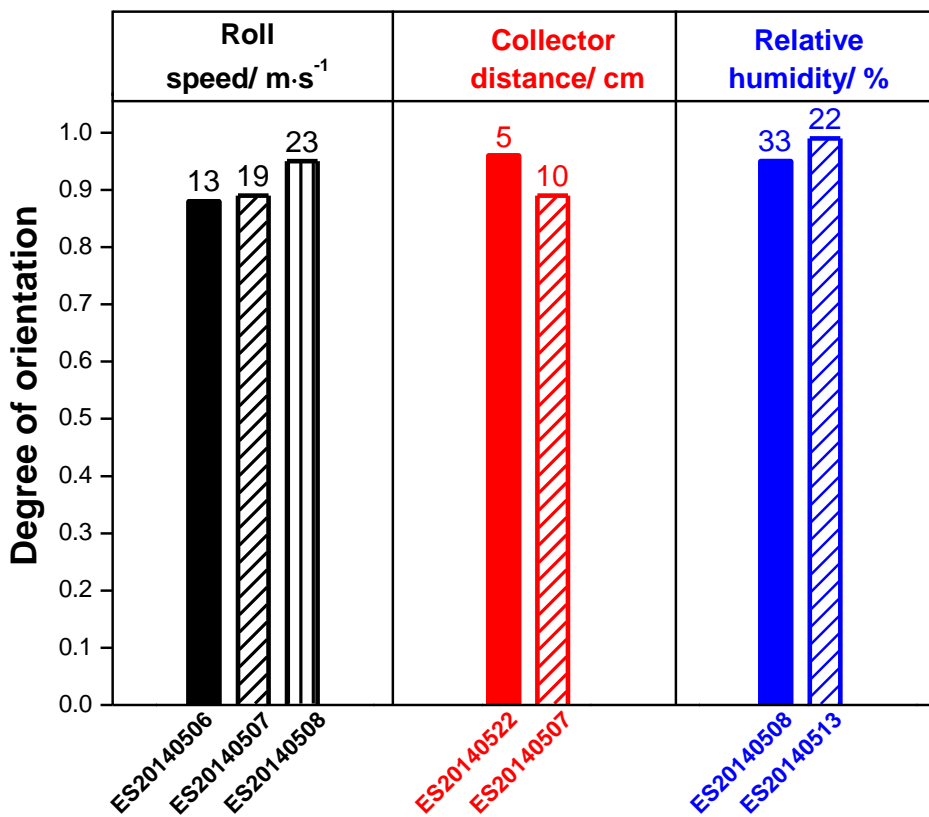


Figure 3-30. The degree of orientation *S* increased with higher roll speed, less distance to the collector and higher humidity.

3.3.2 Influence of parameters of sol-gel process on hydrophobicity and orientation of aligned nanofibers

The original nanofibers showed some certain orientations depending on the preparations. Therefore, there should be two typical dip directions of aligned nanofibers: parallel or vertical to the nanofiber orientation. (**Figure 3-31**) Moreover, oriented nanofibers compacted very densely to each other. In comparison with parallel coating direction, the influence of vertical direction should be much stronger. The nanofibers with the vertical coating may hold the sol-gel solution during the coating process, which could create films between nanofibers.

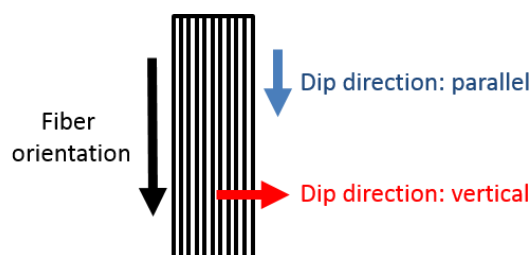


Figure 3-31. Illustration of two dip directions of aligned nanofibers: parallel or vertical to the fiber orientation, blue and red arrows respectively.

Table 3-7. List of samples before and after siloxane coating.*

Sample before coating	Dip direction	Sample after coating
ES20140506	Vertical	DC20140509-4
ES20140507		DC20140509-5
ES20140508		DC20140509-6
ES20140506	Parallel	DC20140509-10
ES20140507		DC20140509-11
ES20140508		DC20140509-12

* All the samples were coated with an immerse speed of 250 mm/min and a lift speed of 10 mm/min. The sol-gel solution was 8.5 wt% corresponding to the amount of TEOS for all the samples.

3 Two-dimensional Superhydrophobic Nonwovens *via* Green Electrospinning

Table 3-8. Diameters and contact angles of siloxane-coated aligned nanofibers.

Sample	Dip direction	Fiber diameter/ nm	Contact angle/ Degree	S
DC20140509-4	Vertical	277±68	141±3	0.83
DC20140509-5		320±74	143±3	0.87
DC20140509-6		285±55	138±2	0.9
DC20140509-10	Parallel	336±69	146±2	0.83
DC20140509-11		287±82	143±2	0.84
DC20140509-12		285±60	140±3	0.85

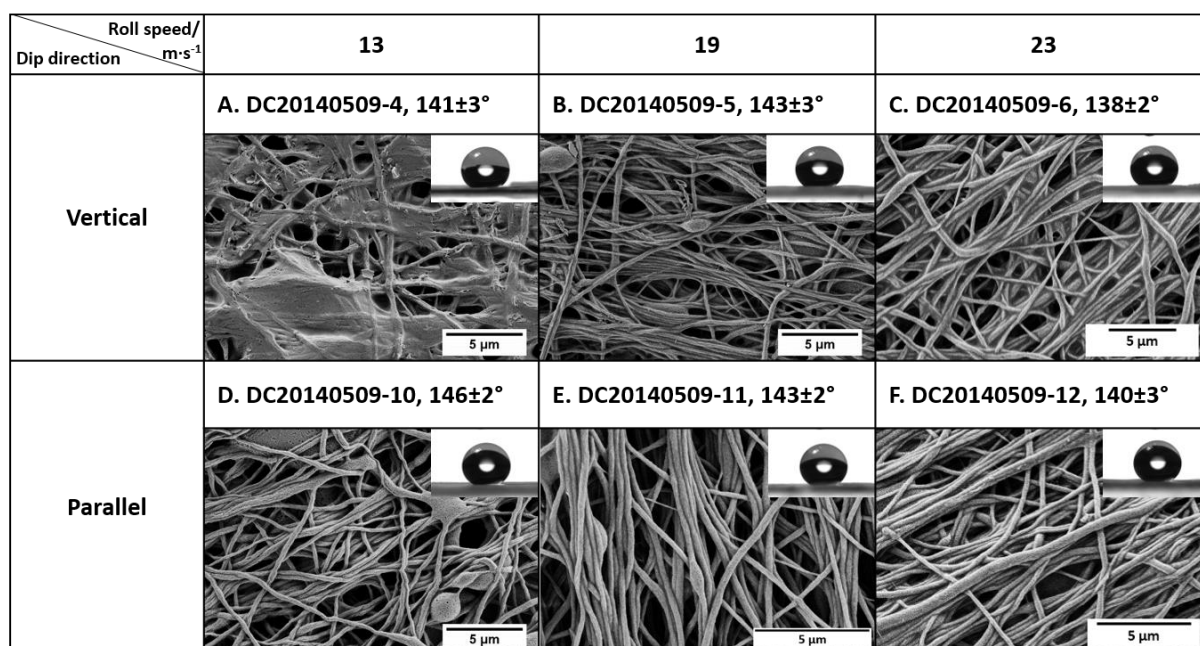


Figure 3-32. The alignment of nanofibers reduced after siloxane coating. Nanofibers stuck together; meanwhile, the formation of films was observed in samples with vertical dip direction. The samples turned less hydrophobic in comparison with nonwovens.

Aligned nanofibers were very thin, less than 250 nm, and they compacted to each other very densely. Coating with siloxane made them stick together; therefore, the nanofibers lost their orientation. For example, the as-spun nanofibers (**Figure 3-29_D**) have an orientation degree of 0.95. The orientation with different coating direction became worse, the degree of orientation S was 0.9 for vertical coating (**Figure 3-32_C**) and 0.85 for parallel coating (**Figure 3-32_F**). Moreover, the formation of films between fibers was also observed with vertical dip direction; samples with parallel dip direction showed no film formation. (**Figure 3-32_A**) This phenomenon agreed with the hypothesis as the discussion at the beginning. The bonded nanofibers and the formation of films reduced the areal fraction of air in the fiber mats, and the fiber mats became less hydrophobic than nonwovens. Generally, the contact angles to water of coated aligned nanofibers were around 140° .

Similar to nonwovens, dip time and cure time also have an influence on the hydrophobicity of aligned nanofibers. The contact angles with different dip times are almost the same (around 140°). The dip time was changed from 5 s to 15 s. Samples with 10 s dip time (**Figure 3-33_B** and **E**) obtained the thinnest nanofibers. Films are barely observed between fibers because all the samples were coated with parallel direction; however, they still tended to stick together after coating. Moreover, there are almost no pores on the fiber surface as comparing to nonwovens.

3 Two-dimensional Superhydrophobic Nonwovens *via* Green Electrospinning

Table 3-9. List of samples before and after siloxane coating.*

Sample before coating	Dip time/ s	Sample after coating
ES20140507	5	DC20140509-11
ES20140508		DC20140509-12
ES20140507	10	DC20140716-1
ES20140508		DC20140716-2
ES20140507	15	DC20140716-8
ES20140508		DC20140716-9

* All the samples were coated with an immerse speed of 250 mm/min and a lift speed of 10 mm/min. The sol-gel solution was 8.5 wt% corresponding to the amount of TEOS for all the samples.

Table 3-10. Diameters and contact angles of siloxane-coated aligned nanofibers.

Sample	Dip time/ s	Fiber diameter/ nm	Contact angle/ Degree	S
DC20140509-11	5	287±82	143±3	0.84
DC20140509-12		285±60	140±3	0.85
DC20140716-1	10	251±46	142±2	0.83
DC20140716-2		226±55	137±2	0.84
DC20140716-8	15	288±64	140±2	0.82
DC20140716-9		277±51	140±3	0.85

3 Two-dimensional Superhydrophobic Nonwovens *via* Green Electrospinning

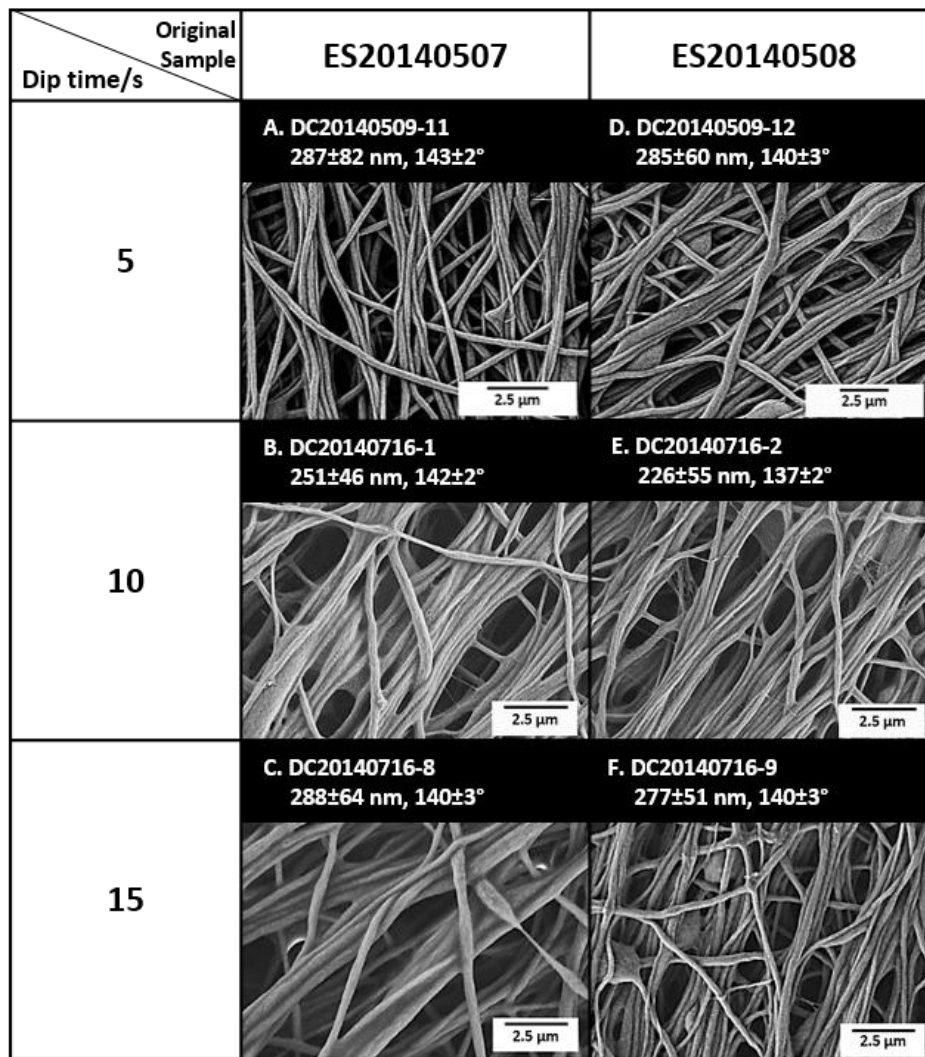


Figure 3-33. Morphologies of aligned nanofibers with different dip time. The coated aligned nanofibers stuck together and lost their orientation; therefore, the degree of orientation decreased as compared to the original samples.

The contact angles are quite the same with different cure time; however, the fiber diameters reached maximum thickness with 10 min, 287±82 nm and 285±60 nm respectively. The reason for this phenomenon should be the same as the one with nonwovens. With less curing time, the siloxane layers could still protect the fluorinated polymer particles from melting. This function became yet weaker with longer cure time. As the curing time increases up to 15 min, polymer particles melted and formed extra fluorinated layers and combined with siloxane

layer showed a higher contact angle with thinnest fibers. This could also be observed in SEM images. (**Figure 3-34**)

Table 3-11. List of samples before and after siloxane coating.*

Sample before coating	Cure time/ min	Sample after coating
ES20140507	5	DC20140804-2
ES20140508		DC20140804-3
ES20140507	10	DC20140509-11
ES20140508		DC20140509-12
ES20140507	15	DC20140804-9
ES20140508		DC20140804-10

* All the samples were coated with an immerse speed of 250 mm/min and a lift speed of 10 mm/min. The sol-gel solution was 8.5 wt% corresponding to the amount of TEOS for all the samples.

Table 3-12. Diameters and contact angles of siloxane-coated aligned nanofibers.

Sample	Cure time/ min	Fiber diameter/ nm	Contact angle/ Degree	S
DC20140804-2	5	259±48	143±1	0.83
DC20140804-3		249±74	141±1	0.84
DC20140509-11	10	287±82	143±2	0.84
DC20140509-12		285±60	140±3	0.85
DC20140804-9	15	237±48	141±2	0.83
DC20140804-10		277±50	141±3	0.85

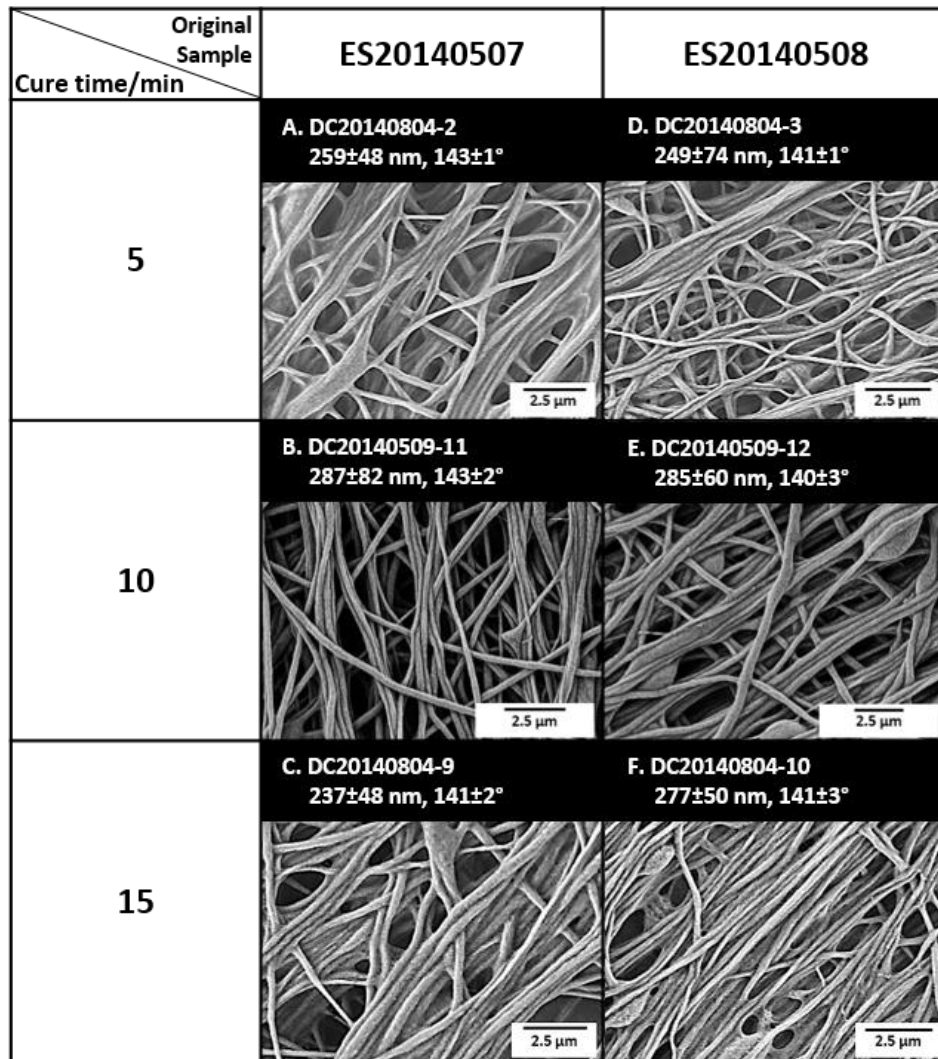


Figure 3-34. Morphologies of aligned nanofibers with different cure time: the degree of orientation reduced due to the bonded fibers. Film formation was strongly retarded by virtue of parallel coating direction. The nanofibers showed relative smooth surface morphology, there were almost no pores on the fiber surfaces.

3.4 Conclusion

Superhydrophobic nonwovens are successfully prepared by green electrospinning from an aqueous dispersion. This material possesses a contact angle higher than 160° and a small roll-off angle less than 5°; moreover, it showed good self-cleaning property.

The Poly (perfluorodecyl acrylate) was successfully synthesized through emulsion polymerization. After mixing this dispersion with PVA, the viscous

solution is created and stable for green electrospinning. There are no organic solvents, this technique is thus environmentally friendly. The acrylate polymer has a spherical structure and its diameter is 90 ± 14 nm. The initial electrospun nanofibers composed of 17 wt% of PVA and 83 wt% of poly-PFDA. The nanofibers are covered with numerous particles. The polymer particles are the main composed part of nanofibers and PVA is like the adhesive and combined particles together. This could be proved by SEM images of the cross-section of nanofibers. The resulting electrospun nonwovens showed different contact angles to water, as the concentration of PVA is changed. Higher concentration of PVA (4 wt%) led to lower water contact angle $49\pm 1^\circ$ and thicker nanofibers 542 ± 109 nm, and less PVA (3.5 wt%) the contact angle is $82\pm 5^\circ$ and the nanofiber diameter decreased to 507 ± 89 nm.

The electrospinning technique provides a surface roughness of the nonwovens; meanwhile, the use of fluorinated acrylate polymer reduces the surface tension. The original nonwovens are still hydrophilic due to PVA, the introduction of another material to reduce the surface energy further is needed. Therefore, siloxane coating with sol-gel treatment comes into concern. After this post-treatment, the water contact angle increases up to 160° and the roll-off angle is less than 5° . The fiber diameter also increased slightly along with more PVA in the composition. With help of SEM, the surface morphologies of siloxane-coated nanofibers are determined. The particles disappeared from the surface after coating with siloxane. Instead, there are a lot of pores on the fiber surface. The pores have an average diameter of around 55 nm. The surface of the coated nonwovens consists of nanofibers and air pockets. The calculated areal fraction of air using Cassie-formula is over 92%. That means, the water droplet sits almost on the air, less than 10% area is covered with nanofibers. The pores disappear or become shallower as coating with more coating cycles or diluted sol-gel solutions.

Therefore, the areal fraction of air decreased dramatically to 75%. The contact angle of these nonwovens with smooth nanofiber morphology is only 146°.

The curing temperature of sol-gel treatment is 85°C, which is higher than the melting point of the fluorinated acrylate polymer. The created siloxane layers could protect the particles from melting, yet only for short duration. Thicker layers exhibit the better protective effect. A diluted coating solution, less dip time or longer cure time, lead to thin siloxane layers. Therefore, the acrylate particles melted and formed an extra layer over the fibers, this lowered the surface energy together with the siloxane layer; however, the areal fraction of air decreases due to the formation of films between fibers. All of these hypotheses could be proved by SEM images and the contact angle measurements.

By use of a rotated collector for electrospinning, only nonwovens but also aligned nanofibers could be produced. In this case, the dip directions to fiber orientation also play an important role in the future hydrophobicity. As also shown with the electrospun nonwovens, thicker fibers could prevent film formation between nanofibers during siloxane coating. In contrast, thinner fibers have lots of films; therefore, the porosity of nonwovens is sacrificed. With a rotating collector, the nanofibers are not only aligned but also stretched. The fiber diameter decreases a lot as compared with the same composition of nonwovens. As a result of the alignment, nanofibers are closed to each other. The coating with siloxane forces them to stick together; on the other hand, films formation with vertical coating direction is also observed. There are also smaller and fewer pores along the fibers after siloxane coating. With the reasons above, the aligned nanofibers only showed contact angle around 145° and higher roll-off angle as comparing with nonwovens.

3 Two-dimensional Superhydrophobic Nonwovens *via* Green Electrospinning

This water-born superhydrophobic surface showed really high water contact angle and low roll-off angle. The potential applications could be as self-cleaning textile or another anti-fouling coating. As compared to the two-dimensional nonwovens, three-dimensional structure has much higher specific surface area. With advantages of the three-dimensional structures, more applications could be realized. In chapter 4, polyamide 6.6 short fibers are used as the starting material to create a three-dimensional structure. This matrix could be applied as a multifunctional platform with different modifications.

4 Three-Dimensional Matrixes with Versatile Functionalities *via* Flocking Technique

In the textile industry, the appearance or properties of the subjects can be changed with three-dimensional coatings of small particles or short fibers. This is the so-called flocking technique. The resulted three-dimensional matrix has a high porosity (as pores are the area between short fibers), and also high roughness. These special factors provide a unique three-dimensional platform with various properties. On the other hand, the surface characteristics are also tunable with a second coating with other materials. This brings other additional functionalities into the three-dimensional matrixes.

4.1 Preparation and characterization of three-dimensional matrixes *via* flocking with Polyamide 6.6

The commercial polyamide 6.6 short fibers are applied for the preparation of three-dimensional matrixes; their physical and chemical parameters are listed in **Table 4-1**. The short fibers are firstly put inside the chamber of a MiniFlock machine from Maag-Flock Company (**Figure 4-1**). Under high voltage, they are deposited on a substrate, which is already coated with adhesive. After solidification, a quite stable three-dimensional grass-like coating, consisting of polymer fibers, is successfully introduced on the substrate. One of the applied adhesives is D564/1 (water dispersion of polyurethane-basis), which is dried at room temperature for 72 h. The other one is D590 (water dispersion of acryl polymers) and should be dried first at 80 °C for 20 min then 40 min at 140 °C. The voltage of the flock process was altered from 30 kV to 70 kV. PA 6.6 fibers can deposit

4 Three-Dimensional Matrixes with Versatile Functionalities *via* Flocking Technique

on the substrate either upward or downward (**Figure 4-2**). The spin-coating method is used to distribute adhesive onto substrates.

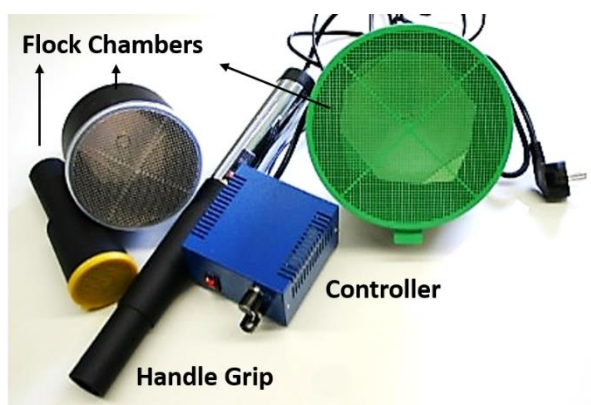


Figure 4-1. Photo of the MiniFlock machine from Maag-Flock Company.

Table 4-1. Physical and chemical parameters of three commercial PA flock fibers.

PA fiber color	Length/ μm	Diameter/ μm	$M_n/\text{g}\cdot\text{mol}^{-1}$	\bar{D}	$T_c/^\circ\text{C}$	$T_m/^\circ\text{C}$
Black	520 ± 20	18 ± 1	49,500	1.67	260	213
Blue	970 ± 60	18 ± 3	49,000	1.64	257	212
White	2250 ± 150	57 ± 6	48,400	1.70	261	210

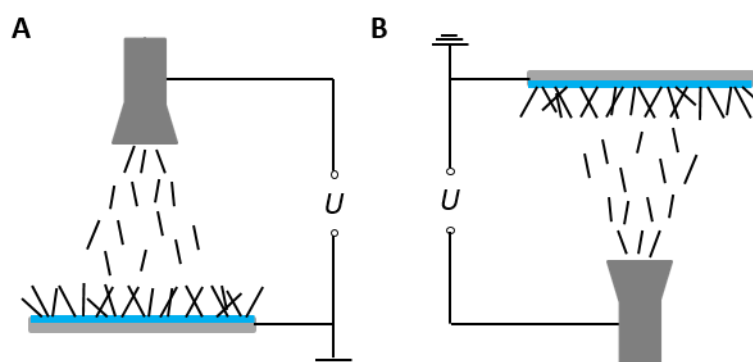


Figure 4-2. Schematically illustration of deposition directions of PA 6.6 flock fibers: downward (A) and upward (B).

4.1.1 Hydrophilicity of initial polyamide 6.6 matrix

Considering the flock fibers matrix as a three-dimensional coating, the resulted surface is thus heterogeneous, which consists of fibers, adhesives, and air. Due to the different hydrophilicity of adhesive materials themselves, samples' water contact angles also differ from each other. Polyurethane prefers to form hydrogen bonds with water than the acryl polymer; therefore, the contact angle with D564/1 is much lower than the one with D590. On the other hand, the flocking direction didn't change the standing structure of fiber grasses on the substrate. There is no obvious difference between contact angles in two systems (**Figure 4-3**).

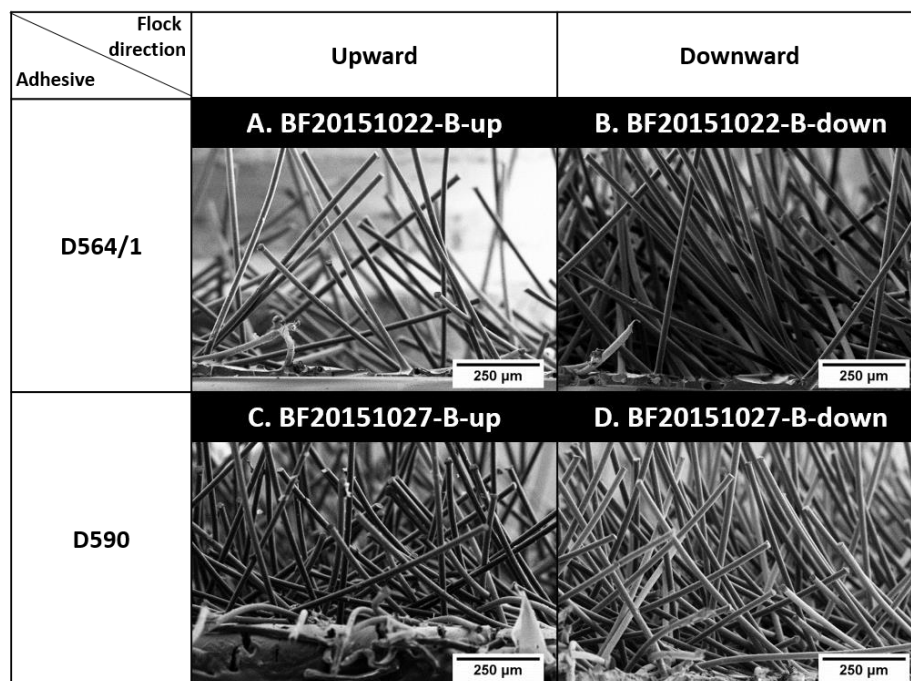


Figure 4-3. SEM images of two flock directions with flock length 1 mm.

The water droplets penetrate the original three-dimensional coating surface within 1 min due to the hydrophilicity of PA 6.6 flock fibers. The water droplet maintains its spherical structure for a few seconds, and then wets the surface; the contact angle is then unmeasurable. (**Figure 4-**

4) The spherical structure of water droplets, which are kept for the longest time, is taken for the measurements of water contact angles; the results are listed in **Table 4-2**.

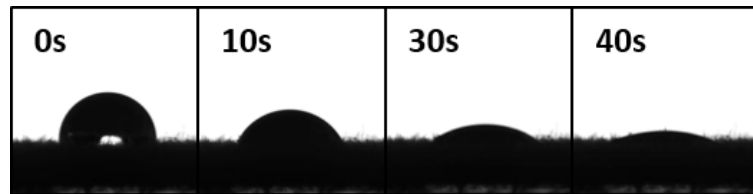


Figure 4-4. The change of a water droplet on the original flock sample BF20151022-B-up along with time.

Table 4-2. Water contact angles of initial PA 6.6 matrixes.

Sample	Flock direction	Adhesive	Contact angle/ Degree
BF20151022-S-up*	upward	D564/1	72±1
BF20151022-S-down	downward		61±1
BF20151022-B-up**	upward		53±4
BF20151022-B-down	downward		44±4
BF20151027-S-up	upward	D590	133±1
BF20151027-S-down	downward		127±1
BF20151027-B-up	upward		97±1
BF20151027-B-down	downward		108±1

* S represents 0.5 mm PA 6.6 short fibers.

** B represents 1 mm PA 6.6 short fibers.

4.1.2 Improve the hydrophobicity of polyamide 6.6 flock

As discussed in chapter 3, superhydrophobic materials are applicable in various fields. However, the original three-dimensional PA 6.6 matrix is mainly hydrophilic. To enrich its properties and expand its application

fields, a secondary coating can be helpful. Introduction of an additional siloxane or PPX layer, the PA 6.6 matrix can turn hydrophobic.

4.1.2.1 Siloxane as the secondary coating material

In the first step, siloxane layers are coated onto the three-dimensional polymer matrix. The procedure is alike to the one for two-dimensional nonwovens. As shown in **Figure 4-5**, water droplets demonstrate different behaviors on surfaces of initial and coated PA 6.6 flock matrix. The original PA 6.6 flock matrixes are hydrophilic; the surface is thus wetted. In contrast, water droplets sit on the surface of coated matrixes, instead of penetrating into the surface; the contact angles range from 120° to 135°.

Flock length/ mm	H ₂ O behaviors on flock surfaces		CA on treated flock
	Original	Treated	
0.5	 BF20150327-S-1	 DC2015402-S-1	121±1° 
1	 BF20150327-B-1	 DC2015402-B-1	122±1° 

Figure 4-5. The behaviors of water droplets on original and siloxane-coated PA 6.6 flock matrixes.

On the other hand, the thickness of siloxane layers is unlike at different positions, the results are shown in **Table 4-3**. The bottom parts have relative more siloxane layers; therefore, the contact angles are also slightly higher than the upper parts. As the voltage during preparation

increased, flock density also increased and there are more fibers under the same volume of the water droplet. Meanwhile, the polymer flock fibers orient themselves more vertical to the substrates.

Table 4-3. Contact angles of siloxane-coated PA 6.6 matrixes on different positions.

Sample*	Fiber length/ mm	Voltage/ kV	Contact angle/ Degree		
			up	middle	bottom
DC20150402-S-1	0.5	50	107±1	121±2	124±1
DC20150402-B-1	1		117±2	122±1	131±2
DC20150402-S-2	0.5	70	110±1	125±1	125±1
DC20150402-B-2	1		130±1	133±2	130±2

* The adhesive is D564/1. The flock duration is 2 s. All the samples are coated with an immerse speed of 250 mm/min and a lift up-speed of 10 mm/min.

4.1.2.2 Poly (para-xylene) as the secondary coating material

Besides siloxane, Poly (para-xylene) (PPX) was also used to change the surface hydrophobicity. The contact angle of pure PPX is around 90°; therefore, thicker PPX layer lead to lower contact angles. As expected, the contact angles with thinner PPX layers, ranging from 135 to 140°, are slightly higher than the thicker ones; moreover, the contact angles on samples with D590 were slightly higher than D564/1. That means the roughness is more important in this three-dimensional system. Although the PPX-coated PA 6.6 matrixes became only hydrophobic, samples with 150 nm PPX layer showed smaller roll-off angles; therefore, water droplets are blown away easily, and the surfaces remained dry.

4 Three-Dimensional Matrixes with Versatile Functionalities *via* Flocking Technique

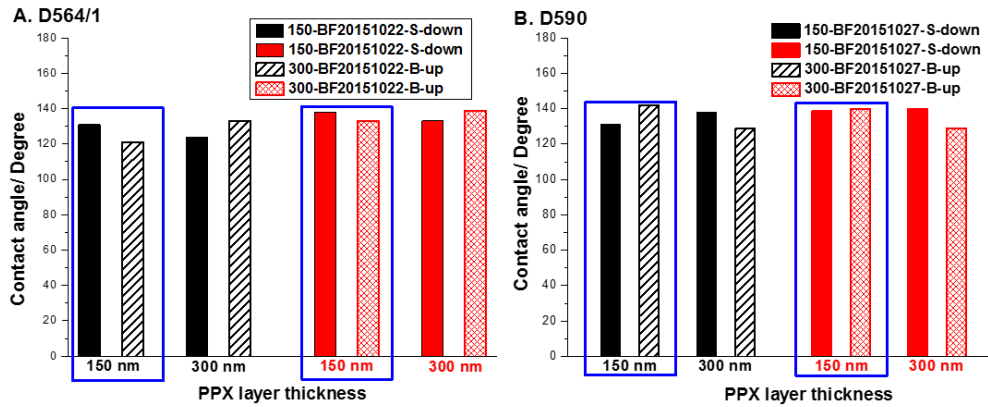


Figure 4-6. Water contact angles on PPX-coated PA 6.6 matrixes.

4.1.3 Stability of polyamide 6.6 flock matrixes

The PA 6.6 fibers are immobilized with adhesives on the substrates. Their stability is very important for the future applications; hence, a tape test is carried out (**Figure 4-7**). Firstly, an original PA 6.6 matrix is fixed on a substrate. Then, a scotch tape strip from Tesa is pressed on the fibers with adhesive side down. After removal of the tape strip, the loose fibers go with it. This step is repeated for 20 times, and the results are recorded with a digital camera.

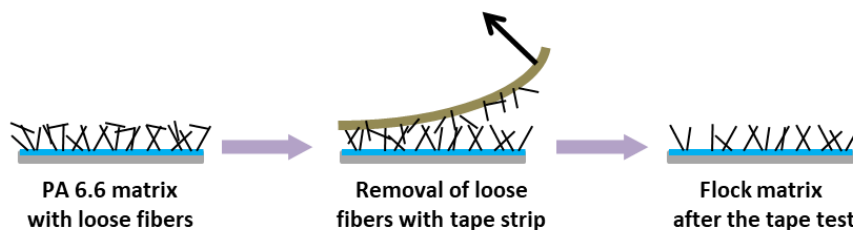


Figure 4-7. Schematically illustration of a scotch tape test.

During the flocking process, not all the fibers are fixed on the substrate. In the first several repetitions, lots of fibers adhered to the tape strips (lower parts on tapes). The tape strips remained clean with more

repetitions, and flock matrixes still kept their grass-like structures. Generally speaking, the flock matrixes are quite stable, and most of the fibers adhere firmly to the substrates.

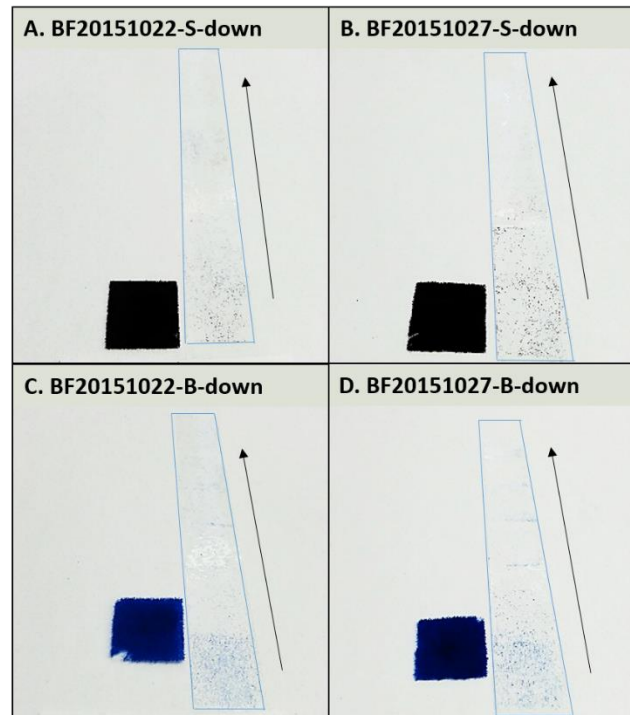


Figure 4-8. Stability test of fresh-made PA 6.6 matrixes with the scotch tape test. Black arrows represent the test directions.

4.1.4 The density of polyamide 6.6 fibers and porosity of three-dimensional matrixes

This grass-like surface consists of short fibers, and the fiber density is an important factor to figure out the relationship between flock conditions and the resulted matrixes. The fiber density on PA 6.6 matrixes represents the numbers of fibers per unit area. Here, 1 mm PA 6.6 fibers are used. The flock duration ranged from 5 s to 20 s, and the applied voltage changed from 30 kV to 70 kV. The standing structure of PA 6.6 fibers could be adjusted by changing the flocking parameters. The sample I in **Figure**

4-9 is prepared with the highest voltage and the longest flock duration; fibers oriented themselves more vertical to the substrate than others.

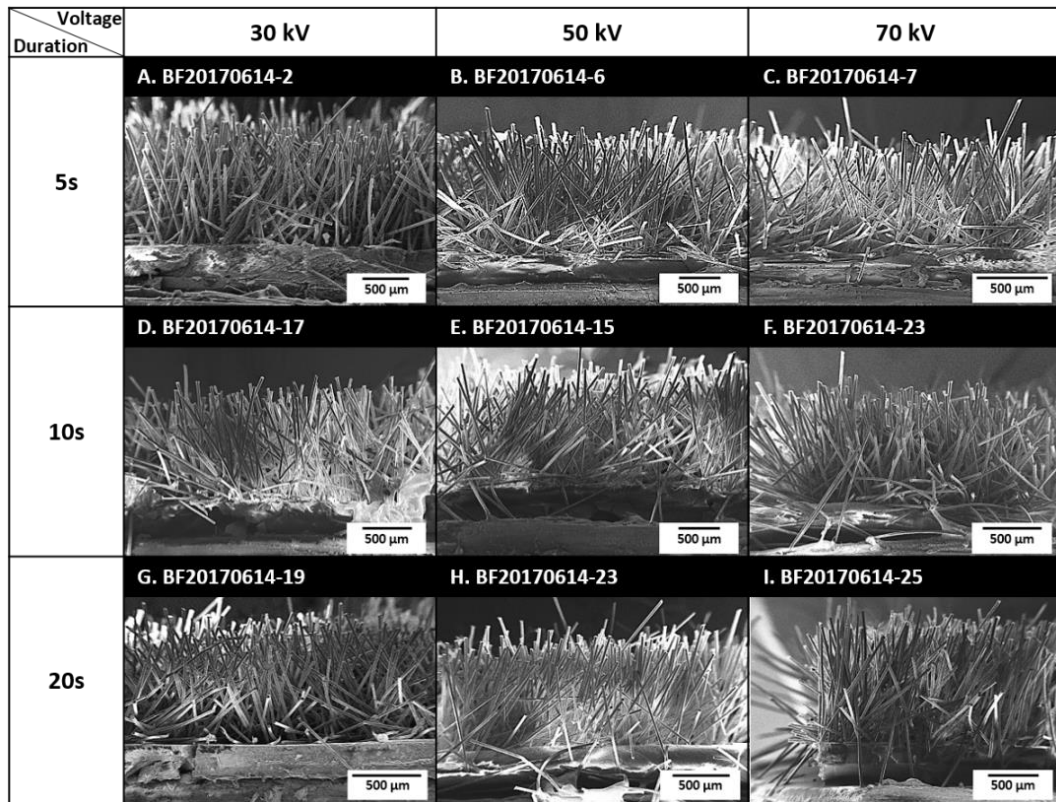


Figure 4-9. SEM images of PA 6.6 flock matrixes with different flock durations and applied voltages.

With longer flock duration, more fibers are deposited on substrates; hence, the fiber density should increase too. As shown in **Figure 4-10**, with the same process voltage, higher fiber density was achieved with longer flock duration. In addition, the fibers are charged during the flocking process, and with higher process voltage the charging effect on fibers was also higher. Therefore, more short fibers could be charged with the same flock duration, thus resulted in higher fiber density.

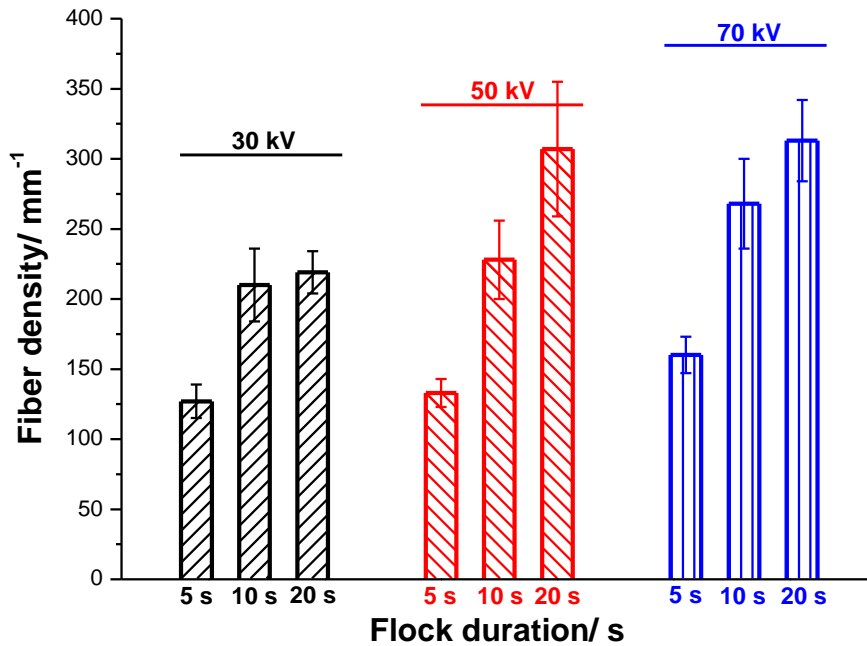


Figure 4-10. Fiber density differs with flock duration and process voltages. Longer flock duration and higher applied voltage lead to higher fiber density of PA 6.6 matrixes.

The three-dimensional matrix can be used in tissue engineering as scaffolds for cell culturing; its porosity is an important criterion for this application. Walther and coworkers [128] calculated the porosity of flock matrix through the volume of the scaffold and all fibers,

$$Porosity = \frac{V_s - V_f}{V_s} \times 100\% \dots \dots \dots (6)$$

where V_s means the volume of the total scaffold, calculated by fiber length and substrate diameter; V_f is the volume of all the fibers inside the scaffold, estimated by volume of single fibers and fiber density. As discussed above, longer flock duration and higher process voltage could increase the fiber density; therefore, the porosity of the total matrix reduces simultaneously.

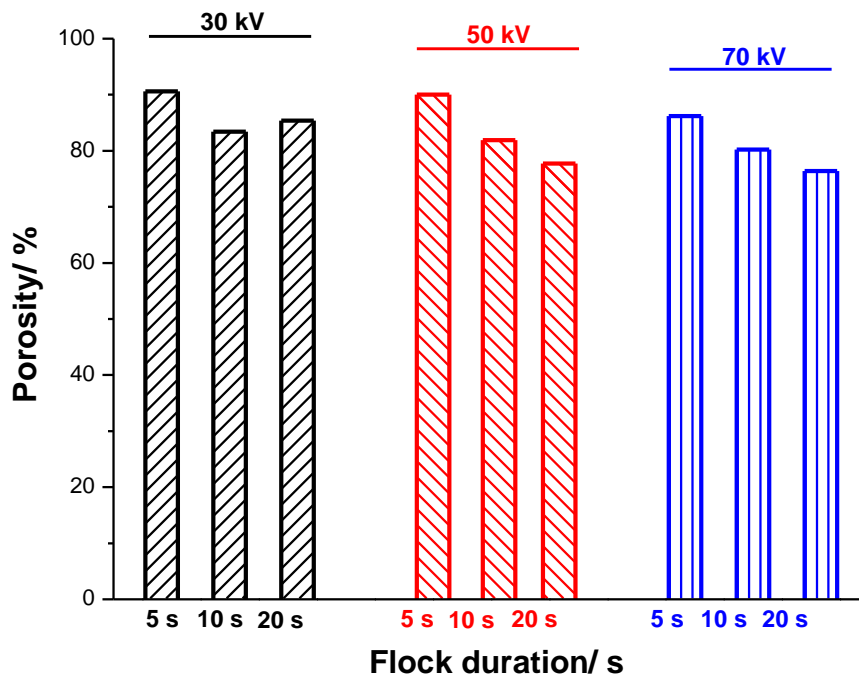


Figure 4-11. The porosity of the PA 6.6 matrix differs with flock durations and process voltages. In brief, fibers arrange themselves more densely with higher fiber density. Therefore, high voltage and long flock duration cause low matrix porosity.

4.1.5 Tribological property of polyamide 6.6 matrixes

Comparing to the common anti-friction materials, the surface of the three-dimensional matrixes consist of numerous PA 6.6 fibers and is therefore quite uneven. As already shown in **Figure 4-9**, not all the flock fibers arranged themselves vertically to the substrate. Moreover, the three-dimensional structure is stable under certain compressive force. These two key factors enable the PA 6.6 flock matrix to be applied as an anti-friction coating material.

Coating the flat substrate with PA 6.6 flock fibers offers a rough surface with high porosity. This kind of coating could minimize the friction strength, which is not desired in many fields. The friction test is carried out with a Thwing-Albert friction test machine (Model FP-2255). (**Figure**

4-12) The static and kinetic coefficients of friction are calculated. The measurements are carried out both in dry and lubricate states with distilled water and isopropanol (IPA) as lubricants. Meanwhile, short flock fibers are dissolved in Hexafluoride isopropanol (HFIP) and poured on a copper plate, a PA 6.6 film is made after evaporation of HFIP; it is the reference for the comparison of different dimensions.

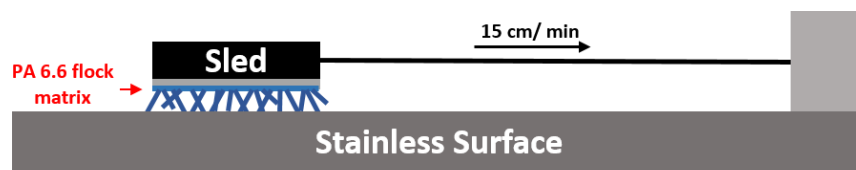


Figure 4-12. Schematically illustration of tribological measurement.

The static and kinetic coefficients of a PA 6.6 fiber-coated aluminum plate in the dry state are 0.30 and 0.28, respectively. The copper plate after coating with flock fibers has slightly lower coefficients of friction (0.27 and 0.26). Films exhibited lower coefficients of friction than three-dimensional fiber matrix. In the lubricated state, the samples are filled with lubricants until saturation. During the measurement, no liquids overflowed from the matrix. Samples with three-dimensional coatings showed much lower coefficients of friction in the lubricated state. The static and kinetic coefficients are 0.07 and 0.06 on an aluminum substrate, 0.08 and 0.07 on a copper substrate. Their values are similar to PTFE. In contrast, the change with film system is not obvious, only maximal 50% reduction of coefficients could be observed. In general, the IPA lubrication system showed better results than distilled water.

4 Three-Dimensional Matrixes with Versatile Functionalities *via* Flocking Technique

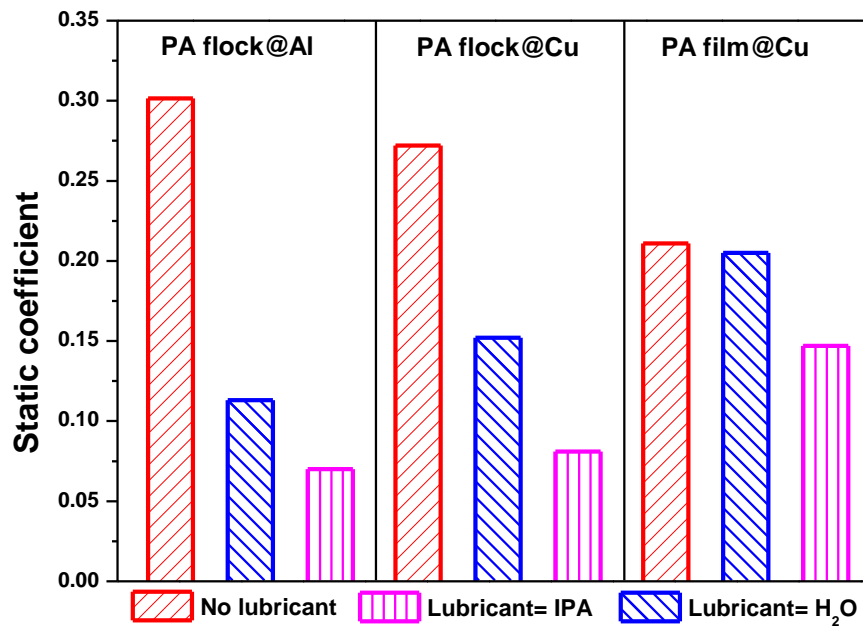


Figure 4-13. The static coefficient of friction of different samples with or without lubricants.

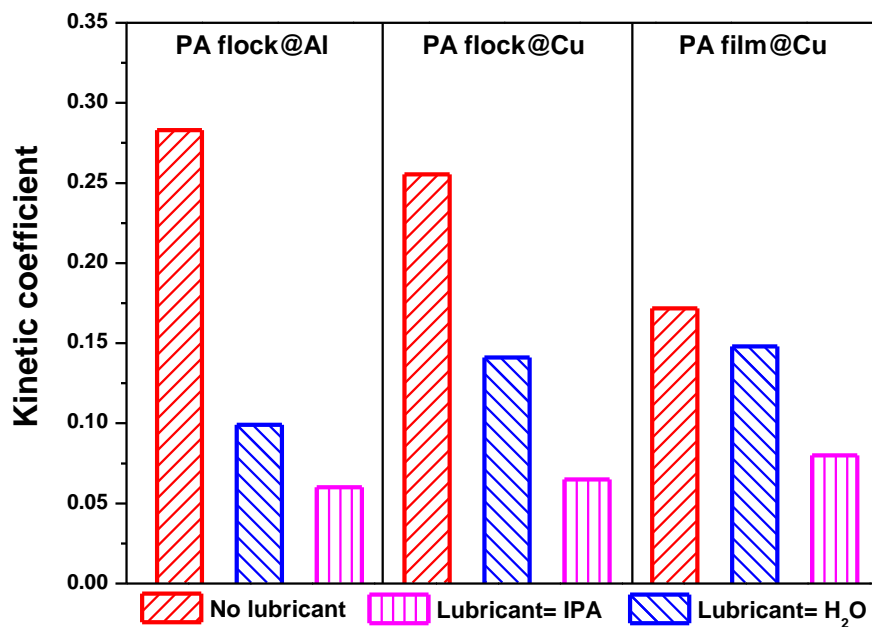


Figure 4-14. The kinetic coefficient of friction of different samples

4 Three-Dimensional Matrixes with Versatile Functionalities *via* Flocking Technique

As compared to other normal materials, the flock samples already showed less coefficient of friction in a dry state, such as glass, aluminum, cast iron or copper. Nevertheless, their frictions are still higher than PTFE. (Figure 4-15)

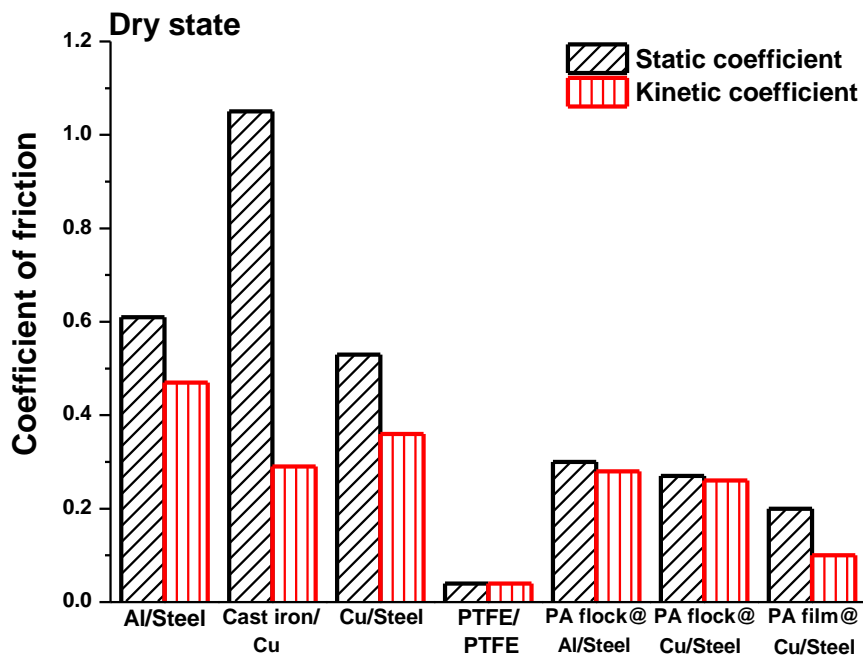


Figure 4-15. The coefficient of friction of different materials in dry states. ^[136-141] The flock matrixes showed better anti-friction property than aluminum or copper.

In the lubricated state, the lubricants are restored between short fibers. Thus, they form extra layers, which could reduce friction and lead to a lower coefficient. The flock fiber system exhibits the similar results to PTFE. (Figure 4-16)

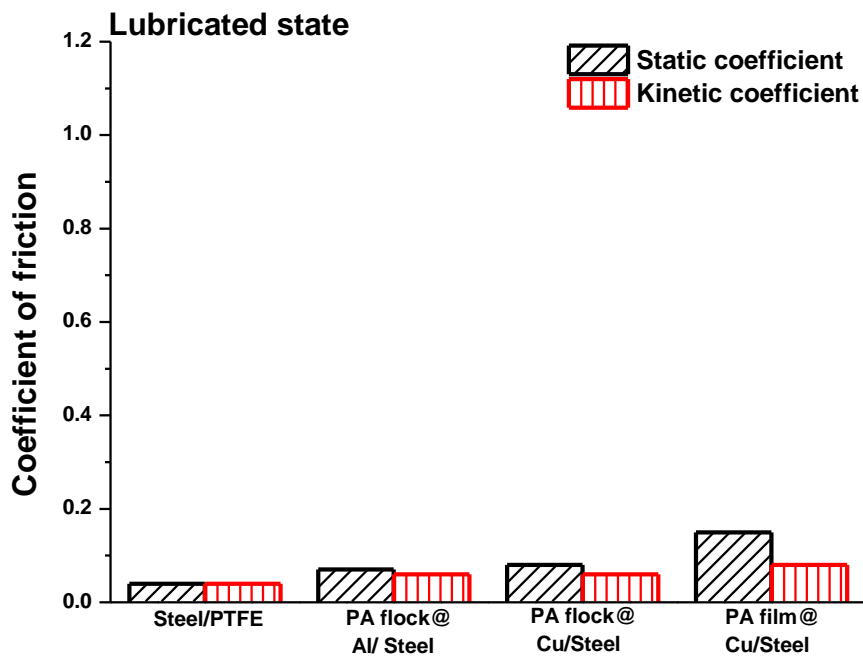


Figure 4-16. The coefficient of friction of different materials in dry states. ^[136-141] The flock matrixes showed the similar anti-friction property to PTFE in the lubricated state.

In order to use this secondary coating method as an antifriction method, the three-dimensional structure must be stable and sustain certain compression. **Figure 4-17** shows the structures of PA 6.6 flock matrixes before and after pressure. Their structures remained the same as the initial flock samples. The flock fibers maintain their three-dimensional structure under pressure; the results are also reproducible. The lower coefficients of friction and its stable porous three-dimensional structure enable flocking of PA 6.6 short fibers as a simple method to create an anti-friction material.

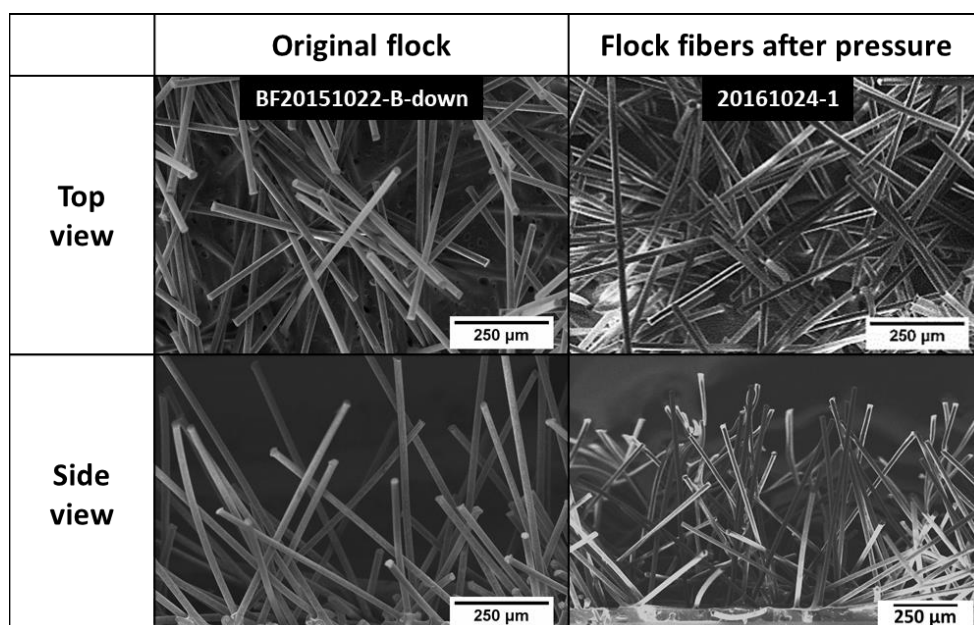


Figure 4-17. SEM images of flock fibers before and after pressure.

4.2 Three-dimensional flock fibers matrix as the loading material for artemisone

Due to its high porosity and complex three-dimensional structures, the flocked fibers offer lots of open pores. Similar to macroporous sponges, the flock fiber matrix is also possible to be applied for drug release. Macroporous sponges, made by a sol-gel process or cryogelation, have high surface-to-volume ratios; meanwhile, their large pore volume ensures the successful loading of drugs. ^[128-129] Comparing to sponges, flock fiber matrix also has high porosity and high surface-to-volume ratio; therefore, it is possible to be applied for drug loading. In this part, artemisone is loaded inside the PA 6.6 flock matrix; the cumulative release behavior of artemisone from this three-dimensional matrix was studied. The artemisone was dissolved in *tert*-Butanol (t-BtOH) and loaded into the PA 6.6 flock matrix. The samples were then frozen in liquid Nitrogen and dry in the freeze dryer over two days. Samples are put into 10 mL buffer solution. After certain time intervals, 1 mL solution is taken out and the

4 Three-Dimensional Matrixes with Versatile Functionalities *via* Floccing Technique

concentration of artemisone in the solution will be measured with HPLC. The signal of sulfur in artemisone with EDX measurement explains the successful loading of artemisone on PA 6.6 flock matrix. In the SEM image of 20160302-42, it is clear, that a high amount of artemisone is found at the bottom of flock fibers. The sample is directly put into the buffer solution; after releasing of artemisone, the signal of sulfur in sample 20160321-42 is quite small and the amount of sulfur reduces a lot. That represents for a successful release of artemisone from the PA 6.6 flock matrix.

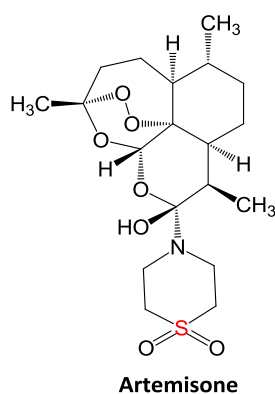


Figure 4-18. Chemical structure of artemisone. The signal of sulfur was detected with EDX and considered to be the proof of the existence of artemisone in the matrix.

Sample	SEM	EDX (blue dots= Sulfur)	wt. % of Sulfur
After loading	<p style="text-align: center;">20160302-42</p> <p style="text-align: right;">50 μm</p>	<p style="text-align: right;">50 μm</p>	Pt1=3.16
			Pt2= 3.4
			Pt3=10.67
After release	<p style="text-align: center;">20160321-42</p> <p style="text-align: right;">50 μm</p>	<p style="text-align: right;">50 μm</p>	Pt1= 0.6
			Pt2=0.81
			Pt3= 0.85

Figure 4-19. SEM and EDX images of samples before and after cumulative release.

4 Three-Dimensional Matrixes with Versatile Functionalities *via* Flocking Technique

In order to compare with the three-dimensional structure, artemisone is also loaded on flat substrates (here: D590 coated glass). For the flat substrate, the fiber length is considered as 0 mm. Taking the fiber length into concern, the longer fibers have much higher surface and higher porosity than shorter ones. Their loading capacity is, therefore, three times higher. Due to the low surface-to-volume ratio, there should be much less artemisone loaded on flat substrates than on three-dimensional PA 6.6 flock matrix. Besides, the cumulative release of artemisone should reach its maximum amount in quite a short while. On the other hand, the flock fibers have an open structure; the loaded artemisone is almost exposed in the air. An extra PPX layer is coated on loaded flock samples to reduce the release rate and make it controllable. Samples without PPX coating layer should have a fast release rate and the fully cumulative release should be achieved in a short time duration. The PPX layer acts as a barrier and could reduce the release speed of artemisone; thus, the cumulative release of artemisone from the sample with the PPX layer should be slower than the one without the PPX layer. Therefore, samples are coated with different PPX layer thickness to find out the influence of the layer thickness on the cumulative release of artemisone.

4 Three-Dimensional Matrixes with Versatile Functionalities *via* Flocking Technique

Table 4-4. Samples coated with PPX-C for the cumulative release of artemisone.

No.	Sample*	Flock length/ mm	Artemisone/ mg	PPX-C/ nm
A	20160513-2**	0	0.7	50
B	20160302-42	0.5	1.8	0
C	20160302-41		1.5	100
D	20160513-34	1	4.6	100
E	20160513-35		4.1	50
F	20160513-33		4.5	20

* D590 is used as the adhesive for all the samples.

** D590 coated glass as a substrate.

D590 coated glass is the substrate for sample 20160513-2, and no more flocking was carried out on this substrate; therefore, it had a two-dimensional structure. Its loading capacity of artemisone was much lower than other three-dimensional flock matrixes in **Table 4-4**. Artemisone was not loaded sufficiently due to the flat structure. After coating with 50 nm PPX-C, artemisone were covered under the hydrophobic layer and not able to be released totally. Therefore. the highest cumulative release amount of sample A was only 46% achieved after 150 min. In contrast, there was no PPX layer in sample B and the highest cumulative release reached 94.3% just after 15 min. (**Figure 4-20**)

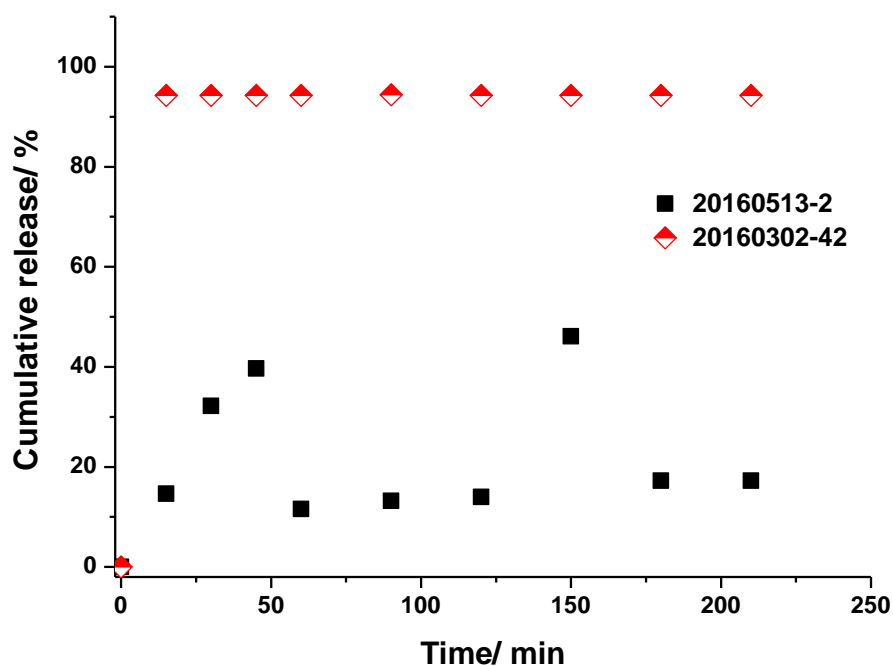


Figure 4-20. Cumulative release of artemisone from the two-dimensional substrate and three-dimensional PA 6.6 flock matrixes.

Keeping the flocking fiber length constant (1 mm), with altering the PPX-C layer changes the cumulative release of artemisone changed as well. (**Figure 4-21**) The thicker PPX-C layer was, the longer it took for artemisone to be released from the substrates, and it took a longer time to reach the maximum cumulative release. The blocking effect for 20 nm PPX-C layer was not as sufficient as thicker ones; the release was thus not controllable and the standard deviations were also very high. The highest cumulative release of the sample with 20 nm PPX was only 70% after 30 min. With 100 nm PPX layer, the release was quite stable. After 150 min, it just reached the highest cumulative release around 90%.

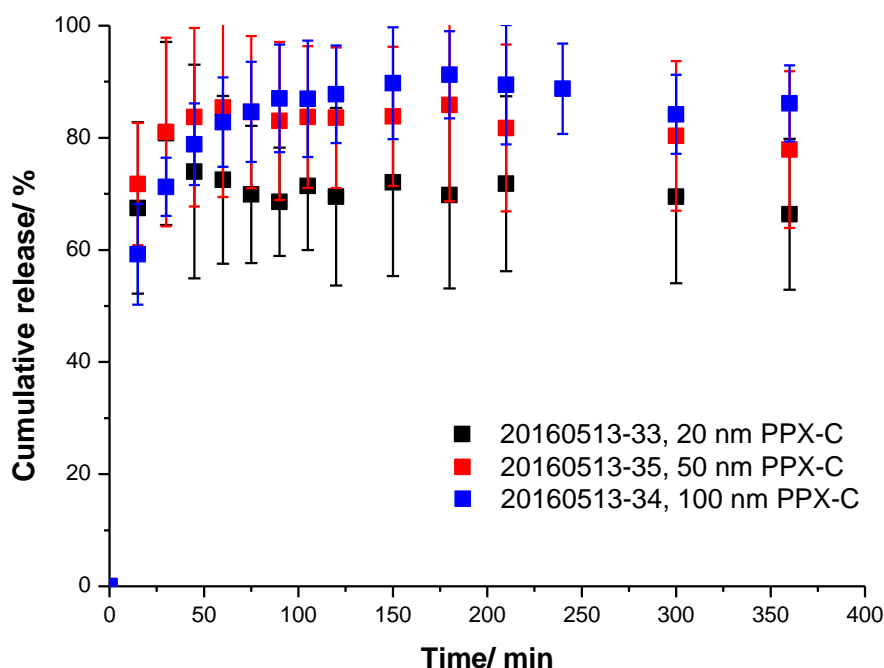


Figure 4-21. Cumulative release of artemisone of PPX-C coated flock matrixes. With an increasing thickness of the PPX layer, the release of artemisone became much more controllable.

4.3 Preparation and characterization of copper flocks

Besides polysiloxane and PPX, copper is also used as a secondary coating material to improve the conductivity of this three-dimensional platform. Consequently, accesses for other applications are added into this system. Its properties such as hydrophilicity/hydrophobicity, conductivity, thermal effect vary with controlled adjustment of the metallization time.

4.3.1 Characterizations of the copper flocks and their conductivity

Metallization of copper was improved by Langner and the details are written in the experimental part. ^[144] In brief, the initial flock samples are at first immersed into an aqueous PEI solution for two hours. The samples maintain their original color during this step. Then, the samples are coated with silver nanoparticles (AgNP) whereby, the color becomes

darker. After metallization with copper, it changes to copper brown. Both the color change and the EDX measurements are convincing evidence of a successful preparation of copper flocks. (**Figure 4-22** and **23**) The original PA 6.6 flock fibers have a relatively smooth surface morphology. After coating with copper, the fibers obtain extra layers, which are clearly seen in SEM images. (**Figure 4-24**)

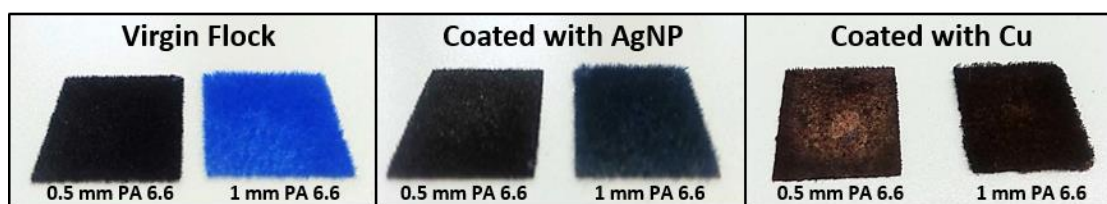


Figure 4-22. Color change of PA 6.6 flocks matrix during metallization with copper.

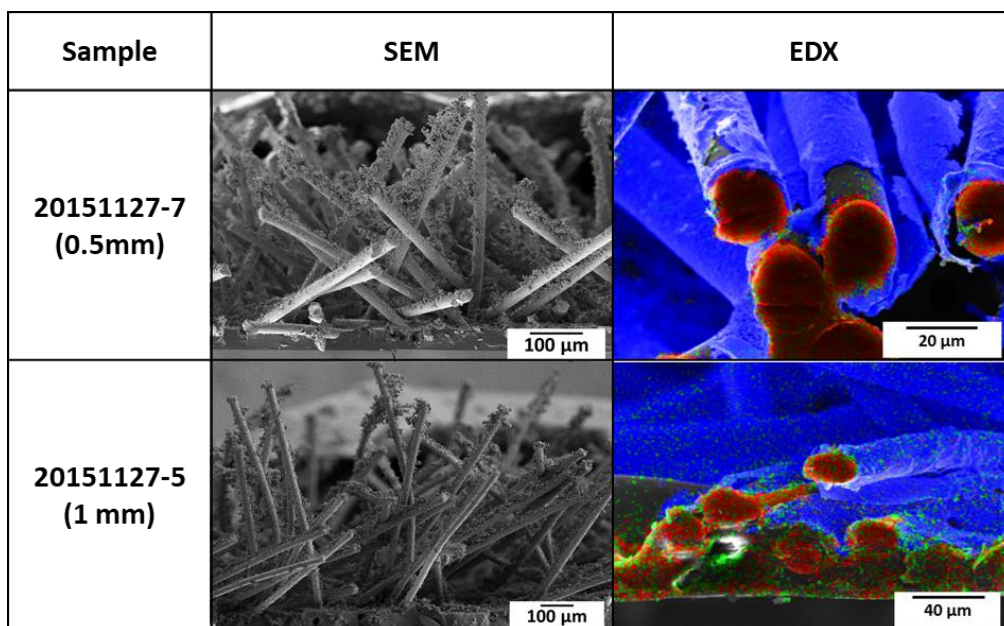


Figure 4-23. SEM and EDX images of different copper flock fibers. The blue color in EDX images represents copper.

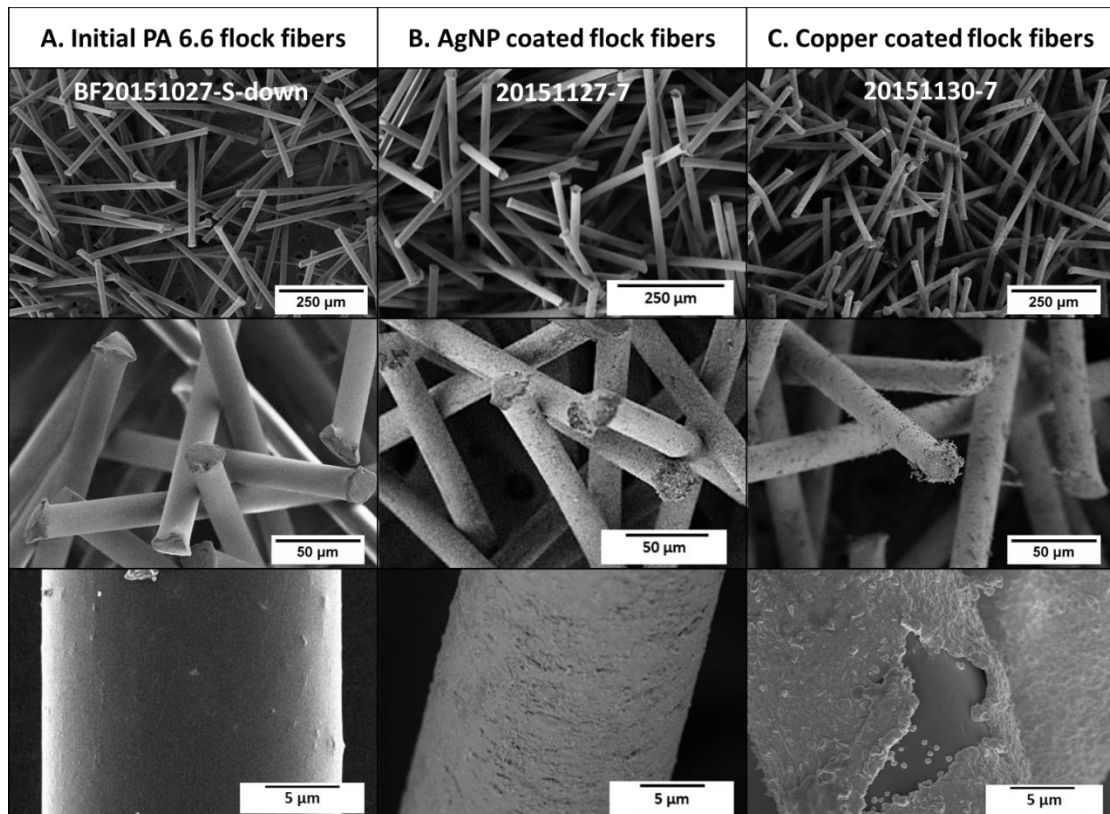


Figure 4-24. SEM images of flock fibers with an initial length of 0.5 mm before coating with AgNP (A), after coating with AgNP (B) and after metallization with copper (C).

The copper density on the surface is strongly dependent on the metallization time and the original PA 6.6 fiber length. As shown in **Table 4-5**, the copper density on the surface increased with longer time for the same fiber length. Meanwhile, copper density on longer fibers was higher than on shorter ones. Sample 20160301-13 was fabricated with 0.5 mm PA 6.6 flock fibers, while 20160301-23 made of 1 mm length. When both were metallized with copper for 1.5 h, the density of copper on the surface increased from 50 g/m² to 104 g/m². This is due to the higher specific surface area of longer fibers. That is why there are much more contact areas for silver nanoparticles, which catalyzed the copper deposition in the following step.

4 Three-Dimensional Matrixes with Versatile Functionalities *via* Flocking Technique

Table 4-5. List of different metallized samples. (Sample size: 18×18 mm²)

Sample	Adhesive	Time/ min	Copper density/ g·m ⁻²	Conductivity*/ S·m ⁻¹
20160301-11**	D564/1	30	20	3490
20160301-12**		60	35	5740
20160301-13**		90	50	8820
20160301-14**		180	61	8570
20160301-21***		30	28	520
20160301-22***		60	69	2450
20160301-23***		90	104	3360
20160301-24***		180	157	4970
20160301-31***	D590	30	16	414
20160301-32***		60	40	2510
20160301-33***		90	46	2670
20160301-34***		180	140	3690
20160301-41**		30	12	981
20160301-42**		60	26	3040
20160301-43**		90	44	5890
20160301-44**		180	108	7710

* Conductivity σ is calculated through electrical resistivity ρ .

$\rho = R_s \frac{A}{l}$, $\sigma = \frac{1}{\rho}$, where R_s means the sheet resistance, l is the sample width and A is the cross-sectional area of a flock ($A = \text{fiber length} \times \text{sample length}$).

** Samples are prepared with flocked fibers of 0.5 mm length.

*** Samples are prepared with flocked fibers of 1 mm length.

4.3.1.1 Control of hydrophilicity/hydrophobicity of copper flock

The copper amount on a flock fibered matrix after metallization is strongly dependent on the reaction duration. As listed in **Table 4-5**, more copper is deposited on flocks with longer metallization duration. When the duration was increased from 0.5 h to 3 h, the increment of copper density on the surface varied from 40 g/m² to more than 120 g/m², depending on the fiber lengths. Simultaneously, their hydrophobicity changes. With a lower density of copper on the surface, matrixes were still hydrophilic and water droplets could penetrate the surface. When the surface density of copper increased to 157 g/m², the surface of copper-flock matrix turned to be hydrophobic. Water droplet suspended on the surface and was easily blown away.

The samples 20160301-13, 20160301044 and 20160301-24 (**Figure 4-25_A, B, and C**) were chosen as examples to explain the tunable hydrophobicity of the copper flock matrixes. Sample A and B were made of flocked PA 6.6 with a length of 0.5 mm. The duration of metallization reaction was 1.5 h for A and 3 h for B. Sample C was fabricated from 1 mm long PA 6.6 fibers with duration of metallization step of 3 h. For flocks of the same initial fiber length (A and B), longer reaction duration led to the higher surface density of copper and higher contact angles. Keeping the duration of metallization the same (B and C), flocks of longer PA 6.6 fibers reached a higher value of copper density due to their higher surface-to-volume ratio. Thus, its contact angle to water was higher than in the case of short fibers.

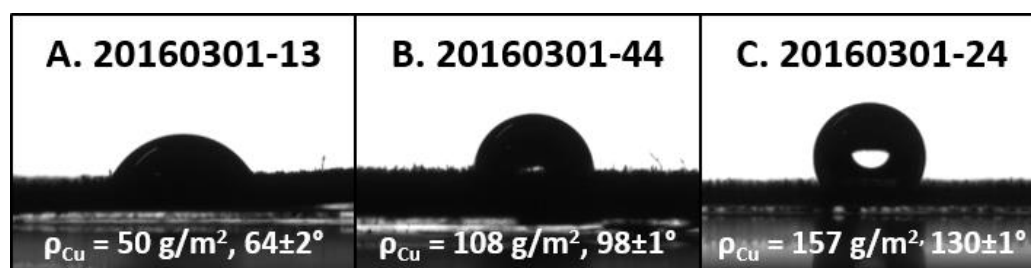


Figure 4-25. The contact angle of water (8 μ L) against copper deposited PA 6.6 flocks depending on the surface density of copper. The higher the surface density of copper is, the more hydrophobic the matrix becomes.

In addition to the different contact angles on flat samples, water droplets behaved also different on tilted ones. With help of a high-speed camera, the behavior of water droplets on three surfaces was recorded. The surface density of copper on sample A in **Figure 4-25** was the lowest among three, and a water droplet stuck on the tilted surface. (**Figure 4-26_B**) With the highest contact angle, water droplet did multiple jumping on the flat surface of sample B; meanwhile, a water droplet bounced from the tilted sample and flipped away. The surface of sample B remained dry. Sample C was less hydrophobic than sample B; a water droplet stuck on the flat surface but bounced away from a tilted one. In conclusion, it is possible to adjust the samples' hydrophobicity and hydrophilicity by changing the length of the flocced polymer fibers and the metallization durations. Overall, hydrophilic copper flock surfaces are created with short polymer fibers and less metallization duration, while hydrophobic copper flocks are made of longer PA 6.6 fibers and extended duration of metallization.

4 Three-Dimensional Matrixes with Versatile Functionalities *via* Flocking Technique

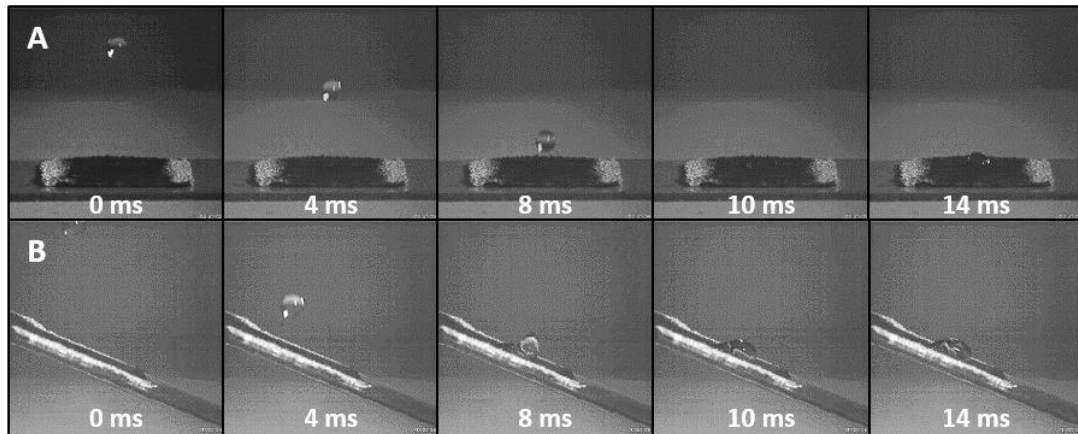


Figure 4-26. The water droplet stuck on either flat (A) or tilted (B) copper-flock surface with lowest copper density. The angle of the tilted surface is 27° .

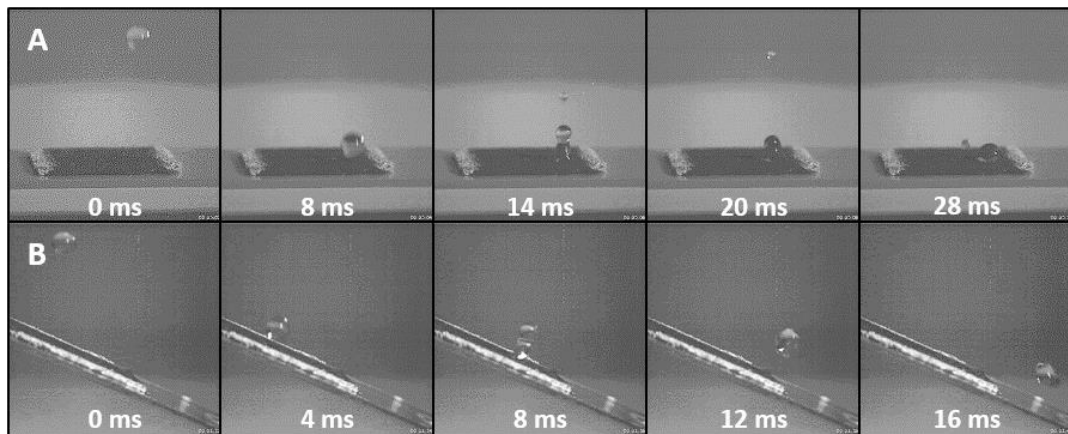


Figure 4-27. By increasing the copper density on the flock, the water droplet stuck on the flat (A) copper flock surface and was bounced away from the tilted surface (B).

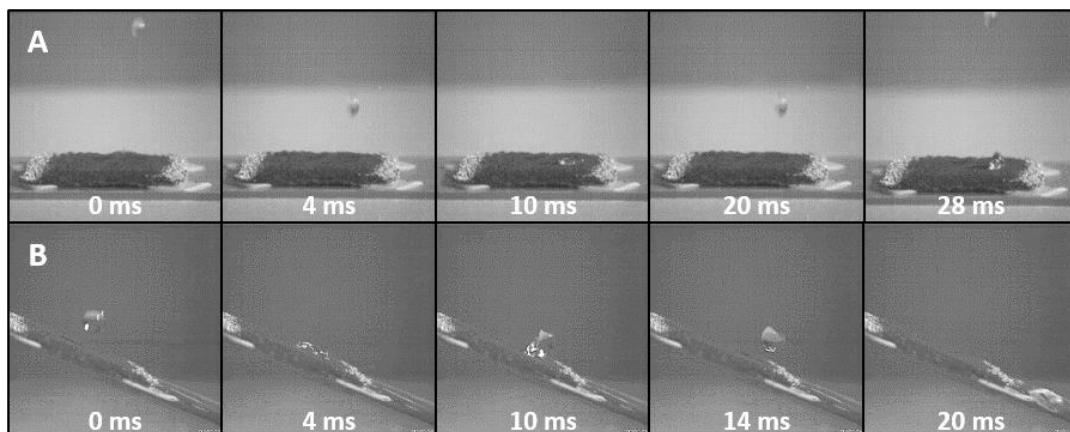


Figure 4-28. With the highest copper density, the water droplet made multiple jumps on a flat surface (A) and was bounced away from a tilted surface (B).

4.3.1.2 The conductivity of copper flocks

The initial PA 6.6 flock matrix was not electrically conductive, yet. After a secondary coating of the PA 6.6 flock with copper, a metal well-known for its high electrical conductivity, the resulting copper flock matrix also became electrically conductive. To determine the electrical conductivity, its sheet resistance is measured as shown in **Figure 4-29**. Two lines of silver glue are drawn on opposing sides of the copper flock matrix, and the measurements were conducted at two diagonally located points. The sheet resistance is calculated according to the formula below,

$$R = \frac{\rho}{t} \times \frac{L}{W} = R_s \frac{L}{W} \dots \dots \dots (7)$$

where R_s represents the sheet resistance and R is the measured value. ^[143]

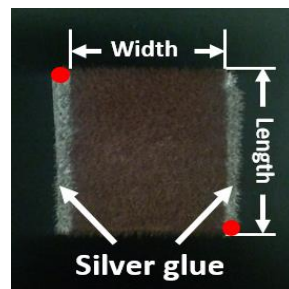


Figure 4-29. Two lines of silver glue were drawn each side of a copper flock and the red dots indicated the two measuring points.

The original PA 6.6 flock matrixes were not electrically conductive, and their resistances are too high to be measured. After 1.5 h of metallization with copper, the sheet resistance decreased significantly and the samples became electrically conductive.

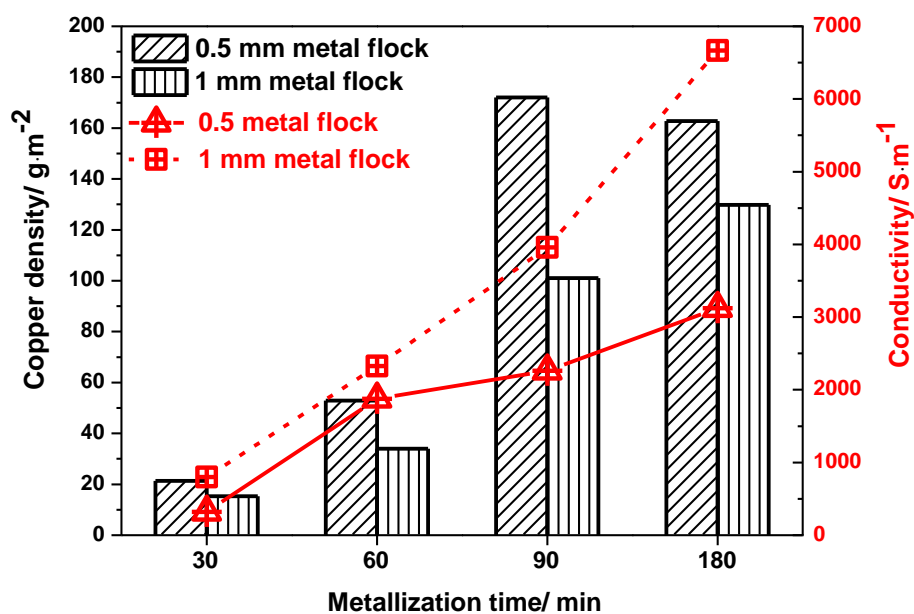
Table 4-6. Change of sheet resistances with metallization of copper for 1.5 h.

Sample*	Sheet resistance/ M Ω	Sample**	Sheet resistance / Ω	Conductivity/ S·m ⁻¹
BF20151022-S-down	immeasurable	20160302-43	0.34	4760
BF20151022-B-down		20160302-33	0.39	2104
BF20151027-S-down		20160302-13	0.23	6667
BF20151027-B-down	6.9	20160302-23	0.31	2577

* Samples of PA 6.6 flocks.

** Samples of copper flocks.

Figure 4-30 showed the relationship between conductivity and metallization duration. Generally, the electrical conductivity increased with longer reaction times for both 0.5 mm and 1 mm long copper flocks. Due to the limited surface area of short flocked fibers, the trend was not as distinctive as with the longer ones.

**Figure 4-30.** The conductivity of different copper flocks in relation to the metallization time.

4.3.1.3 Energy transfer of copper flocks

The electrical energy can be transformed into thermal energy. This is why different copper flock samples also showed a different amount of heat produced in the conductivity measurements. In order to examine the influence of the three-dimensional structure on their electro-thermal-effect, a self-made setup shown in **Figure 4-31** is used. According to formula (8),

$$Q = I^2 R t \dots\dots\dots (8)$$

It is known, that the thermal energy Q only depends on the resistance of samples, if the current I and the time t are kept constant.

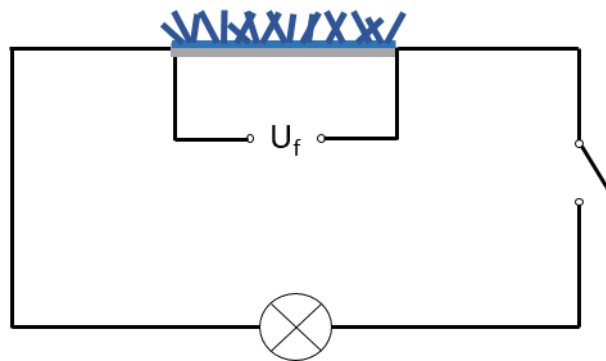


Figure 4-31. Sketch of the setup to determine the conductivity of copper flocks. The temperature of each sample is simultaneously measured with an IR camera.

Copper flocks generally have a far higher surface-to-volume ratio compared to bulky copper films. Moreover, the copper flocks are also very porous, if they are considered as a three-dimensional coating layer of the substrate. Accordingly, the thermal energy can be transferred to the environment more effectively compared to copper films. Therefore, the maximum temperature of copper flocks should be lower than films. To confirm this hypothesis, pure glass and D590-coated glass are used as the

substrates for copper films. Additionally, flock samples are prepared by downwards deposition of PA 6.6 fibers onto the D590-coated glass.

Table 4-7. The resistance of copper films and copper flock.

No.	Sample	Flock length / mm	Copper density/ g·m ⁻²	Measured resistance ^{***} / Ω
A	20161130-1*	0	44	182
B	20161130-2**	0	45	18 kΩ
C	20161130-3	0.5	102	167
D	20161130-4	1	172	112

* The substrate of the copper film is pure glass and no more flocking is carried out.

** The substrate of the copper film is D590-coated glass and no more flocking is carried out.

*** The values are measured at a current flow of 4 A.

In general, copper films on a D590-coated substrate (**Table 4-7_A**) showed the highest resistance at the identical current flow. Copper flocks with longer fiber lengths are more conductive compared to those with shorter fibers. Increasing the current, all the samples exhibit higher peak temperatures (**Table 4-8**). Due to the extraordinary high resistance of 18 kΩ, sample B shows the highest peak temperature. It was burnt when the current increased to 4 A. Sample D with the highest surface density of copper has the highest conductivity. The heat was being transferred all over the highly structured surface more effectively to the environment than in the case of two-dimensional copper films. Therefore, copper flocks showed lower peak temperatures than bulky copper films. As mentioned

above, the surface density of copper also differed as for the flock length changes, which strongly influenced the flocks' resistance. In contrast, the surface density of copper in films stays almost the same. However, here the adhesive material showed considerable influence on the films' resistance.

Table 4-8. Peak temperatures of copper films and flocks at different currents.

No.	Sample	$T_{\text{peak}} / ^\circ\text{C}$			
		@1.5 A	@2 A	@3 A	@4 A
A	20161130-1*	23	23	29	39
B	20161130-2**	30	34	61	burnt
C	20161130-3	23	26	32	43
D	20161130-4	24	25	31	40

* The substrate of the copper film is pure glass and no more flocking is carried out.

** The substrate of the copper film is D590-coated glass and no more flocking is carried out.

Nevertheless, it has to be stated, that the copper films distributed inhomogeneous though copper deposition procedure. Therefore, an inhomogeneous temperature distribution was observed in copper films. It could be seen from the IR camera photographs in **Figure 4-32**, that the temperature distribution on copper flocks was more homogenous than on copper films at a current of 3 A. In case of sample 20161130-2, the temperature rise at a time of 40 s, followed by a temperature drop. After a few seconds, the temperature rose again. However, the copper flocks showed a continuous rise of the peak temperature over time. (**Figure 4-**

33) Considering the copper flocks as three-dimensional coating layers on substrates, it obtained a quite porous structure. Therefore, the heat was transferred to the environment more sufficiently. Comparing to copper flocks, the copper films were much denser and the heat distribution was also quite inhomogeneous. Hence, it led to local overheating and burning of the sample after a few seconds at a current of 4 A on 20161130-2.

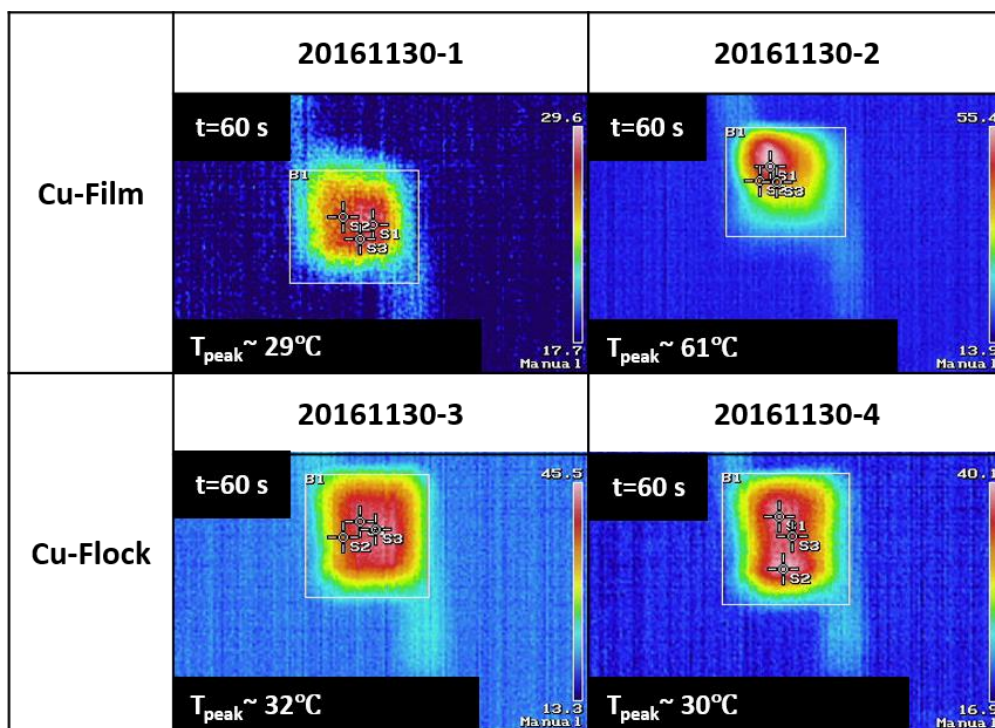


Figure 4-32. Images with IR camera for each system at a current of 3 A at 60 s showed inhomogeneous distribution of heat of copper film and better heat transfer of copper flock.

4 Three-Dimensional Matrixes with Versatile Functionalities *via* Flocking Technique

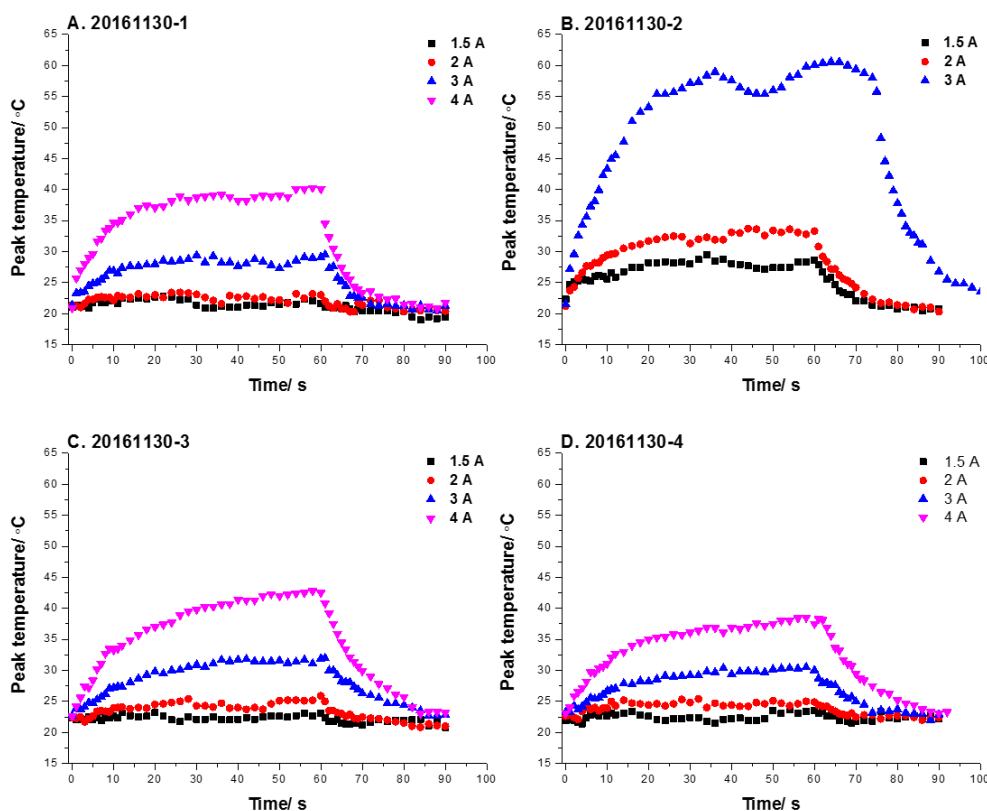


Figure 4-33. Temperature profiles of copper films (A and B) and copper flocks (C and D) at different currents. By virtue of high porosity and low resistance, the peak temperatures of copper flocks (C and D) are much lower.

4.3.2 Applications of copper flocks

Comparing to bulky copper films, copper flock matrixes possess higher surface-to-volume ratios and porous three-dimensional structures. To benefit from the advantages of copper flock matrixes, some applicable possibilities are showed in the following parts.

4.3.2.1 Applied as new electrode materials for microbial fuel cells

Three-dimensional structures such as sponges have already shown high electrical conductivity in different studies. ^[144-145] As copper flocks can be also considered as a three-dimensional coating on the substrate, this layer has open pores; meanwhile, it shows electrical conductivity. In the first application study, It was tried to be used as an electrode material for

microbial fuel cells (MFC). The substrates in these studies are D590-coated copper plates with a size of $2 \times 2 \text{ cm}^2$. Fibers of different lengths are flocked onto the substrate to analyze the influence. The resulting bio-electro catalytic current was generated with help of a secondary, acetate-based electrochemically active biofilm at copper in a semi-batch model experiment. Even though the system is not optimal yet, the copper flock matrixes already showed their potential to be applied as an advanced electrode material in MFCs.

4.3.2.2 Applied as solar thermal energy materials

Although the flocked fibers are vertically aligned to the substrate, they orient themselves into random directions. The copper flock samples were exposed to light and the reflectance was measured in dependence of wavelength. During the reflection measurement, it was found that the copper flock samples absorb light; meanwhile, the slight temperature increase is also observed. It means the photon energy was transferred into thermal energy. Therefore, it is possible to use this energy conversion to make a solar-thermal energy harvesting setup.

4.4 Conclusion

In this part of the work, a multifunctional three-dimensional platform originating from flocked Polyamide 6.6 fibers was successfully produced. Copper flock fibers are fabricated in following processing steps. These matrixes, both the polymer and copper flocks, have a lot of outstanding properties and show high potential in different application fields. (**Figure 4-34**)

4 Three-Dimensional Matrixes with Versatile Functionalities *via* Flocking Technique

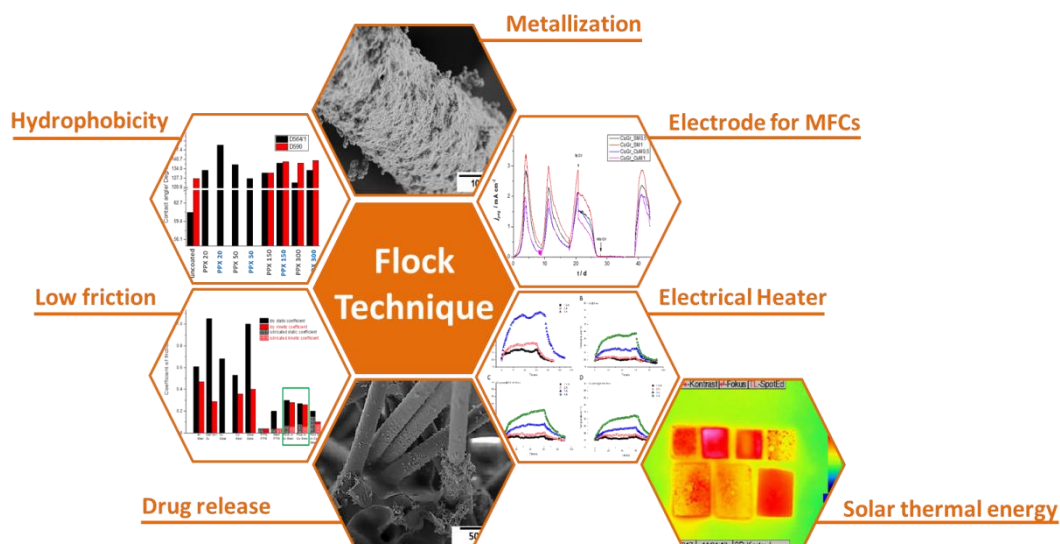


Figure 4-34. Three-dimensional platform *via* flocking technique possess outstanding properties and show high potential in different application fields.

The original polymer flock matrix is very rough and has a heterogeneous surface consisting of fibrous structures and open pores in between. While the samples already showed a relatively low coefficient of friction in the dry state; it could furthermore be decreased by lubrication with water or isopropanol. The anti-frictional properties of the lubricated polymer flocks are similar to PTFE. In addition, there are lots of empty spaces between polymer flock fibers and its high surface-to-volume ratio makes it an interesting candidate for a controlled drug release system. In this study, samples were loaded with artemisone, an antimalarial drug. The cumulative release of artemisone from the pure polymer flock matrix is quite fast and not controllable. To slow down the release rate and to make the process more controllable, artemisone loaded flocks were coated with different PPX-C layers. With PPX-C layer of 100 nm thickness, the release is quite controllable. After 150 min, around 90% of artemisone were released.

4 Three-Dimensional Matrixes with Versatile Functionalities *via* Flocking Technique

For further studies, polymer flock matrixes were also coated with other materials. Firstly, the initial flock samples are coated with siloxane or PPX, through sol-gel treatment and chemical vapor deposition process respectively. By doing this, the polymer flock becomes hydrophobic. The siloxane coated flock samples exhibit water contact angles between 120° and 130°. The siloxane layer thickness increases from the upper to lower points of the fibrous structures. Similar to the application of siloxanes, a coating with PPX can also make polymer flock matrixes hydrophobic. The contact angle of water is approximately independent of PPX layer thickness. The average values are between 135° and 140°. With a PPX layer of 150 nm, the roll-off angle is less than 5°, a water droplet can be blown away easily.

Furthermore, the initial flock samples are plated with copper. By this procedure, they become electrically conductive. The surface density of copper on this three-dimensional matrix is tunable by variation of the metallization time and the length of the flocked fibers. Meanwhile, the hydrophobicity is also dependent on the surface density of copper and is, in consequence, adjustable, as well. These copper flock matrixes can be applied as electrodes for MFCS due to their electrical conductivity. As electric current flows through copper flocks, their temperature increases. Nevertheless, they also show a photo-thermal energy conversion and can be used in energy harvesting facilities.

In comparison to the nanofibers with complex structures which are produced *via* electrospinning, the fiber morphology of polyamide 6.6 fibers is still too simple. Thus, using electrospun fibers as the starting material for the flocking technique might offer a lot of other benefits.

5 Flocking with Short Fibers Prepared *via* Electrospinning

The structure of nanofibers, which are fabricated through electrospinning technique, is usually complex and adjustable with different the electrospinning parameters. Unfortunately, this method is mainly used for the preparation of two-dimensional fabrics, thus limits its applications. On the other hand, flock short fibers, which are made from natural or synthetic materials, are usually milled or cut. The resulted three-dimensional flock matrix has fewer functionalities, due to the simple fiber morphology. Therefore, using electrospun nanofibers as the initial materials for the flocking technique is interesting; meanwhile, the combination of these two classical techniques may add other special properties to the three-dimensional matrix. This part of work is mainly focused on utilization of electrospun nanofibers for flock technique. The electrospun nanofibers are firstly cut into the desired length. Then it is studied, whether the short nanofibers is possible or suitable to be used as flock materials.

5.1 Preparation and characterization of short nanofibers *via* electrospinning

5.1.1 Short PA 6.6 nanofibers and the possibility as flock materials

The commercial PA 6.6 flock fibers are dissolved in hexafluoro-2-propanol (HFIP) or formic acid; the solutions are used for electrospinning. The electrospinning parameters are listed in **Table 5-1**. The concentration of PA 6.6 in HFIP is 15 wt.%; the electrospun nanofibers have a diameter of 3.5 ± 0.75 μm . The weight ratio of PA in concentrated formic acid is increased up to 30wt.% to avoid beads formation. The nanofibers are only 439 ± 63 nm, which is much thinner than prepared one from the HFIP

solution. These PA 6.6 electrospun nanofibers have smooth fiber morphologies. PA electrospun nanofibers from Formic acid solution are used for the preparation of short fibers.

Table 5-1. Parameters of electrospinning of PA 6.6 with different solvents.

Sample	ES20150708	ES20150709
Solvent	HFIP	Formic acid
Voltage/ kV	13	12
Flow rate/ ml/h	5.5	0.35
Relative Humidity/ %	30	50
Temperature/ °C	22	22
Collector distance/ cm	20	20

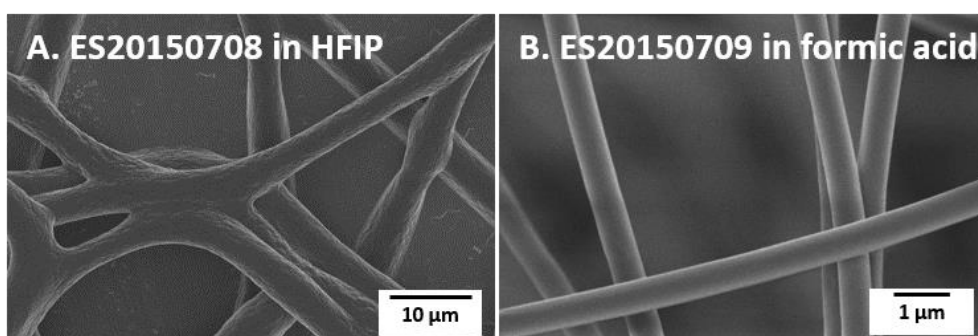


Figure 5-1. SEM images of electrospun PA 6.6 nanofibers. A. HFIP as the solvent, fiber diameter= $3.5\pm 0.75\ \mu\text{m}$. B. Formic acid as the solvent, fiber diameter= $439\pm 63\ \text{nm}$.

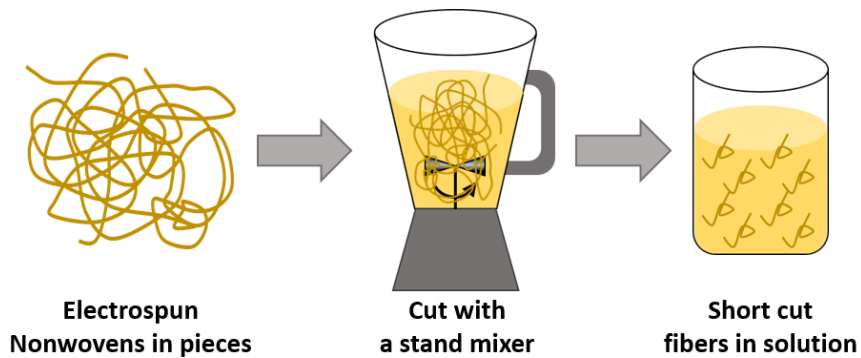


Figure 5-2. Illustration of the cutting process of electrospun nonwovens.

The commercial PA 6.6 flock fibers have a diameter from 20 μm to 60 μm , and their length varies from 0.5 mm to 2 mm. Therefore, their aspect ratios alter from 25 to 50. The electrospun nanofibers are usually very long, and their aspect ratio is extremely high. In this work, the electrospun nanofibers are cut into shorter fibers with the stand mixer to reduce their aspect ratio. As shown in **Figure 5-2** above, the electrospun nonwovens are at first cut into small pieces with a scissor, then a stand mixer is used to cut them into short fibers. The cutting solution is composed of isopropanol/water and Dioxane/water. The composition is listed in the experimental part. The short fibers are first suspended in the solvents mixture and dried on a freeze-drier for two days. To determine the fiber length under a digital microscope, 1mL short fiber dispersion is mixed with 10 wt% PVA solution, to prevent the fibers from aggregation. After freeze-drying, the short fibers are also observed under SEM.

The cutting parameters of short PA electrospun nanofibers are listed in **Table 5-2**. PA nanofibers, prepared with formic acid (Sample ES20150709), were firstly cut for 2 minutes in the stand mixer. The short nanofibers have a length distribution of $718 \pm 325 \mu\text{m}$, and the aspect ratio is around 1500, which is much higher than the one of PA flock fibers. To reduce the

aspect ratio, the short nanofibers were suspended again in solvents mixture and cut for another 2 min, and the resulted sample is 20150916. Although the cutting time increased, the fiber length distribution didn't change a lot. The fiber diameter of the new batch decreased to 600 nm, but the aspect ratio was still way too high. With HFIP as the solvent for electrospinning, thicker PA fibers were produced (Sample ES20180708). Small pieces of this fiber mat are cut in a stand mixer for 2 min, and the short fibers are named of 20150901. On the basis of the thicker diameter, the aspect ratio of these short fibers is reduced to 355. Short fibers suspend very well in solutions with lower concentrations, the fibers are separated from each other. However, it is impossible to separate them as single fibers in the dry state. Comparing to the commercial PA 6.6 flock fibers, the short PA electrospun nanofibers are too long, and they tend to wrap together. (**Figure 5-3**) Their aspect ratios are also too high, and the short nanofibers prefer to agglomerate in the dry state, as shown in **Figure 5-5**.

Table 5-2. Cutting parameters and the fiber length of PA 6.6 nanofibers.

Sample **	Solvent Mixture	Cut time/ min	Fiber length* / μm	Fiber diameter/ μm	Aspect ratio
20150828	IPA/H ₂ O	2	718 \pm 325	0.4 \pm 0.06	1795
20150901	Dioxane/H ₂ O	2	1243 \pm 559	3.5 \pm 0.75	355
20150916	Dioxane/H ₂ O	4	603 \pm 369	0.4 \pm 0.06	1508

* Values are measured with a digital microscope.

** 20150828 and 20150916 are PA nanofibers from formic acid solution, 20150901 is produced with HFIP.

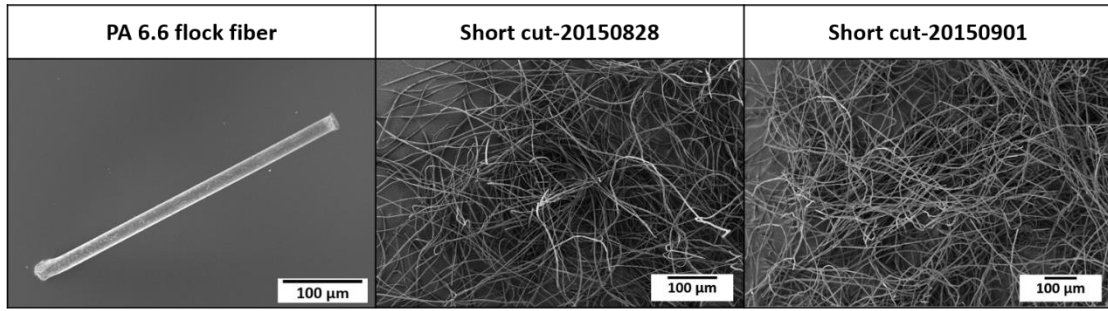


Figure 5-3. SEM images of a single PA flock fiber and short PA 6.6 electrospun nanofibers. The short PA nanofibers are much thinner than the PA flock fiber and tend to wrap together. It is impossible to separate them from each other afterwards.

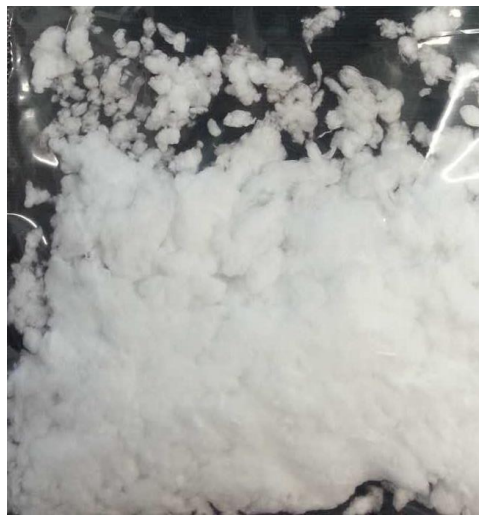


Figure 5-4. Short PA nanofibers (Sample: 20150901) aggregate in the dry state and they are unable to be flocked.

By virtue of the agglomeration of short PA electrospun nanofibers, they are unable to pass through the filtration mesh, which is equipped in the front of the flock chamber. Based on this point, electrospaying of fiber suspension is carried out. On the basis of the high aspect ratio of short nanofibers, the fibers are too flexible to orient themselves vertically to the substrate, when the substrate is lying on the table. Thus, the electrospaying is carried out in direction of parallel to the horizontal with a vertically placed substrate. **(Figure 5-5)** The substrate is previously

covered with the adhesive D564/1. In addition, concentrations of fiber suspensions are also changed.

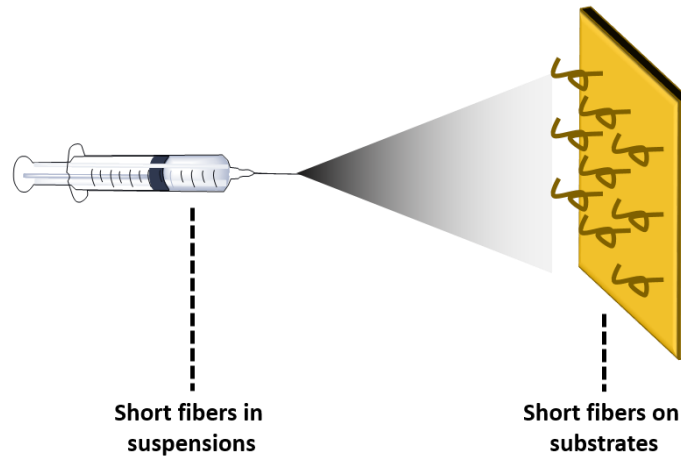


Figure 5-5. Illustration of electrospaying of short PA fiber suspension.

Table 5-3. Parameters of electrospaying of short fiber suspension.

Voltage/ kV	14.5
Flow rate/ mL·h ⁻¹	1.2
Temperature/ °C	21
Relative humidity/ %	22
Distance to collector/ cm	15

Unfortunately, all the short nanofibers are stuck or lying on the substrate. Instead of a three-dimensional grass-like structure, only two-dimensional nonwovens, composed of short nanofibers, are created. This is caused by the higher flexibility of short PA electrospun nanofibers. They prefer to orient themselves paralleled instead of vertically to the substrate. (**Figure 5-6**)

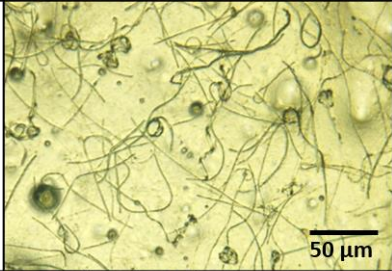
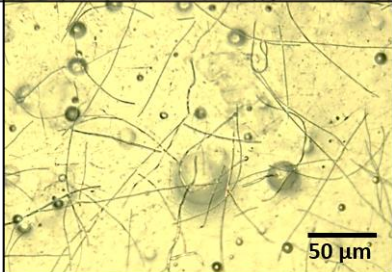
Sample	Concentration/ g·L ⁻¹	Digital microscope
ESP20160127-1	0.44	
ESP20160127-2	0.22	
ESP20160172-3	0.11	

Figure 5-6. Digital microscopic images of sprayed short PA nanofibers with different concentrations of electrospinning solutions. The nanofibers orient themselves parallel instead of vertically to the adhesive substrate.

5.1.2 Short Polyimide nanofibers and the possibility as flock materials

The Polyimide (PI) nanofibers are prepared in DMF solution with a fiber diameter of 487 ± 84 nm; then cut into short fibers with the similar procedure to PA short fibers in IPA/water mixture. ^[146] The short fibers are washed with water, suspended again in water, and freeze-dried. Comparing to the PA nanofibers, the PI nanofibers are much shorter after cutting. **(Figure 5-7)** On the other hand, most of the short PI nanofibers have the similar length. The distribution of fiber length is 2.9 ± 1.3 μm . Their aspect ratio reduced dramatically to less than 6, which is too short for flocking. Besides, the electrostatic interaction between short PI fibers

and the chamber wall is very strong. Thus, the fibers stuck on the wall, and it is impossible to carry out the flocking process. (**Figure 5-8**)

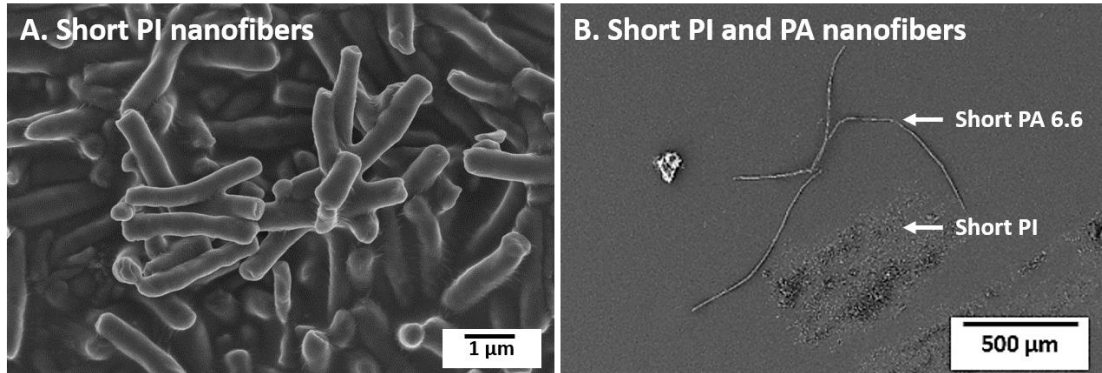


Figure 5-7. Short PI nanofibers (Sample 20150819) have a diameter of 487 ± 84 nm, and the length distribution is 2.9 ± 1.3 μm.

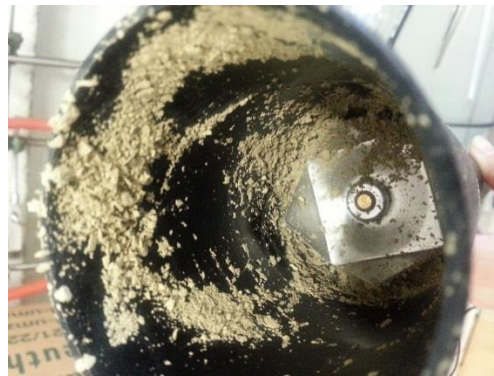


Figure 5-8. The strong electrostatic interaction between short PI fibers and the chamber wall prohibits the flocking process.

5.2 Preparation and characterization of short yarn fibers and the possibility as flock materials

The short electrospun nanofibers, prepared with the stand mixer, tend to agglomerate and wrap together. It's impossible to make flocking of these agglomerations. The main problem of short electrospun nanofibers are the extremely high aspect ratios, and there are two ways to reduce them:

either to increase the nanofiber diameter or reduce the length of short fibers. Usually, the electrospun nanofibers have a diameter in the range of several hundred nanometers to several micrometers. With the existed cutting methods, it is quite hard to reduce the length of short fibers. Therefore, the fiber diameter must be increased. Based on this consideration, yarn fibers are favorable. The yarn fibers, prepared by electrospinning, consist of thousands of single nanofibers; the diameter is usually in the range of micrometers. In this work, the yarn fibers of polyacrylonitrile (PAN) was used.

5.2.1 Preparation of short yarn fibers

PAN is dissolved in DMF/Acetone mixture. The numerous single nanofibers are firstly collected on the rotating funnel with help of a moving cotton thread, the composed single yarn fiber wraps on the rotating collector. The sketch in **Figure 5-9** shows the setup. The polymer solution is loaded in two syringes, which are equipped on the opposite sites of the rotating funnel. A cotton thread is hanged on the collector. During electrospinning, thousands of nanofibers reach firstly the funnel, which rotates at a certain speed. Simultaneously, nanofibers wrap together on the cotton thread and form a single yarn fiber. The yarn fiber is pulled upwards and collected on the rotating collector.

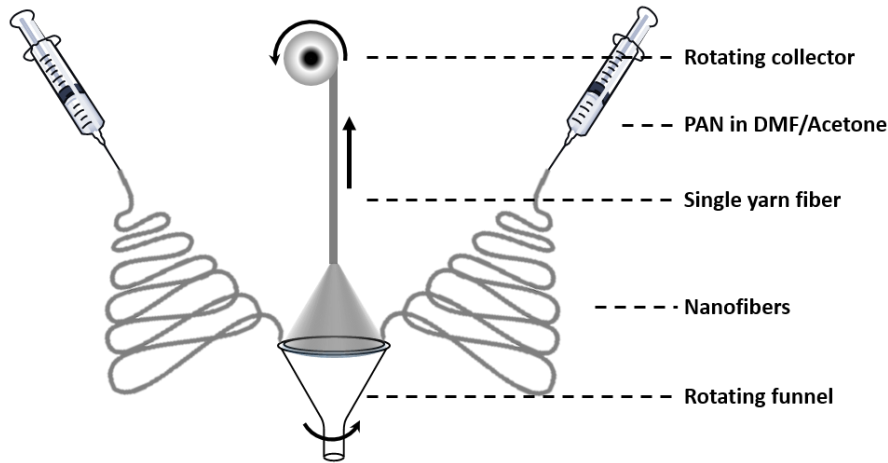


Figure 5-9. Illustration of preparation of yarn fibers.

As discussed, the stand mixer could not reduce the short fiber length sufficiently. In this part of work, the yarn fibers were frozen in liquid N₂ and cut with a blade. However, the cutting process is quite complicated with a low productivity. To increase the productivity, two cutting models are carried out. In the first one, the yarn fibers were wrapped on a glass plate. Then, the PVA/H₂O solution was poured onto the plate. After solidification of PVA, the PAN-immobilized PVA film is prepared and will be cut into 1 mm long slices with a paper cutter. The short PVA slices are then dissolved in distilled water to remove the PVA matrix. (**Figure 5-10**)

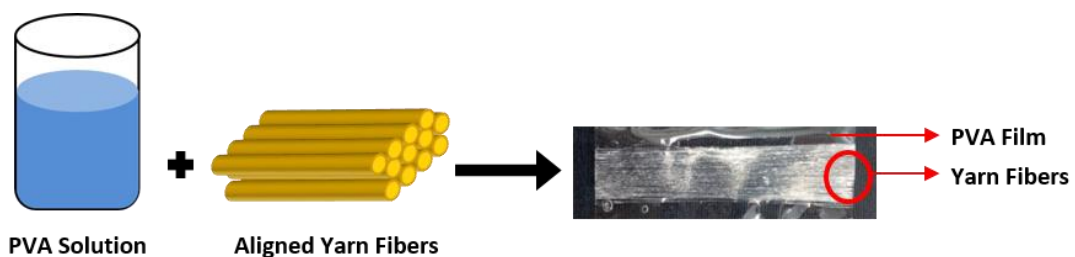


Figure 5-10. Schematically illustration of the cutting model I. Aligned PAN yarn fibers are immobilized in PVA film and then cut into short fibers. After removal of the PVA matrix, 1 mm short yarn fibers are made.

Although the productivity of the cutting model I is already increased as compared to cutting with a blade, it still takes usually 1-2 hours to cut a 10 cm long film. Furthermore, the length of the short fiber is not uniform. To shorten the cutting time and to control the fiber length, using the electronic bread cutter is the key idea in the cutting model II. In this case, a cutting block with a certain thickness is recommended. It is way too thin for the machine with only the PVA film. If the film was increased to the desired thickness, it is too hard to be cut. Therefore, the thin films are piled up and covered with another matrix material. The material should be solid at room temperature. Moreover, it is soft enough to be cut with the electronic cutter. Candle wax is considered to be a good choice in this case. The preparation of this cutting method is shown in **Figure 5-11**.

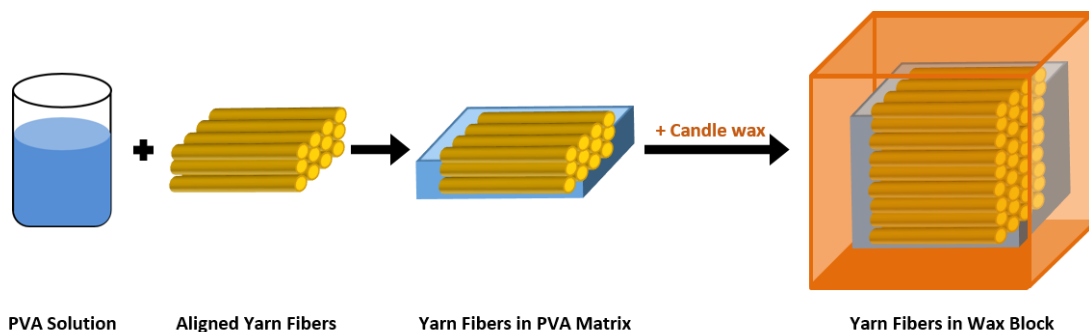


Figure 5-11. Schematically illustration of the cutting model II. Similar to the first cutting model, multilayers of yarn fiber/PVA matrix are piled up and covered with candle wax.

The blocks were easily cut into thin strips, and then they were washed with organic solvents to remove the rest wax. The resulted strips are shown in **Figure 5-12**. They are then dissolved in distilled water to remove the PVA.



Figure 5-12. 1 mm yarn fibers immobilized PVA strips, prepared by the cutting model II.

5.2.2 Flock possibility of yarn fibers

As discussed, the flock fibers should be in a certain range of aspect ratio. Additionally, short fibers could separate from each other. The as-spun yarn fibers were like to stick together. After stretching, the fibers were smoother, and they did not stick together. In this work, both the original and the stretched yarn fibers are cut into short fibers. As shown in **Figure 5-13**, the as-spun yarn fibers have a diameter of $155\pm 12\ \mu\text{m}$, and the stretched ones are $109\pm 3\ \mu\text{m}$. Both of them are thicker than the commercial PA 6.6 flock fibers. When they are cut into 1 mm, the aspect ratios are 6.5 and 9, respectively. The short yarn fibers are observed in PVA solution under a digital microscope.

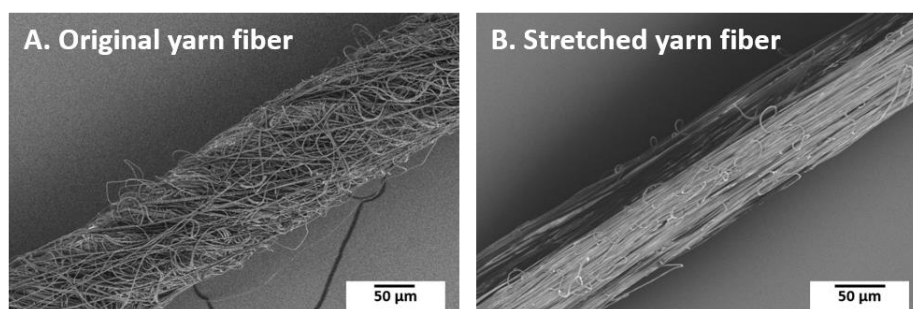


Figure 5-13. SEM images of original yarn fiber (A) and 4-times stretched yarn fiber (B).

The nanofibers in the original yarn fiber twist together and form one single thicker fiber. Therefore, its fiber alignment is not good. At high temperature, the original yarn fibers are stretched 4-times longer to improve the nanofiber alignment. Simultaneously, the stretched fibers are thinner. By virtue of the different morphologies, the nanofibers in original yarn fibers are wrapped compactly together; the stretched yarn fibers are crossly very loose. Accordingly, the nanofibers in the stretched yarn fibers separate from each other and lost their yarn structure in the solution. The original short yarn fibers maintain their single fiber structure in the solution.

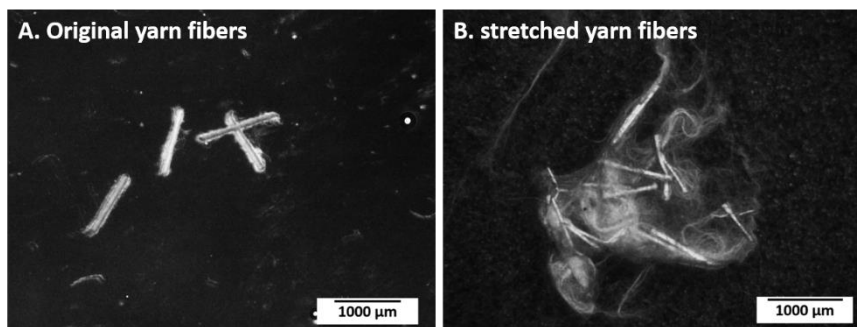


Figure 5-14. Digital microscopic images of short yarn fibers in PVA solution.

As shown in the digital microscope, the stretched short yarn fibers are surrounded with numerous nanofibers. As a consequence, it is impossible to get single short fibers in the dry state with the stretched ones. For the original yarns, the short fibers separate from each other very well in solution. Nevertheless, the short fibers tend to stick together in a dry state, which makes the flocking process impossible.

To get separated single short yarn fibers, the as-spun yarns are coated with a siloxane layer. The obtained short fibers separate well both in solution and in the dry state. Unfortunately, the electrostatic interaction

between the short fibers and the chamber wall is still too strong. Consequently, it is not possible to use these short yarn fibers as flocking material.

5.3 Conclusion

Electrospinning provides nanofibers with different morphologies, and there is no limit on material selection. With this technique, it is possible to create a three-dimensional fiber matrix with various functionalities. This part of work is focused on the study of using electrospun nanofibers as flocking materials.

Firstly, common electrospinning of PA 6.6 and PI was carried out. The as-spun nanofibers were very thin, and their fiber diameters varied from 500 nm to 1 μm . The stand mixer is used to cut the fiber mats. Although the cutting duration was varied, the average length of short fibers did not change a lot. Meanwhile, the distribution of fiber length is very broad. Accordingly, the aspect ratio of these short nanofibers is extremely high as compared to PA flock fibers. On the other hand, the short nanofibers wrapped with each other, which led to the agglomeration both in solution or in the dry state. In addition, the electrostatic interaction between the short fibers and the chamber wall is too strong. As a result of these reasons, the electrospun nanofibers are not suitable for flocking technique.

The aspect ratio of electrospun short fibers should be reduced, and there are two methods to realize this purpose: either to reduce the fiber length or to increase the fiber diameter. According to the existing cutting methods, it is very difficult to reduce the fiber length further.

Consequently, the only possibility is to increase the fiber diameter. Based on this consideration, yarn fibers are advantageous. A single yarn fiber consists of numerous nanofibers, which twist together during electrospinning with a rotating funnel and a rotating collector. The obtained yarn fibers are also endless, similar to nanofibers, yet much thicker. Their diameters are usually several micrometers, which is similar to the PA 6.6 flock fibers. In this work, Polyacrylonitrile (PAN) is dissolved in DMF/acetone mixture, and the PAN yarn fibers have a thickness of ca. 155 μm .

To increase the produce efficiency of the cutting process, the paper cutter and the electronic bread cutter are used. Meanwhile, the aligned yarn fibers are immobilized in PVA or PVA/wax matrixes. Moreover, the fiber length with the electronic bread cutter is more controllable. The original and stretched yarn fibers are used as initial materials. Nanofibers in the stretched yarns are much aligned, and the twisting force is much less than the as-spun ones. Accordingly, the short stretched yarns lost their yarn-structure, and they are surrounded by single nanofibers. In contrast, the as-spun yarn fibers could still maintain their structure under the same condition. However, the dry short fibers tend to stick together, and it makes the flocking process impossible. Coating the original yarn fibers with siloxane layers, the short fibers could be separated both in solution and in the dry state. However, the electrostatic interaction is still so high, that the short fibers stick on the chamber wall and could not be deposited on the substrate.

The short yarn fibers are until this step not capable for flocking technique, and some improvements might be helpful for the future work. Firstly, the

length of short yarns should be increased to reach the aspect ratio range of PA 6.6 flock fibers. Secondly, to coat yarn fibers with a charged outer layer. As discussed, the electrostatic interaction is very strong, so that the short fibers stick inside the chamber. If the yarn fibers are coated with charged outer layers, they will separate from each other due to the electrostatic repulsion. Moreover, yarn fibers could also be fabricated from charged polymers, which should have the similar effect of the charged coating layers.

6 Experimental Part

6.1 Materials

The Table below shows used materials, producers and their purities.

Table 6-1. List of chemicals, producer and their purity.

Material	Producer and purity
Acetone	Industrial grade, distilled before use
2,2'-Azo-bis(2-methylpropion-amidin)-dihydrochloride	Acros Organics, 97%, used as received
Cetyltrimethyl-ammonium bromide	Roth, $\geq 98\%$, used as received
Copper sulfate pentahydrate	Sigma-Aldrich, $\geq 99\%$, used as received
D564/1 (adhesive)	Borcher+Moller GmbH & Co. KG, used as received
D590 (adhesive)	Borcher+Moller GmbH & Co. KG, used as received
Ethanol	Industrial grade, distilled before use
Formaldehyde	Grüssing GmbH, 37%, used as received
Polyisocyanate (Hardener)	Borcher+Moller GmbH & Co. KG, used as received

^1H , ^1H , ^2H , ^2H -Perfluorodecyl Acrylate	Sigma-Aldrich, 97%, used as received
Hydrochloride acid	Grüssing, 25%, used as received
Mowiol®56-98	Aldrich, used as received
n-Decyltrimethoxysilane	Alfa Aesar, 98%, used as received
Parylene-C	SCS coatings, used as received
Parylene-N	SCS coatings, used as received
PEG 300	VWR, used as received
Polyamide 6.6 (Flock fibers)	Borcher+Moller GmbH & Co. KG, used as received
Poly(ethylene imine)	Sigma-Aldrich, 50% w/v in water, used as received
Potassium sodium tartrate tetrahydrate	Sigma-Aldrich, 99%, used as received
Pyridine	VWR, > 99%, used as received
Sodium citrate (anhydrous)	Sigma-Aldrich, $\geq 99.5\%$, used as received
Sodium borhydride	Sigma-Aldrich, $\geq 96\%$, used as received
Sodium hydroxide	VWR, > 99%, used as received

Silver nitrate	Merck, $\geq 99.8\%$, used as received
Tetraethyl orthosilane	Aldrich, $> 99\%$, used as received

6.2 Characterization

6.2.1 Contact angle measurement

Water contact angles were measured with Drop shape analyzer DSA25 from Krüss GmbH and Advance as analysis program. At least five droplets of 8 μL of distilled water were taken to get an average value.

6.2.2 Digital microscopy

Digital microscope of KEYENCE VHX-100 equipped with VH-Z500 and VH-Z35 was used as a method to premeasure of nanofibers, particles and flock fibers. The exact results were given by scanning electron microscope (SEM).

6.2.3 Solid-state NMR

The ^{13}C spectrum (solid-state NMR) is recorded on a Bruker Advance II spectrometer operating at a B_0 field of 7.1 T using a triple-resonance 4 mm Bruker MAS probe and at a rotation frequency of 12.5 kHz. The ^{13}C one-pulse experiments was acquired using a 90° pulse lengths of 3.7 μs with a recycle delay of 60 s. During acquisition proton broadband decoupling was applied using a spinal-64 sequence with a radio-frequency field of 70 kHz. The ^{13}C spectrum is referenced indirectly with respect to tetramethylsilane (TMS) using adamantane as secondary reference.

6.2.4 Electron microscopy

Surface characterization was carried out with scanning electron microscope (SEM). Small fragments of the sample were mounted on a standard sample holder by conductive adhesion graphite-pad (Plano) and examined with a Zeiss LEO 1530 (FE-SEM with Schottky-field-emission cathode; in-lens detector, SE2 detector or Back Scattered Detector) using an accelerating voltage of 3 kV. The samples were sputtered with platinum (1.3 nm using a Cressington HR208 sputter coater and a Cressington mtm20 thickness controller) or vapor coated with carbon (10-20 nm using a Leica EM ACE600) prior to SEM imaging.

Energy-dispersive X-ray spectroscopy (EDX) was used to characterize element distribution of metallized flock samples. Sample preparation is the same process as for SEM, but it would be coated with carbon with a thickness of 10 to 20 nm. The equipment is from Thermo Fisher with a SDD-detector. The analysis system is a Noran-system.

For characterization of bacteria structures, Low-Vacuum-SEM (FEI Quanta 250, ETD detector, LFD detector) was used. An accelerating voltage of 5 kV was applied and the vacuum is 1.05×10^{-3} Pa, 60 Pa or 130 Pa. The sample was mounted on a standard sample holder by conductive adhesion graphite-pad (Plano) without coating of platinum or carbon.

6.2.5 Thermal gravimetric Analysis

To determine the thermal stability of polymers NETZSCH TG 209 F1 Libra was used. Samples were heated to 800 °C with Al₂O₃-pan and 610 °C with Al-pans. Approximately 7 mg polymers were measured with a balance and put in a sample-pan. Whole measurement was taken under nitrogen atmosphere with a heat rate of 10 °C/min. Evaluation of decomposition

curves was done with NETZSCH Proteus software (Thermal Analysis-Version 6.1.0). The curves which showed in this dissertation were replotted with OriginPro 8.5.

6.2.6 Differential scanning calorimetry (DSC)

The DSC measurement was carried out with Mettler Toledo DSC 821c. 3 mg to 7 mg samples were used with a heating/cooling rate of 10 K/min. Aluminum pan was used as sample holders. Evaluation was first done with Mettler STAR^e Software and then replotted with OriginPro 8.5.

6.2.7 Dynamic mechanical analysis (DMA)

The DMA measurement was carried out with METTLER TOLEDO DMA 1 STAR^e System. 20-30 mg Poly-PFDA powders were put inside the sample holder. The measure range is -180°C to 80°C with a heating rate of 2 K/min. Evaluation was done with Mettler STAR^e Software and replotted with OriginPro 8.5.

6.2.8 Gel permeation chromatography (GPC)

For fluorinated polymer GPC measurements was performed with a HFIP-GPC. Chloroform GPC was used to determine molecular weight of polyamide 6.6.

6.2.9 Small angle X-ray scattering (SAXS)

All small-angle X-ray scattering (SAXS) data reported here were measured using the small-angle X-ray system “Double Ganesha AIR” (SAXSLAB, Denmark). The X-ray source of this laboratory-based system is a rotating anode (copper, MicoMax 007HF, Rigaku Corporation, Japan). The data are recorded by a position sensitive detector (PILATUS 300K, Dectris). To cover the range of scattering vectors between 0.002-1.0 Å⁻¹, different detector positions were used. The measurements were done in 1mm

glass capillaries (Hilgenberg, code 4007610, Germany, which were inserted in a linkam heating stage (TST350). The temperature was adjusted from 25-80°C. The data analysis was performed with the software Scatter (version 2.5).

6.2.10 Dynamic light scattering (DLS)

ALV Correlation system was used for particle size measurement, equipped with an ALV-SP 125 compact goniometer, an ALV 5000/E cross correlator and a He-Ne laser ($\lambda = 632.8$ nm). With distilled water diluted solution was put into a cylindrical scattering cell with a diameter of 10 mm and measured with a fixed scattering angle of 90° for 120 s. Each sample was measured at least three times to get a mean value.

6.2.11 Thickness measurement of PPX coating

The thickness of PPX layer was measured with Veeco Dektak 150 Profiometer. For each sample at least three positions would be chosen and the mean value took as final results.

6.2.12 Tribological study of initial PA 6.6 flock matrix

The friction test is carried out with Thwing-Albert friction test machine (Model: FP-2255) The initial PA 6.6 matrix has a size of 5×5 cm², and is fixed on the sled. It is pulled on a flat stainless surface with a constant speed of 15 cm/min. The measuring time is 10 s.

6.3 Synthesis of Poly(perfluorodecyl acrylate)

6.3.1 Emulsion polymerization

Emulsion polymerization was performed using a reactor equipped with 250 mL pressure glass bottle, thermometer and blade-type stirrer. Typically polymerization was performed under argon (Ar) with 1000 rpm of stirring rate.

0.73 g Cetyltrimethyl-ammonium bromide (CTAB), 50.9 g Water, 14.2 g Acetone and 22.6 g ^1H , ^1H , ^2H , ^2H -Perfluorodecyl acrylate (PFDA) were given into a 250 mL pressure glass bottle at room temperature. The mixture will be stirred sufficiently and the solution will be bubbled with Ar for 20 min in order to remove oxygen. After evacuation and charged again with Ar for several cycles, solution was heated with water-bath up to 60 °C. 0.57 g 2,2'-Azo-bis(2-methylpropionamidin)-dihydrochloride (V-50) will be added to the reaction mixture. The polymerization will be started and the stirring speed increased up to 1000 rpm and stopped after 5 h. After precipitation in methanol, the colorless solid could be dried at 46°C and used for further study.

6.3.2 Electrospinning

A typical setup of electrospinning will be used. A high voltage of 30 kV was employed to electrodes. Poly (vinyl alcohol) (Mowiol®56-98, Mw~195,000, PVA) was dissolved in distilled water and blended with Poly-PFDA dispersion in a weight ratio of 17 to 83. This solution is used for electrospinning and PVA amount in solution was kept as 3.5 wt%. Flow rate during the spin process was 0.9 mL/h and whole was carried out at room temperature with a relative humidity around 20%. The electrospun fiber mats was collected on aluminum foil which pre-attached on the counter. The fiber mats were dried in oven at 30°C over night to remove the rest solvent.

6.3.3 Siloxane formation with sol-gel treatment

The sol-gel solution was prepared to modify the surface hydrophobicity of electrospun nonwoven and made by hydrolysis and polycondensation of tetraethyl orthosilane (TEOS) and n-decyl-trimethoxysilane (DTMS).^[151]

Solution mixture would be stirred at room temperature for 1h before use. The coating process was carried out with a dip-coater (RDC-21, Bungard Elektronik GmbH & Co.KG). Subsequently, the nonwoven was cured at 80°C for 10 min. Here, the coating time, coating cycles and solvent concentration will be altered.

Table 6-1. Molar ratio of chemicals in sol-gel solution.

Chemical	Ethanol	TEOS	DTMS	HCl
Equivalent	24.3	0.5	0.1	0.008

6.4 Preparation of multifunctional three-dimensional platform via flocking

6.4.1 Preparation of initial flock samples

MiniFlock machine from Maagflock Company was used for flocking process. Three lengths of flock fibers were used 2 mm (dtex 22), 0.5 mm and 1 mm (dtex 3.3). The mix ratio of adhesive and hardener is 95 to 5 in weight percent. Spin coater was used to apply adhesive mixture onto substrates. Short PA fibers were put into the front chamber of flock machine. Under high voltage (70 kV) they were shot out and stuck onto a glass slide which was pre-covered with adhesive. The flock time was 10 s and the distance to collector was 10 cm. Then the samples would be dried either at room temperature for 24 h (with D564/1) or at 140°C for 40 min (with D590). After washing with distilled water for at least three times to remove the loose flocks, samples are ready for further applications.

Table 6-2. Parameters of adhesive and hardener.

	Chemical composition	Viscosity* / mPas
D564/1	H ₂ O-dispersion of PU	30,000
D590	H ₂ O-dispersion of acrylate polymer	58,000
	Chemical composition	NCO-Content** / %
Hardener	Polyisocyanate	23

* Measured with Brookfield RVT with Spindel of 7.20 rpm at 20°C.

** DIN 53185.

6.4.2 Preparation of artemisone loaded flock samples

First, 47.65 mg artemisone will be dissolved in 2.5 mL *tert*-Butanol to make a solution with concentration of 19.06 mg/mL. Then, with help of 1 mL syringe the solution will be dropped onto flocking samples. The samples will be frozen in liquid nitrogen then hanged on freeze dryer over two days. When the samples are totally free from *t*-BuOH the release process will start. 1 g SDS will be dissolved in 100 mL Milli-pure water and stirred at 37°C for 3 hours to make the puffer solution. The pH-value will be measured with pH-meter from Mettler Toledo-seven compact. The NaHCO₃ solution will be added into puffer solution in order to change the pH to 7.4±0.1. The resulted puffer solution has a pH-value of 7.2 at 37°C.

Artemisone loaded flock samples will be put into 10 mL puffer solution and after a certain period, 1 mL solution will be taken out and the concentration of Artemisone in the solution will be measured with HPLC. The experiment is carried out for three times.

6.4.3 Preparation of siloxane coated flock samples

The sol-gel solution was prepared to modify the surface hydrophobicity of electrospun nonwoven and made by hydrolysis and polycondensation of TEOS and DTMS. The solution would be stirred at room temperature for 1h before use. Subsequently, sample was heated at 80 °C for 10 min. The change of water contact angle will be proved.

6.4.4 Preparation of PPX coated flock samples

Chemical vapor deposition was carried out with Labcoter®1 Parylene Deposition Unit Model PDS 2010 from SCS Coatings. Some certain amount of Parylene monomer was put in the oven and then the temperature would be stepwise increased up to 180°C. The PPX layer thickness was controlled with different amount of monomer Parylene and later measured with Dektak.

Table 6-3. Parylene amount and PPX layer thickness.

Parylene/ mg		70	120	300	600
PPX thickness/ nm	predicted	20	50	150	300
	measured	15	66	170	358

6.4.5 Preparation of copper flock samples^[144]

6.4.5.1 Coating samples with Poly (ethylene imine) (PEI)

Immersing initial flock samples with 40 mg Poly (ethylene imine) (PEI) in 200 mL distilled water for 2 h. Dry samples were used for next step.

6.4.5.2 Preparation of citrate stabilized silver nanoparticle (AgNP)

In 1000 mL distilled water, 42 mg silver nitrate (AgNO₃) and 65 mg sodium citrate will be dissolved. 0.55 mg sodium borhydride (NaBH₄) dissolved in

3 mL distilled water and added to silver solution rapidly under strong stirring for 2 min. The solution turned from colorless to green-brown.

6.4.5.3 Coating flocking sample with silver nanoparticle (AgNP)

With PEI pre-coated samples will put into 10 mL AgNP-solution and shake for 24 h. As long as the color of solution changed, solution should be changed until no obvious color change. Then dried in oven over night at 50 °C.

6.4.5.4 Metallization with copper

Preparation of metallization solutions: 1. 60 g/L copper sulfate pentahydrate ($\text{CuSO}_4 \cdot 5\text{H}_2\text{O}$) in water; 2. 150 g potassium sodium tartrate tetrahydrate ($\text{KNaC}_4\text{H}_4\text{O}_6 \cdot 4\text{H}_2\text{O}$), 60 g sodium hydroxide (NaOH), 12 g PEG 300 and 360 mg Pyridine in 1 L distilled water; 3. 180 mL/L formaldehyde in water.

Procedure: take 50 mL of each solution and diluted with 150 mL distilled water in a flask and heated with a water bath at 45 °C. Immerse AgNP-coated samples into solution under stirring until solution turned to colorless. If necessary, fresh solution would be used to increase the copper density on flock fibers. At the end the samples will be washed with distilled water for several times to get rid of the rest copper and dried in the oven over night at 50 °C.

6.5 Flocking of electrospun nanofibers

6.5.1 Preparation of short cut electrospun fibers

The commercial polyamide 6.6 was dissolved in HFIP or concentrated formic acid. The concentration of each system is 15 wt% and 30 wt%. The electrospinning of these solutions was carried out in high humidity environment, with help of humidifier.

Cutting of PA as-spun fibers: fiber mats was cut into small pieces. Stand mixer was firstly cooled with Ice-water mixture; the cutting solution consists of 100 mL Dioxane and 300 mL distilled water, or 150 mL IPA and 250 mL water. The mixture was frozen with liquid N₂. During the frozen process, solvent was stirred with a spatula. Peel the frozen ice off from the beaker and put into the already cooled mixer. Start the mixer slowly, as long as the frozen ice melted and created a viscose liquid; then put fiber mat pieces into the mixer. At first, cut them for 10 seconds at low rate level and the further 50 seconds at highest level. The mixture was frozen again and repeat the frozen-cutting process again. The total cutting time is 2 min.

The short cut electrospun polyimide fibers and short cut electrospun polyamic acid fibers are produced in the similar methods.

6.5.2 Preparation of short Polyacrylonitrile (PAN) yarn

10 g Polyacrylonitrile was dissolved in 50 mL DMF and 80 mL acetone. With two needles, loaded with polymer solution, nanofibers could be collected on the high-speed rotated funnel. With help of a moving cotton thread, the nanofibers will be collected along the thread, and then forming the yarn fibers.

Cutting with paper cutter: aligned PAN yarn fibers are immobilized in PVA film matrix. After dried on hot plate, the resulted composite membranes are cut with the paper cutter. The cutting length is 1 mm. PVA matrix polymer is removed by washing with distilled water for several times. The dried short fibers are used for flocking.

Cutting with bread cutter: in order to use the bread cutter, single PVA membrane is too thin to be fixed and cut. Candle wax is used as additional

matrix. The in PVA immobilized yarn will be fixed in candle wax and used for cutting. The cutting length is also 1 mm. The wax layer will be washed by organic solvents, such as Acetone or pentane. The PVA membrane will be washed away with distilled water. The short yarn fibers are used for flocking.

Coating yarn with siloxane: the yarn fibers will be wrapped on glass slide with certain alignment. The glass slide is immersed into sol-gel solution (preparation see chapter 6.3.3) for 10 min. After drying in oven, fibers will be immobilized first in PVA and then in candle wax. The cutting procedure is like above. The short yarn fibers are used for flocking.

7 Summary

Two-dimensional superhydrophobic nonwovens and three-dimensional multifunctional matrixes are successfully prepared through electrospinning and flocking techniques. The main objective of this work is to design and produce materials with versatile functionalities and to develop a three-dimensional coating technique, which enriches the application possibilities.

Electrospinning is widely used to prepare nanofiber composed materials; however, in most cases, only organic solvents are used. To use water as the solvent during electrospinning can confer several benefits; it is less toxic, more environmentally friendly, and does not cause health problems. In this work, superhydrophobic nonwovens are successfully produced by green electrospinning from an aqueous dispersion. The two-dimensional nonwovens showed already many outstanding properties and applications; however, lots of other applications demand more complex structures, such as three-dimensional matrix, which has much higher porosity, higher specific surface area, and more complex structure. Flocking, a well-developed classic textile technique, offers the opportunity to create a three-dimensional Polyamide 6.6 matrix; moreover, many surface modifications could be introduced into the matrixes. Moreover, using electrospun nanofibers as flock materials has drawn great interest since the combination of these two techniques can create a more complex three-dimensional matrix, which should have more functionalities.

In the third chapter, an intensive study on the preparation and characterization of superhydrophobic nonwoven fabrics *via* green

electrospinning of aqueous dispersion was reported. The resulting nonwovens are superhydrophobic and possess self-cleaning property. Firstly, poly (perfluorodecyl acrylate) particle dispersion was successfully synthesized by emulsion polymerization. Particles had a diameter of 90 ± 14 nm, as evidenced by dynamic light scattering and scanning electron microscope. A viscous aqueous solution of Poly-PFDA and PVA was used for green electrospinning. The fabricated nanofibers had a diameter of around 550 nm. Altering the concentration of PVA, the fiber diameter and contact angle to water were also adjustable. The nanofibers consisted mainly of poly-PFDA particles. The particles covered the fibers' surfaces and made them rough. Coating with siloxane through sol-gel treatment can reduce the surface energy; moreover, there are many pores instead of particles on the surface of the coated nanofibers. This special nanofiber morphology is the essential matter of its superhydrophobicity. The superhydrophobic nonwovens had a heterogeneous surface, which consists of siloxane-coated nanofibers and air. The areal fraction of air inside the superhydrophobic nonwovens was more than 92%, which was enhanced by numerous micropores (diameter ca. 55 nm); therefore, the nonwovens have contact angles up to 160° . The areal fraction of air decreased to 75% with smaller pores; furthermore, these coated nanofibers possess much smoother surfaces and the contact angles were only 146° . According to thermal behavior studies, the siloxane layer is responsible not only for the formation of pores but also for the protection of poly-PFDA particles from melting. However, the protection effect depends on the layer thickness and the exposure duration at higher temperatures. In addition, fiber alignment also showed a large influence on the hydrophobicity. The aligned thin nanofibers tend to stick together

during the siloxane coating process, whereby the areal fraction of air decreases. The nonwovens are hydrophobic and exhibit contact angles of around 145°.

In chapter four, the multifunctional three-dimensional matrix with commercial polyamide short fibers was fabricated by flocking technique. The obtained three-dimensional matrix provides higher compressive strength, high porosity, and can be used as scaffolds in tissue engineering. In addition, further modifications on this three-dimensional matrix were established, and additional functions were achieved. The initial polymer-grass matrix showed a lower coefficient of friction. The lubricated ones exhibited similar results to polytetrafluoroethylene and might be applied as an anti-friction coating. Moreover, the porous polymer matrixes can be loaded with drugs; coated with PPX-C, a controllable cumulative release of artemisone is achieved after 150 min approximately 90%. Simultaneously, the three-dimensional matrix was also coated with secondary materials, which enlarges its applications. Firstly, the PA 6.6 flock fibers are coated with siloxane layers and PPX, so that the polymer flocks became hydrophobic. Moreover, the polymer flocks were coated with copper and are electrically conductive. The copper flocks can be hydrophobic or hydrophilic depending on the surface density of copper. To conclude, the three-dimensional matrixes, polymer and copper flocks, can be applied as anti-friction coating, drug release system, electrical electrode, and in energy harvesting facilities.

To manipulate the advantages of electrospinning and flocking technique, the preparation of short electrospun nanofibers and the possibility to use them for flocking were studied in chapter five. The short nanofibers

possess a high aspect ratio by virtue of their extremely thin diameters. The yarn fibers, produced by electrospinning with a rotating funnel and a rotating collector, exhibit the similar fiber diameter as PA flocks. The short yarn fibers have an aspect ratio of less than 10. Nonetheless, the short yarns stick together and cannot be flocked. Coating the yarn fibers with siloxane, separated short yarn fibers were observed in dispersion; however, they agglomerated again after dry. Overall, the electrostatic interaction between short yarn fibers and chamber is too strong; it is not possible to flock short yarn fibers. Further modifications of the yarn fibers are still needed.

8 Zusammenfassung

In der vorliegenden Arbeit wurden zweidimensionale superhydrophobe Materialien und dreidimensionale multifunktionale Matrizen mittels Elektrosponnen und elektrostatischer Beflockung erfolgreich hergestellt. Das Forschungsziel liegt in dem Entwurf und der Herstellung von Materialien mit vielseitigen Funktionalitäten. Zudem strebt diese Forschung nach der Entwicklung von dreidimensionaler Beschichtung, wodurch die Anwendungsmöglichkeiten stark bereichert werden können.

Das Elektrosponnen ist eine typische Methode um Nanofasern aus bestehenden Materialien zu präparieren. Die Verwendung von Wasser als Lösungsmittel für das Elektrosponnen könnte einige Vorteile wie z. B. geringere Toxizität, Umweltfreundlichkeit und weniger Gesundheitsprobleme zur Folge haben. In dieser Arbeit wurde superhydrophobes Material aus wässriger Dispersion mittels grünem Elektrosponnen erfolgreich hergestellt. Obwohl diese zweidimensionalen Stoffe herausragende Eigenschaften und Anwendungsmöglichkeiten besitzen, erfordern viele andere Anwendungen noch komplexere Strukturen, z. B. dreidimensionale Matrizen. Eine dreidimensionale Struktur weist hohe Porosität und große spezifische Oberflächen auf, zudem bereichern ihre komplexen Strukturen die Möglichkeiten für zukünftige Anwendungen. Die Beflockung, eine klassische Technik in Textil-industrie, präpariert solche dreidimensionale Beschichtung aus PA 6.6 kurzen Fasern. Durch verschiedene Modifikationen der Oberfläche wird ein noch breiteres Anwendungsspektrum für das System erhalten. Außerdem, ist es auch von Interesse ein neuartiges dreidimensionales Material aus elektrogenesponnenen Nanofasern und der Beflockung-

Technik herzustellen. Die Kombination dieser beiden Techniken kann eine komplexere dreidimensionale Matrix mit mehr Funktionalitäten erzeugen.

Im Kapitel 3 wird eine intensive Studie über die Herstellung und Charakterisierung von superhydrophoben Fasermatten durch grünes Elektrosponnen aus wässriger Dispersion durchgeführt. Die superhydrophobe Fasermatte zeigen auch Selbstreinigende Eigenschaft. Zuerst wurde die Partikel-Dispersion von Poly (Perfluorodecyl Acrylate) mit Hilfe einer Emulsionspolymerisation erfolgreich synthetisiert. Die Teilchen besitzen eine Durchmesser-Verteilung von 90 ± 14 nm, nachgewiesen durch Dynamische Lichtstreuung und Rasterelektronenmikroskopie. Die viskos wässrige Lösung aus Poly-PFDA und PVA wurde für das grüne Elektrosponnen verwendet. Die Nanofasern besaßen einen Durchmesser von ca. 550 nm. Durch Änderung der Konzentration von PVA können sowohl der Faserdurchmesser als auch der Kontaktwinkel eingestellt werden. Die Nanofasern bestehen hauptsächlich aus Acrylate-Polymerpartikeln, welche durch PVA stabilisiert sind. Die Oberfläche der Nanofasern ist ebenfalls mit Partikeln bedeckt, wodurch eine ungleichmäßige Oberfläche entsteht. Die Beschichtung von Siloxane durch ein So-Gel-Verfahren kann die Oberflächenenergie weiter reduzieren. Anstelle von Partikeln entstehen viele Poren entlang der Fasern. Die beschichteten Nanofasern zeigten eine spezielle Morphologie, die für die Superhydrophobizität von essentieller Bedeutung ist. Die superhydrophoben Faservliese weisen eine heterogene Oberfläche auf, welche aus polymeren Nanofasern und Luft besteht. Der Flächenanteil der Luft innerhalb der Fasermatten ist durch zahlreiche Mikroporen (Durchmesser ca. 55 nm) ausreichend erhöht worden. Es beträgt mehr als 92%, wodurch Kontaktwinkel bis zu 160° erhalten werden können. Wird

die Porengröße verringert, fällt der Flächenanteil der Luft auf 75%. Die Faserflächen werden ebener und der Kontaktwinkel beträgt nur noch 146°. Thermische Untersuchungen zeigen, dass die Siloxane-Beschichtung nicht nur für die Poren-Bildung zuständig ist, sondern verhindert sie auch durch ihre Wärmeschutzfunktion das Verschmelzen der Poly-PFDA Partikeln. Der Schutzeffekt hängt hierbei von der Schichtdicke und der Expositionsdauer bei höheren Temperaturen ab. Zusätzlich hat die Faserorientierung einen großen Einfluss auf der Hydrophobizität. Da die dünnen ausgerichteten Nanofasern neigen diese dazu, während des Beschichtungsprozesses zusammenzukleben. Daher verringert sich der Flächenanteil der Luft und das Material zeigt nur Kontaktwinkel von etwa 145°.

Im Kapitel vier wurden multifunktionale dreidimensionale Matrizen mit kommerziellen Polyamid-Kurzfasern durch Beflockung-Technik hergestellt. Die Beflockungsmatrizen liefern eine höhere Druckfestigkeit, sowie eine hohe Porosität, welche als Grundlage in der Textil-Gestaltung verwendet werden könnte. Weitere Modifikationen der Oberfläche werden untersucht, wodurch zusätzliche Funktionen erreicht werden. Die ursprüngliche Polymer-Gras-Matrix zeigte schon einen geringeren Reibungskoeffizienten. Nach der Befeuchtung zeigt es ähnliche Ergebnisse wie Polytetrafluorethylen (PTFE), und konnte als Antihaf-Beschichtung verwendet werden. Weiterhin können die poröse Polymer-Gräser mit Medikaments geladen werden. Mit Hilfe einer PPX-Schicht wird eine kontrollierbare kumulative Freisetzung von Artemisone mit einem Umsatz von ca. 90% innerhalb von 150 min verwirklicht. Gleichzeitig wurde die Matrix auch mit anderen Materialien beschichtet, weitere Anwendungen zu realisieren. Zunächst wurde die Polymer-Gras-

Matrix mit Siloxane und PPX beschichtet, wodurch das resultierende Material hydrophob wurde. Abgesehen davon, wurde die original Polymermatrix mit Kupfer metallisiert und die Kupferflocks weisen eine elektrische Leitfähigkeit auf. Die Hydrophobizität von Kupferflocks kann sowohl hydrophob als auch hydrophil sein, die von der Kupferdichte steuerbar ist. Zusammenfassend, können die dreidimensionalen Matrizen aus Polymer- oder Kupferflocks in unterschiedlichen Bereichen verwendet werden, z.B. als Antihaft-Beschichtung, bei der Freisetzung von Medikamenten, als Elektrode und auch als Energiegewinnungsanlagen.

Um die Vorteilen des Elektrosinnens und der Beflockung zu benutzen, wurden die Präparation der kurzen elektrogenesponnenen Nanofasern und die Möglichkeit, solche kurzen Fasern für die Beflockung zu verwenden, wurden in Kapitel fünf untersucht. Die kurz geschnittenen Nanofasern besaßen ein sehr hohes Aspekt-Verhältnis wegen ihre extrem dünnen Durchmesser. Garnfasern, die durch Elektrosinnen mit gedrehtem Trichter und Kollektor hergestellt werden, zeigen die ähnliche Faserdurchmesser wie PA-flocks. Die Kurzschnittgarnfasern weisen ein Aspekt-verhältnis weniger als 10 auf. Dennoch neigen die kurzen Garnfasern zum Zusammenkleben und ist daher keine Möglichkeit solche Materialien in der Beflockung einzusetzen. Durch eine Siloxane-Beschichtung der Garnfasern sollten separierte Fasern erhalten werden. Dies war allerdings nur in Dispersion und nicht im trockenen Zustand stabil. Ebenfalls ist die elektrostatische Wechselwirkung zwischen den Fasern und der Flockungskammer zu stark. Weitere Modifikationen der Garnfasern stehen noch aus.

9 Outlook

Design, preparation, and application of multifunctional materials are presented in this thesis, which provides the fundamental establishment of different surface modification methods. Either two-dimensional nonwovens or three-dimensional matrixes exhibited versatile functionalities and can be applied in diverse fields. As compared to the two-dimensional structure, matrixes with more complex structure and morphologies show more advantages.

In chapter 3, a green electrospinning process is carried out by using water as the solvent. However, the polymer particles include fluoride, which is now under discussion for its sustainability. To make this process much “greener”, the fluorinated acrylate polymer should be substituted. Polydimethylsiloxane and other silicon polymers have been applied in various fields and can be good choices here. ^[254-270] On the other hand, the fluorinated acrylate particles are produced through emulsion polymerization, and their sizes are around 90 nm. To explore the influence of the particle size on the hydrophobicity, particles of different sizes should be prepared.

Compared to nonwovens, the three-dimensional matrixes manifest a variety of properties and functionalities. For the application as an antifriction coating, the initial flock showed fewer coefficients after lubrication. However, the polymer flock matrix has an open structure, which means the lubricants could not be stored inside the coating layers. To solve this problem, the polymer matrix could be immobilized in some certain materials such as hydrogels, which could absorb lubricants. Poly (N-isopropyl acrylamide) (PNIPAM) absorbs water at a lower temperature

and is applied as hydrogel materials. When PNIPAM microgels are grafted onto the PA 6.6 flock fibers, they uptake water, and the lubricant is then entrapped inside the matrix. On the other hand, the flock matrix could form a thermal insulation layer over the object; it may also protect the objects from freeze or slow down the frozen process.

In the present work, there are a lot of problems with short electrospun yarn fibers. The PAN yarn fibers tend to stick together and are not able to be flocked. Coating the fibers with siloxane layer helps to separate them in dispersion but not in solid states. Under this circumstance, this short fiber dispersion could be used for needless electro spraying or electrospinning, to make a grass-like structure. On the other hand, the charged yarn fibers may reduce the interaction between short fibers, due to the electrostatic repulsive force. Furthermore, yarn fibers of other polymers, such as PA 6.6, PLA or PMMA, could also enlarge the functionalities, as a result of different chemical properties.

Furthermore, the three-dimensional multifunctional polymer matrix has already shown different application possibilities. Till now, the three-dimensional coatings were carried out on flat surfaces. Three-dimensional coatings on substrates with complex geometric structures can also be of interest for more functionalities. Last but not least, the application fields of these platforms will be widely expanded by using functional adhesives, such as pH-responsive or electrical/thermal-conductive.

10 References

1. Polat N. H.; Kap Ö; Farzaneh A.. *Turkish Journal of chemistry* **2018**, *42* (3), 672-682.
2. Mouterde, T.; Lehoucq, G.; Xavier, S.; Checco, A.; Black, C. T.; Rahman, A.; Midavaine, T.; Clanet, C.; Quere, D. *Nature Materials* **2017**, *16* (6), 658-663.
3. Pakdel A.; Zhi C.; Bando Y; Nakayama T. and Golberg D. *ACS NANO* **2011**, *5* (8), 6507-6515.
4. Sun T.L.; F. L.; Gao X.F. and Jiang L. *Accounts of Chemical Research* **2005**, *38*, 644-652.
5. Butt, H.-J.; Semperebon, C.; Papadopoulos, P.; Vollmer, D.; Brinkmann, M.; Ciccotti, M. *Soft Matter* **2013**, *9* (2), 418-428.
6. Li, X. M.; Reinhoudt, D.; Crego-Calama, M. *Chemical Society Reviews* **2007**, *36* (8), 1350-1368.
7. Teo, W. E.; Ramakrishna, S. *Nanotechnology* **2006**, *17* (14), 89-106.
8. Jeevahan, J.; Chandrasekaran, M.; Britto Joseph, G.; Durairaj, R. B.; Mageshwaran, G. *Journal of Coatings Technology and Research* **2018**, *15* (2), 231-250.
9. Wang, N.; Zhao, Y.; Jiang, L. *Macromolecular Rapid Communications* **2008**, *29* (6), 485-489.
10. Ma, M.L.; Mao, Y.; Gupta, M.; Gleason, K.K. and Rutledge, C. C. *Macromolecules* **2005**, *38*, 9742-9748.

11. Liu, Z.; Wang, H.; Wang, E.; Zhang, X.; Yuan, R.; Zhu, Y. *Polymer* **2016**, *82*, 105-113.
12. Chen, Y.; Kim, H. *Applied Surface Science* **2009**, *255* (15), 7073-7077.
13. Zhu, M.; Zuo, W.; Yu, H.; Yang, W.; Chen, Y. *Journal of Materials Science* **2006**, *41* (12), 3793-3797.
14. Patel, S. U.; Manzo, G. M.; Patel, S. U.; Kulkarni, P. S.; Chase, G. G. *Journal of Nanotechnology* **2012**, *2012*, 1-7.
15. Xue, Y.; Wang, H.; Yu, D.; Feng, L.; Dai, L.; Wang, X.; Lin, T. *Chemical Communications (Camb)* **2009**, *42*, 6418-20.
16. Jiang, L.; Zhao, Y.; Zhai, J. *Angewandte Chemie* **2004**, *116* (33), 4438-4441.
17. Zhu, M.; Hua, D.; Pan, H.; Wang, F.; Manshian, B.; Soenen, S. J.; Xiong, R.; Huang, C. *Journal of Colloid and Interface Science* **2018**, *511*, 411-423.
18. Ji, H.; Zhao, R.; Li, Y.; Sun, B.; Li, Y.; Zhang, N.; Qiu, J.; Li, X.; Wang, C. *Colloids and Surfaces A: Physicochemical and Engineering Aspects* **2018**, *538*, 173-183.
19. Jiang, S.; Hou, H.; Agarwal, S.; Greiner, A. *ACS Sustainable Chemistry & Engineering* **2016**, *4* (9), 4797-4804.
20. Bubel, K.; Zhang, Y.; Assem, Y.; Agarwal, S.; Greiner, A. *Macromolecules* **2013**, *46* (17), 7034-7042.
21. Giebel, E.; Getze, J.; Röcker, T.; Greiner, A. *Macromolecular Materials and Engineering* **2013**, *298* (4), 439-446.
22. Giebel, E.; Mattheis, C.; Agarwal, S.; Greiner, A. *Advanced Functional Materials* **2013**, *23* (25), 3156-3163.

23. Agarwal, S.; Greiner, A. *Polymers for Advanced Technologies* **2011**, 22 (3), 372-378.
24. Hollister, S. J. *Nature Materials* **2005**, 4, 518-524.
25. Pfister, A.; Landers, R.; Laib, A.; Hübner, U.; Schmelzeisen, R. and Mülhaupt, R. *Journal of Polymer Science: Part A: Polymer Chemistry* **2004**, 42, 624-638.
26. Liao, C. J.; Chen, C. F.; Chen, J. H.; Chiang, S. F.; Lin, Y. J.; Chang, K. Y. *Journal of Biomedical Materials Research* **2002**, 59 (4), 676-81.
27. Yong, J.; Chen, F.; Yang, Q.; Huo, J.; Hou, X. *Chemical Society Reviews* **2017**, 46 (14), 4168-4217.
28. Subhash Latthe, S.; Basavraj Gurav, A.; Shridhar Maruti, C. and Shrikant Vhatkar, R. *Journal of Surface Engineered Materials and Advanced Technology* **2012**, 02 (02), 76-94.
29. Sas, I.; Gorga, R. E.; Joines, J. A.; Thoney, K. A. *Journal of Polymer Science Part B: Polymer Physics* **2012**, 50 (12), 824-845.
30. W. Barthlott, C. N. *Planta* **1997**, 202, 1-8.
31. Yoshimitsu, Z.; Nakajima, A.; Watanabe, T.; Hashimoto, K. *Langmuir* **2002**, 18 (15), 5818-5822.
32. Feng, L.; Li, S.H.; Li, Y.S.; Li, H.J.; Zhang, L.J.; Zhai, J.; Song, Y.L; Liu, B.Q.; Jiang, L. and Zhu, D.B. *Advanced Materials* **2002**, 14 (24), 1857-1860.
33. Law, J. B.; Ng, A. M.; He, A. Y.; Low, H. Y. *Langmuir* **2014**, 30 (1), 325-331.
34. Watson, G. S.; Cribb, B.W. and Watson J. A. *ACS NANO* **2010**, 4 (1), 129-136.

35. Falde, E. J.; Yohe, S. T.; Colson, Y. L.; Grinstaff, M. W. *Biomaterials* **2016**, *104*, 87-103.
36. Lee, J. Y.; Han, J.; Lee, J.; Ji, S.; Yeo, J. S. *Nanoscale Research Letters* **2015**, *10* (1), 505.
37. Guo, Z.G.; Liu, W.M. *Progress in Chemistry-Beijing-* **2006**, *18* (6), 721.
38. Wagner, P.; Fürstner, R.; Barthlott, W.; Neinhuis, C. *Journal of Experimental Botany* **2003**, *54* (385), 1295-1303.
39. Koch, K.; Bhushan, B.; Barthlott, W. *Progress in Materials Science* **2009**, *54* (2), 137-178.
40. Bormashenko, E.; Gendelman, O.; Whyman, G. *Langmuir* **2012**, *28* (42), 14992-14997.
41. Gao, X.F.; Jiang, L. *Nature* **2004**, *432* (4), 36.
42. Bormashenko, E.; Bormashenko, Y.; Stein, T.; Whyman, G.; Bormashenko, E. *Journal of Colloid and Interface Science* **2007**, *311* (1), 212-216.
43. Fang, Y.; Sun, G.; Bi, Y.; Zhi, H. *Science bulletin* **2015**, *60* (2), 256-263.
44. Parker, A.R. and Lawrence, C.R. *Nature* **2001**, *414*, 33-34.
45. Gao, X.; Yan, X.; Yao, X.; Xu, L.; Zhang, K.; Zhang, J.; Yang, B.; Jiang, L. *Advanced Materials* **2007**, *19* (17), 2213-2217.
46. Hosono, E.; Fujihara, S.; Honma, I.; Zhou, H. *Journal of the American Chemical Society* **2005**, *127* (39), 13458-13459.
47. Tan, S.; Xie, Q.; Lu, X.; Zhao, N.; Zhang, X.; Xu, J. *Journal of Colloid and Interface Science* **2008**, *322* (1), 1-5.

48. Borrás, A.; Barranco, A.; and González-Elipe, A. R. *Langmuir* **2008**, *24*, 8021-8026.
49. Forsberg, P.; Nikolajeff, F.; Karlsson, M. *Soft Matter* **2011**, *7* (1), 104-109.
50. Ming, Z.; Jian, L.; Chunxia, W.; Xiaokang, Z.; Lan, C., *Soft Matter* **2011**, *7* (9), 4391-4396.
51. Marmur, A. *Langmuir* **2003**, *19*, 8343-8348.
52. Ding, B.; Ogawa, T.; Kim, J.; Fujimoto, K.; Shiratori, S. *Thin Solid Films* **2008**, *516* (9), 2495-2501.
53. Zhang, X.; Zhang, J.; Ren, Z.; Li, X.; Zhang, X.; Zhu, D.; Wang, T.; Tian, T.; Yang, B. *Langmuir* **2009**, *25* (13), 7375-7382.
54. Cheng, Z.; Gao, J.; Jiang, L. *Langmuir* **2010**, *26* (11), 8233-8238.
55. Sheng, X.; Zhang, J. *Langmuir* **2009**, *25* (12), 6916-6922.
56. Hozumi, A.; Cheng, D. F.; Yagihashi, M., *Journal of Colloid and Interface Science* **2011**, *353* (2), 582-587.
57. Su, R.; Liu, H.; Kong, T.; Song, Q.; Li, N.; Jin, G.; Cheng, G. *Langmuir* **2011**, *27* (21), 13220-13225.
58. Young, T. *Philosophical Transactions of the Royal Society of London* **1805**, *95*, 65-87.
59. Celia, E.; Darmanin, T.; Taffin de Givenchy, E.; Amigoni, S.; Guittard, F. *Journal of Colloid and Interface Science* **2013**, *402*, 1-18.
60. Yan, Y.Y.; Gao, N; and Barthlott, W. *Advances in Colloid and Interface Science* **2011**, *169*, 80-105.

61. Cassie, A. B. D.; Baxter, S. *Transactions of the Faraday Society* **1944**, *40* (0), 546-551.
62. Lee, S. M. a. H. J. *Langmuir* **2007**, *23*, 6004-6010.
63. Guo, Z.; Liu, W.; Su, B. L. *Journal of Colloid and Interface Science* **2011**, *353* (2), 335-355.
64. Kang, M.; Jung, R.; Kim, H.-S.; Jin, H.-J. *Colloids and Surfaces A: Physicochemical and Engineering Aspects* **2008**, *313-314*, 411-414.
65. S. W. IP, J. M. T. *Journal of Materials Science* **1994**, *29*, 688-692.
66. Bedford, N. M.; Steckl, A. J. *ACS Applied Materials & Interfaces* **2010**, *2* (8), 2448-2455.
67. Grignard, B.; Vaillant, A.; de Coninck, J.; Piens, M.; Jonas, A. M.; Detrembleur, C.; Jerome, C. *Langmuir* **2011**, *27* (1), 335-42.
68. Kim, P.; Wong, T. S.; Alvarenga, J.; Kreder, M. J.; Adorno-Martinez, W. E.; and Aizenberg, A. *ACS NANO* **2012**, *6* (8), 6569-6577.
69. Han, D.; Steckl, A. J. *Langmuir* **2009**, *25* (16), 9454-9462.
70. Wang, L.; Yang, S.; Wang, J.; Wang, C.; Chen, L. *Materials Letters* **2011**, *65* (5), 869-872.
71. Viswanadam, G.; Chase, G. G. *Separation and Purification Technology* **2013**, *104*, 81-88.
72. Yohe, S. T.; Colson, Y. L.; Grinstaff, M. W. *Journal of the American Chemical Society* **2012**, *134* (4), 2016-9.
73. Yohe, S. T.; Herrera, V. L.; Colson, Y. L.; Grinstaff, M. W. *J Control Release* **2012**, *162* (1), 92-101.

74. Horbett, T. A. *Biomater: Interfac Phenom Applic* **1982**, 17, 233-244.
75. Feldman, K.; Hähner, G.; Spencer, N.; Harder, P.; Grunze, M. *Journal of the American Chemical Society* **1999**, 121 (43), 10134-10141.
76. Harder, P.; Grunze, M.; Dahint, R.; Whitesides, G.; Laibinis, P. *The Journal of Physical Chemistry B* **1998**, 102 (2), 426-436.
77. Ratner, B. D.; Bryant, S. J. *Annual Review of Biomedical Engineering* **2004**, 6, 41-75.
78. Alves, N. M.; Shi, J.; Oramas, E.; Santos, J. L.; Tomás, H.; Mano, J. F. *Journal of Biomedical Materials Research Part A: An Official Journal of The Society for Biomaterials, The Japanese Society for Biomaterials, and The Australian Society for Biomaterials and the Korean Society for Biomaterials* **2009**, 91 (2), 480-488.
79. Piret, G.; Galopin, E.; Coffinier, Y.; Boukherroub, R.; Legrand, D.; Slomianny, C. *Soft Matter* **2011**, 7 (18), 8642-8649.
80. An, Y.; Friedman, R. *Journal of Hospital Infection* **1996**, 33 (2), 93-108.
81. Crick, C. R.; Ismail, S.; Pratten, J.; Parkin, I. P. *Thin Solid Films* **2011**, 519 (11), 3722-3727.
82. Tang, P.; Zhang, W.; Wang, Y.; Zhang, B.; Wang, H.; Lin, C.; Zhang, L. *Journal of Nanomaterials* **2011**, 2011, 2.
83. Li, L.; Tian, J.; Li, M.; Shen, W. *Colloids and Surfaces B: Biointerfaces* **2013**, 106, 176-180.
84. Xing, S.; Harake, R. S.; Pan, T. *Lab on a Chip* **2011**, 11 (21), 3642-3648.
85. Qing, G.; Sun, T. *Advanced Materials* **2011**, 23 (14), 1615-1620.

86. Wolinsky, J. B.; Colson, Y. L.; Grinstaff, M. W. *Journal of controlled release* **2012**, *159* (1), 14-26.
87. Sridhar, R. and Ramakrishna, S. *Biomatter* **2013**, *3* (3), 24281.
88. Doimoto, M.; Greiner, A. *Macromolecular Materials and Engineering* **2018**, *303*, 1700621.
89. Agarwal, S.; Greiner, A.; Wendorff, J. H. *Progress in Polymer Science* **2013**, *38* (6), 963-991.
90. Wendorff, J. H.; Agarwal, S.; Greiner, A. *Electrospinning: Materials, Processing, and Applications*. Wiley-VCH Verlag GmbH & Co. KGaA. : **2012**.
91. Huang, Z.-M.; Zhang, Y. Z.; Kotaki, M.; Ramakrishna, S., *Composites Science and Technology* **2003**, *63* (15), 2223-2253.
92. Wannatong, L.; Sirivat, A.; Supaphol, P. *Polymer International* **2004**, *53* (11), 1851-1859.
93. Reneker, D. H.; Yarin, A. L. *Polymer* **2008**, *49* (10), 2387-2425.
94. Reneker, D. H.; Yarin, A. L.; Fong, H.; Koombhongse, S. *Journal of Applied physics* **2000**, *87* (9), 4531-4547.
95. Lyons, J.; Li, C.; Ko, F. *Polymer* **2004**, *45* (22), 7597-7603.
96. Stoiljkovic, A.; Venkatesh, R.; Klimov, E.; Raman, V.; Wendorff, J. H.; Greiner, A. *Macromolecules* **2009**, *42* (16), 6147-6151.
97. Stoiljkovic, A.; Ishaque, M.; Justus, U.; Hamel, L.; Klimov, E.; Heckmann, W.; Eckhardt, B.; Wendorff, J. H.; Greiner, A. *Polymer* **2007**, *48* (14), 3974-3981.
98. Ganachaud, F.; Katz, J. L. *ChemPhysChem* **2005**, *6* (2), 209-216.

99. Sun, J.; Bubel, K.; Chen, F.; Kissel, T.; Agarwal, S.; Greiner, A. *Macromolecular Rapid Communications* **2010**, *31* (23), 2077-2083.
100. Agarwal, S.; Horst, S.; Bognitzki, M. *Macromolecular Materials and Engineering* **2006**, *291* (6), 592-601.
101. Sachlos, E.; Czernuszka, J. T. *European Cells and Materials* **2003**, *5*, 29-40.
102. Fang, Q.; Hanna, M. A. *Industrial Crops and Products* **2001**, *13* (3), 219-227.
103. Auras, R.; Harte, B.; Selke, S. *Macromolecular bioscience* **2004**, *4* (9), 835-864.
104. Lim, L.-T.; Auras, R.; Rubino, M. *Progress in polymer science* **2008**, *33* (8), 820-852.
105. Hutmacher, D. W. *Biomaterials* **2000**, *21*, 2529-2543.
106. Duan, G.; Jiang, S.; Jérôme, V.; Wendorff, J. H.; Fathi, A.; Uhm, J.; Altstädt, V.; Herling, M.; Brey, J.; Freitag, R.; Agarwal, S.; Greiner, A. *Advanced Functional Materials* **2015**, *25* (19), 2850-2856.
107. Duan, G.; Jiang, S.; Moss, T.; Agarwal, S.; Greiner, A. *Polymer Chemistry* **2016**, *7* (15), 2759-2764.
108. Jiang, S.; Uch, B.; Agarwal, S.; Greiner, A. *ACS Applied Materials and Interfaces* **2017**, *9* (37), 32308-32315.
109. Jiang, S.; Reich, S.; Uch, B.; Hu, P.; Agarwal, S.; Greiner, A. *ACS Applied Materials and Interfaces* **2017**, *9* (39), 34286-34293.
110. Duan, G.; Bagheri, A. R.; Jiang, S.; Golenser, J.; Agarwal, S.; Greiner, A. *Biomacromolecules* **2017**, *18* (10), 3215-3221.

111. Mikos, A. G.; Lyman, M. D.; Freed, L. E. and Langer, R. *Biomaterials* **1994**, *15* (1), 55-58.
112. Nofar, M.; Park, C. B. *Progress in Polymer Science* **2014**, *39* (10), 1721-1741.
113. Salerno, A.; Oliviero, M.; Di Maio, E.; Iannace, S.; Netti, P. *Journal of Materials Science: Materials in Medicine* **2009**, *20* (10), 2043-2051.
114. Mooney, D. J.; Powell, C.; Piana, J.; Rutherford, B. *Biotechnology Progress* **1996**, *12* (6), 865-868.
115. Inzana, J. A.; Olvera, D.; Fuller, S. M.; Kelly, J. P.; Graeve, O. A.; Schwarz, E. M.; Kates, S. L.; Awad, H. A. *Biomaterials* **2014**, *35* (13), 4026-34.
116. Lam, C. X. F.; Mo, X.; Teoh, S.-H.; Hutmacher, D. *Materials Science and Engineering: C* **2002**, *20* (1-2), 49-56.
117. Bose, S.; Vahabzadeh, S.; Bandyopadhyay, A. *Materials today* **2013**, *16* (12), 496-504.
118. Moss, T.; Paulus, I. E.; Raps, D.; Altstädt, V.; Greiner, A., *e-Polymers* **2017**, *17* (4), 255-261.
119. Chen, Z.; Ren, W.; Gao, L.; Liu, B.; Pei, S.; Cheng, H. M. *Nature Materials* **2011**, *10* (6), 424-428.
120. Du, A.; Zhou, B.; Zhang, Z.; Shen, J. *Materials (Basel)* **2013**, *6* (3), 941-968.
121. Pierre, A. C.; Pajonk, G. M. *Chemical Reviews* **2002**, *102* (11), 4243-4266.
122. Si, Y.; Yu, J.; Tang, X.; Ge, J.; Ding, B. *Nature Communications* **2014**, *5*, 5802.
123. Si, Y.; Wang, X.; Yan, C.; Yang, L.; Yu, J.; Ding, B. *Advanced Materials* **2016**, *28* (43), 9512-9518.

124. Boltnew, A.; Spartanburg, S.C. *United States Patent US 3,356,521*. **1967** Dec. 5.
125. Sieroff, M. *Lenzinger Berichte* **1975**, *38*, 108-121.
126. Kim, Y.K; Lewis, A. F.; Hou, Y. J.; Pottokaran, F. *National textile center annual Report: Nov.* **1999**, F97-D01.
127. BOLGE, S. W. *Journal of Coated Farbrics* **1991**, *21*, 123-131.
128. Walther, A.; Hoyer, B.; Springer, A.; Mrozik, B.; Hanke, T.; Cherif, C.; Pompe, W.; Gelinsky, M. *Materials (Basel)* **2012**, *5* (3), 540-557.
129. Sung, B.-J.; Aly, A.; Lee, S.-H.; Takashima, K.; Kastura, S.; Mizuno, A. *Plasma Processes and Polymers* **2006**, *3* (9), 661-667.
130. Lee, H. J.; Michielsen, S. *Journal of Polymer Science Part B: Polymer Physics* **2007**, *45* (3), 253-261.
131. Mironova, V.S.; Park, M. *Composites Science and Technology* **2000**, *60*, 927-933.
132. Nosonovsky, M.; Bhushan, B. *Multiscale dissipative mechanisms and hierarchical surfaces: friction, superhydrophobicity, and biomimetics*. Berlin: Springer; **2008**.
133. Orowan, E. *Proceedings of the Royal Society of London. Series A* **1970**, *316*, 473-491.
134. Ding, B.; Li, C.R.; Hotta, Y.; Kim, J.H.; Kuwaki O. and Shiratori, S. *Nanotechnology* **2006**, *17*, 4332-4339.
135. Hench, L. L.; West, J. K. *Chemical Reviews* **1990**, *90*, 33-72.
136. Chen, Z.; Ren, W.; Gao, L.; Liu, B.; Pei, S.; Cheng, H. M. *Nature Materials* **2011**, *10* (6), 424-428.

- 137 Yabuki, A.; Arriffin, N. *Thin Solid Films* **2010**, *518* (23), 7033-7037.
- 138 Thewsey, D. J.; Zhao, Y. Y. *physica status solidi (a)* **2008**, *205* (5), 1126-1131.
- 139 Lu, L.; Shen, Y.F.; Chen, X.H.; Qian, Li.H; Lu, K. *Science* **2004**, *304*, 422-426.
140. Tai, C. C.; Rose, J. H.; Moulder, J. C. *Review of Scientific Instruments* **1996**, *67* (11), 3965-3972.
141. Nath, P.; Chopra, K. L. *Thin Solid Films* **1974**, *20*, 53-62.
142. Langner, M.; Agarwal, S.; Baudler, A.; Schröder, U.; Greiner, A. *Advanced Functional Materials* **2015**, *25* (39), 6182-6188.
143. Heaney, M. B., Electrical Conductivity and Resistivity. In *Electrical Measurement, Signal Processing, and Displays*, Webster, J. G., Ed. CRC Press: 2004.
144. Langner, M.; Agarwal, S.; Baudler, A.; Schröder U.; Greiner, A. *Advanced Functional Materials* **2015**, *25*, 6182-6188.
145. Baudler, A.; Schmidt, I.; Langner, M.; Greiner, A.; Schröder, U. *Energy and Environmental Science* **2015**, *8*, 2048-2055.
146. Master Thesis of Markus Langner. *Herstellung, Charakterisierung und Verarbeitung von Polymer-Kurzchnitt-Nanofasersonsuspensionen aus electrogesponnener Fasern*. **2012**.

11 Acknowledgments

At this moment, I would like to declare my deep gratitude to all the people who have involved in this work and assisted me to finish the thesis.

First and foremost, I want to take this occasion to thank my supervisor Prof. Dr. Andreas Greiner, for giving me the opportunity to work in this highly interesting and interdisciplinary topic. He guided me into polymer science step by step. Without his impartial support, patience, and encouragement, I could not achieve so much in the last few years. I learned quite a lot from him, which influences me to be a better person in the future life.

Likewise, I also want to thank Prof. Dr. Seema Agarwal for her helpful support and fruitful scientific discussions throughout my promotion.

Moreover, I would like to express my great thanks to the Graduate School of University of Bayreuth and the Bayreuth Graduate School of Mathematical and Natural Sciences (BayNAT) for the financial support and training courses. I also want to thank Deutsche Forschungsgemeinschaft (DFG) for the financial support during my research.

I want to acknowledge Prof. Dr. Andreas Fery and Prof. Dr. Volker Altstädt for being my BayNAT mentors and for supporting me during my Ph.D. time.

I thank Prof. Dr. Norbert Hampp from the Philipps-University of Marburg, Prof. Dr. Uwe Schröder from the Technical University of Braunschweig and their doctoral candidates for the fruitful cooperation and the regular exchange of ideas and suggestions.

Special thank I would give to Mitusnobu Diomoto, who built up the fundamental study of superhydrophobic nonwovens. Moreover, I would like to thank my lab mates and the entire MCII group for the great working atmosphere and supports

from various aspects. I also want to thank Martina Heider for the support of SEM measurements and Rika Schneider for the GPC measurements. Without them, I could accomplish my research successfully. In addition, I want to thank Gaby Oliver for her patience and her help with all bureaucratic matters.

I am grateful to my colleges who took part in the time-consuming burden of proof-reading of this thesis. Therefore, my thanks are addressed at, no particular order, Marius Feldmann, Mina Heidari, Julia Kronawitt, Mahsa Mafi, Florian Käfer, and Martin Pretscher.

Last but not least, I owe numerous thanks to my mother for her unconditional love, trust, and support. I shared my joy and sorrow with her in the last few years. Her confidence in me encouraged me to face all the toughness and keep going. Without her understanding, patience, and kindness, I could not achieve so much.

(Eidesstattliche) Versicherungen und Erklärungen

(§ 9 Satz 2 Nr. 3 PromO BayNAT)

Hiermit versichere ich eidesstattlich, dass ich die Arbeit selbstständig verfasst und keine anderen als die von mir angegebenen Quellen und Hilfsmittel benutzt habe (vgl. Art. 64 Abs. 1 Satz 6 BayHSchG).

(§ 9 Satz 2 Nr. 3 PromO BayNAT)

Hiermit erkläre ich, dass ich die Dissertation nicht bereits zur Erlangung eines akademischen Grades eingereicht habe und dass ich nicht bereits diese oder eine gleichartige Doktorprüfung endgültig nicht bestanden habe.

(§ 9 Satz 2 Nr. 4 PromO BayNAT)

Hiermit erkläre ich, dass ich Hilfe von gewerblichen Promotionsberatern bzw. -vermittlern oder ähnlichen Dienstleistern weder bisher in Anspruch genommen habe noch künftig in Anspruch nehmen werde.

(§ 9 Satz 2 Nr. 7 PromO BayNAT)

Hiermit erkläre ich mein Einverständnis, dass die elektronische Fassung meiner Dissertation unter Wahrung meiner Urheberrechte und des Datenschutzes einer gesonderten Überprüfung unterzogen werden kann.

(§ 9 Satz 2 Nr. 8 PromO BayNAT)

Hiermit erkläre ich mein Einverständnis, dass bei Verdacht wissenschaftlichen Fehlverhaltens Ermittlungen durch universitätsinterne Organe der wissenschaftlichen Selbstkontrolle stattfinden können.

.....
Ort, Datum, Unterschrift